

**ASSESSMENT OF CLIMATE CHANGE IMPACT ON
HYDROLOGY OF THE GANGES-BRAHMAPUTRA-
MEGHNA BASIN AND IMPLICATIONS FOR FUTURE
WATER RESOURCE MANAGEMENT**

A Dissertation

Submitted to the Faculty of the National Graduate Institute for Policy Studies (GRIPS)

and International Centre for Water Hazard and Risk Management (ICHARM),

Public Works Research Institute (PWRI)

in partial fulfillment of the requirements for the Degree of

DOCTOR OF PHILOSOPHY IN DISASTER MANAGEMENT

by

Muhammad MASOOD

September 2015

(This page is intentionally left blank)

Declaration

Except where specific reference has been made to the work of others the work embodied in this thesis is the result of investigation carried out by the author. No part of this thesis has been submitted or is being concurrently submitted in candidature for any degree at any other institution.

Author

Acknowledgement

The author wishes to express his profound gratitude and sincere appreciation to his supervisor Professor Kuniyoshi Takeuchi, Advisor, International Centre for Water Hazard and Risk Management (ICHARM), Japan, for his constant guidance, invaluable suggestions, and affectionate encouragement, which were extremely helpful in accomplishing this study.

The author wants to express sincere gratitude to Dr. Pat J.-F. Yeh, Assistant Professor, National University of Singapore, for his teaching, which helped the author to understand many hydrological concepts. The author also wants to acknowledge to Dr. Naota Hanasaki, Senior Researcher of National Institute for Environmental Studies, Tsukuba, Japan, for his suggestions and help regarding hydrologic model H08.

The author is indebted to the authority of Nippon Koei Co., Ltd., Japan for the grant from The Kubota Fund and Public Works Research Institute (PWRI), International Centre for Water Hazard and Risk Management (ICHARM), and the National Graduate Institute for Policy Studies (GRIPS), Tokyo, for providing him the opportunity to carry out this research in Japan.

The author dedicates this work to his beloved wife, son, and parents for their continuous encouragement and blessings during this work. Above all, the author expresses his gratitude to Almighty ALLAH to whom belongs ALL GLORY, who has wished to bring this work to reality.

Abstract

The intensity, duration, and geographic extent of floods in Bangladesh mostly depend on the combined influences of three river systems, the Ganges, Brahmaputra, and Meghna (GBM). In addition, climate change is likely to have significant effects on the hydrology and water resources of the GBM basins. However, detail hydro-meteorological analyses including climate change impact assessment with an advanced hydrological model aiming to acquire policy-relevant information necessary for climate change adaptation as well as for local water resources management in the GBM basins have rarely been conducted. To fill this gap, in this study, a macro-scale distributed hydrologic model, H08, was employed to assess impacts of climate change on basin-scale hydrology including runoff, evapotranspiration, net radiation, and soil moisture by using 5 CMIP5 GCMs through 3 time-slice experiments; the present-day (1979–2003), the near-future (2015–2039), and the far-future (2075–2099) periods. The model H08 was calibrated at a relatively fine grid resolution (10 km) via analyzing model parameter sensitivity and validated based on long-term (32 years) observed daily streamflow data. In addition, climate change impacts on manageability of hydrological extremes (both floods and droughts) in terms of necessary storage to smooth out hydrological variations were assessed by using Flood Duration Curves (FDCs) and Drought Duration Curves (DDCs). The results show that by the end of the 21st century, under the highest emission scenario, RCP8.5, (a) the entire GBM basin is projected to be warmed by $\sim 4.3^{\circ}\text{C}$; (b) the changes of mean precipitation (runoff) are projected to be +16.3% (+16.2%), +19.8% (+33.1%), and +29.6% (+39.7%) in the Brahmaputra, Ganges, and Meghna, respectively; and (c) evapotranspiration is projected to increase for the entire GBM (Brahmaputra: +16.4%, Ganges: +13.6%, Meghna: +12.9%) due to increased net radiation as well as warmer temperature. Over all, it is observed that

the impact of climate change on the hydrological processes of the Meghna basin will be larger than those of the other two basins. From the duration curve analyses, it is also observed that, the manageability of the Meghna basin is expected to be more difficult due to increases of seasonal and annual variations of streamflow in the future. This information will contribute to direct water resource management in the basin and improve the design of adaptive measures. The findings can also be considered for risk management, planning for prevention, mitigation of disaster risk, and formulation of policies for water resources development.

.

Table of Contents

	Title	Page
	Declaration	iii
	Acknowledgement	iv
	Abstract	v
	Table of Contents	vii
	List of Tables	xi
	List of Figures	xiii
1	Introduction	1-5
	1.1 Background	1
	1.2 Objectives of the Research	3
	1.3 Outline of the Thesis	4
2	Methodology	6-16
	2.1 Introduction	6
	2.2 Methodology	6
	2.2.1 Hydrologic Modeling: H08	7

2.2.2	Duration curve analysis: Flood Duration Curve (FDC) and Drought Duration Curve (DDC)	10
2.3	Data to be analyzed	13
2.3.1	Meteorological forcing datasets	13
2.3.2	Hydrologic data	14
2.3.3	Topographic data	15
2.3.4	GCM data	16
3	Analysis of the Impact of Climate Change on Hydrological Processes	17-31
3.1	Model performance	17
3.1.1	Parameter sensitivity	17
3.1.2	Calibration and validation	20
3.1.3	Uncertainty in projection due to model parameters	21
3.2	Hydrological processes	23
3.2.1	Seasonal cycle	23
3.2.2	Correlation between meteorological and hydrological variables	25
3.2.3	Interannual variability	27

3.3	Impact of Climate Change on Climatic and Hydrologic	
	Quantities: Projected Mean Changes	27
3.3.1	Precipitation	28
3.3.2	Air temperature	29
3.3.3	Net radiation	29
3.3.4	Runoff	30
3.3.5	Evapotranspiration	30
3.3.6	Soil moisture	31
4	Analysis of the Impact of Climate Change on the Manageability	
	of Hydrological Extremes	32-38
4.1	Introduction	32
4.2	Persistence characteristics of precipitation	33
4.3	Persistence characteristics of streamflow	33
4.4	Manageability of hydrological extremes and inter-basin comparisons	36
5	Analysis of Climate Change Impact on the Meghna Basin	39-47
5.1	Introduction	39
5.2	About the Meghna Basin	39

5.3	Variability of Precipitation	42
5.3.1	Spatial variation of precipitation	42
5.3.2	Temporal variation of precipitation	43
5.4	Variability of Runoff	43
5.4.1	Spatial variation of runoff	44
5.4.2	Temporal variation of runoff	44
5.5	Effect of Climate Change on Discharge	45
5.6	Decadal Changes of Precipitation and Runoff	46
6	Conclusions and Policy Implications	48-56
6.1	Conclusions	48
6.1.1	Hydrological modeling	48
6.1.2	Climate change impact assessment	50
6.1.3	Duration curve analysis	51
6.2	Policy Implications	53
6.3	Recommendations for Future Studies	55
	References	57
	Appendices	108

List of Tables

Table	Title	Page
Table 1-1:	Major characteristics of the Ganges, Brahmaputra and Meghna River basin.	67
Table 2-1:	Basic input data used in this study.	69
Table 3-1:	Sensitive parameters in the H08 model and 10 best performance parameter combinations out of 625 simulations.	71
Table 3-2:	Basic information of the streamflow validation stations in the GBM basin.	72
Table 3-3:	Statistical indices that measure the model performance at three GBM basins during both calibration and validation period.	73
Table 3-4:	Statistical indices (the coefficient of variation (CV) and standard deviation (SD)) of the uncertainty in model simulations due to the uncertainty in model parameters.	74
Table 3-5:	The 22-year (1980-2001) averages of the meteorological (from the WFD forcing data) and hydrologic variables in the GBM river	

	basins.	75
Table 3-6:	The 10-simulation average of annual mean and percentage changes of hydrological and meteorological variables.	76
Table 4-1:	Basic statistics of precipitation and streamflow data for three periods.	77
Table 4-2:	Basin ranking according to degree of difficulty to manage extreme events using the indicators of duration curves.	78
Table 5-1:	Major statistics of the Meghna river basin.	79
Table 5-2:	Percent area of the basin for different classes of average annual (a) precipitation and (b) runoff in three different time slices.	81
Table 5-3:	Percent area of the basin for different classes of percentage change of (a) precipitation and (b) runoff in the near-future (2015-2039) and the far-future (2075-2099) compared to the base-period..	82

List of Figures

Figure	Title	Page
Figure 1-1	The boundary of the Ganges-Brahmaputra-Meghna (GBM) River basin (thick red line), the three outlets (red star): Hardinge bridge, Bahadurabad and Bhairab bazar for the Ganges, Brahmaputra and Meghna River basin, respectively. Green stars indicate the locations of three additional upstream stations; Farakka, Pandu and Teesta. (modified from Pfly, 2011).	83
Figure 2-1	Flow chart of the methodology with input (left) and output (right).	84
Figure 2-2	Flow chart of the methodology followed for future projection.	85
Figure 2-3	A typical Flood duration curve (FDC) and Drought duration curve (DDC) of daily discharge series and its basic terminologies.	86
Figure 2-4	Duration curves of daily streamflow series of three periods with 10-years return period for the Ganges, plotted in linear scale (left) and logarithmic scale (right).	87
Figure 3-1	The 11-year (1980–1990) mean seasonal cycles of the simulated total runoff, surface runoff, and subsurface runoff (unit: mm day ⁻¹) in the Brahmaputra basin. Each of the five lines in each panel represents the average of 5 ³ (=125) runs with one of the four calibration parameters fixed at a given reasonable value.	88
Figure 3-2	The simulated discharges (red line) using the WFD forcing data (both calibration and validation period) compared with observations (green line) at outlets of the (a) Brahmaputra, (b)	89

Ganges, (c) Meghna River, and (d) mean monthly (1980–2001) simulated discharges compared with that of observations at outlets, (e) simulated discharges by using the 10 best performance parameter sets (red line) and the associated uncertainty bands (green shading) in a typical year (1985). Nash–Sutcliffe efficiency (NSE), percent bias (PBIAS), relative Root-Mean Square Error (RRMSE), correlation coefficient (cc), and coefficient of determination (R^2) for both calibration and validation period are noted at subplot (a), (b), and (c).

Figure 3-3 The mean (solid line) and upper and lower bounds (dashed line) 90 of the uncertainty band of the hydrological quantities and net radiation components for the present-day (black), near-future (green) and far-future (red) simulations as determined found from 10 simulation results, with considering 10 best performance parameter set according to Nash–Sutcliffe efficiency (NSE) (cu: present-day, nf: near-future, ff: far-future). Coefficient of variations (CV) for all periods (Table 3-4) are noted on each subplot.

Figure 3-4 Seasonal cycle of climatic and hydrologic quantities during 91 1980–2001. Box-and-whisker plots indicate minimum and maximum (whiskers), 25th and 75th percentiles (box ends), and median (black solid middle bar). Solid curve line represents interannual average value. All abbreviated terms here refer to Table 3-5.

Figure 3-5 The correlation between the monthly means of meteorological 92 variables (WFD) and that of hydrological variables for the Brahmaputra, Ganges and Meghna basins. Three different colors represent the data in three different seasons: Black: dry/winter (November–March); Green: pre-monsoon (April–June); and Red: monsoon (July–October). The correlation

coefficient (cc) for each pair (all 3 seasons together) is noted at each subplot. The units are mm day⁻¹ for Prec, ET, runoff, mm for SoilMoist, °C for T_{air}, and W m⁻² for net radiation. All abbreviated terms here are referred to in Table 3-5.

Figure 3-6	Interannual variation of mean of meteorological and hydrological variables of 5 GCMs for the present day (1979-2003), near future (2015-2039), and far future (2075-2099). Thick blue lines represent the means of 5 GCMs.	93
Figure 3-7	Percentage changes in the monthly means of the climatic and hydrologic quantities from the present-day period to the near-future and far-future periods. The dashed lines represent the annual mean changes.	94
Figure 4-1	Comparison of duration curves of basin-averaged monthly precipitation (P) series of three periods with 10-year return period for three basins.	95
Figure 4-2	Flood and drought duration curves of basin-averaged monthly precipitation (P) series of three periods; observed (1980–2009), near-future (2015–2039) and far-future (2075–2099) with 5-, 10-, 20-, and 50-year return period (<i>T</i>) for the three basins.	96
Figure 4-3	Comparison of duration curves of daily streamflow series of three periods; observed (1980-2009), near future (2015-2039), and far future (2075-2099) with 10-year return period for the three basins.	97
Figure 4-4	Flood and drought duration curves of daily streamflow (Q) series of three periods: observed (1980–2009), near future (2015–2039), and far future (2075-2099) with 5-, 10-, 20-, and 50-year return period (<i>T</i>) at basin outlets for the three basins.	98

Figure 5-1	The Meghna river basin map with major rivers, transportation network, and gauging stations in the study area.	99
Figure 5-2	Topography and land use of the Meghna river basin.	100
Figure 5-3	Spatial distribution of projected precipitation and percentage changes in average annual precipitation of the Meghna basin. All mean annual precipitation presented in the figure are 25-year means, and changes are calculated considering the 1979–2003 as the base period. (a), (b), and (c) are for the base period, the near future, and the far future, respectively. Percentage changes in projected precipitation are presented as (d) and (e) for the near future and the far future, respectively. Light violet colored cells in (d) indicate the area where projected precipitation is zero or negative.	101
Figure 5-4	Probability of exceedance of basin averaged monthly precipitation of the Meghna basin at two gauging stations: (a) and (b) at Bhairab Bazar, (c) and (d) at Amalshid for three time slices: the base period, the near future, and the far future. (b) and (d) are the magnified view of (a) and (c) at 75–100 percentage exceedance (which represent the probability of exceedance of monthly low-precipitation) at Bhairab Bazar and Amalshid, respectively.	102
Figure 5-5	Spatial distribution of projected runoff and percentage changes in average annual runoff of the Meghna basin. All mean annual runoff presented in the figure is a 25-year mean, and changes are calculated considering 1979–2003 as the base period. (a), (b), and (c) are for the base period, the near future, and the far future, respectively. Percentage changes in projected runoff are presented as (d) and (e) for the near future and the far future, respectively. Light violet colored cells in (d) and (e) are	103

indicate the area where projected runoff is zero or negative.

- Figure 5-6 Probability of exceedance of basin averaged monthly runoff of the Meghna basin at two gauging stations: (a) and (b) at Bhairab Bazar, (c) and (d) at Amalshid for three time slices: the base period, the near future and the far future. (b) and (d) are the magnified view of (a) and (c) at 75–100 percentage exceedance (which represent the probability of exceedance of monthly low-flow) at Bhairab Bazar and Amalshid, respectively. 104
- Figure 5-7 Discharge of the Meghna river at Bhairab Bazar station for three time slices: the base-period (bp), the near future (nf) and the far future (ff). Box-and-whisker plots indicate minimum and maximum (whiskers), 25th and 75th percentiles (box ends), and median (black solid middle bar). Solid curve line represents mean monthly value. (b) Mean discharges at Bhairab Bazar station for three time slices. 105
- Figure 5-8 Probability of non-exceedance and return period for Gumbel distribution of annual maxima discharges ($\text{m}^3 \text{s}^{-1}$) at Bhairab Bazar for three time slices; the base period (1979–2003), the near future (2015–2039), and the far future (2075–2099), plotted in a Gumbel probability paper. 106
- Figure 5-9 Projected precipitation and runoff change for the near-future and the far-future. Each point in the plot represents the 10-year mean of runoff increment associated with the corresponding precipitation increment at Bhairab Bazar gauging station. For 2035–2039 and 2095–2099, the mean is taken over 5 years. All increments are computed considering 1979–2003 as the base period. 107

1. Introduction

1.1 Background

Bangladesh is situated in the active delta of three of the world's major rivers, the Ganges, Brahmaputra, and Meghna. Due to its unique geographical location, the occurrence of water-induced disasters in Bangladesh is a regular phenomenon. In addition, the anticipated change in climate is likely to lead to an intensification of the hydrological cycle, have a major impact on the overall hydrology of these basins, and ultimately lead to an increase in the frequency of water-induced disasters in Bangladesh. However, the intensity, duration, and geographic extent of floods in Bangladesh mostly depend on the combined influences of these three river systems. Previous studies have indicated that flood damages have become more severe and devastating when two or more flood peaks in these three river basins coincide (Chowdhury, 2000; Mirza, 2003).

The Ganges-Brahmaputra-Meghna (hereafter referred to as GBM) River basin has a total area of about 1.7 million km² (FAO-AQUASTAT, 2014; Islam et al., 2010) and is shared by a number of countries (Figure 1-1). The Brahmaputra River begins in the glaciers of the Himalayas and travels through China, Bhutan, and India before emptying into the Bay of Bengal in Bangladesh. It is a snow-fed braided river that remains a natural stream with no major hydraulic structures built along its reach. The Ganges River originates at the Gangotri glaciers in the Himalayas and passes through Nepal, China, and India before emptying into the Bay of Bengal at Bangladesh. It is a snowmelt-fed river, and its natural flow is controlled by a number of dams constructed by the upstream countries. The Meghna River is a comparatively smaller, rain-fed, and relatively flashier river that runs through a mountainous region in India before entering

Bangladesh. Major characteristics of the GBM Rivers are presented in Table 1-1. This river system is the world's third-largest freshwater outlet to the oceans (Chowdhury & Ward, 2004). During extreme floods, over $138,700 \text{ m}^3 \text{ s}^{-1}$ of water flows into the Bay of Bengal through a single outlet, which is the world's largest intensity, even exceeding that of the Amazon discharges by about 1.5 times (FAO-AQUASTAT, 2014). The GBM River basin is unique in the world in terms of diversified climate. For example, the Ganges River basin is characterized by low precipitation ($760\text{--}1,020 \text{ mm year}^{-1}$) in the northwest upper region and high precipitation ($1,520\text{--}2,540 \text{ mm year}^{-1}$) along the coastal areas. High precipitation zones and dry rain-shadow areas are located in the Brahmaputra River basin, whereas the world's highest precipitation ($\sim 5,690 \text{ mm year}^{-1}$) area is situated in the Meghna River basin (FAO-AQUASTAT, 2014).

Several studies have focused on the rainfall and discharge relationships in the GBM basin by (a) identifying and linking the correlation between basin discharge and the El Niño-southern oscillation (ENSO) and sea surface temperature (SST) (Chowdhury & Ward, 2004; Mirza et al., 1998; Nishat & Faisal, 2000), (b) analyzing available observed or reanalysis data (Chowdhury & Ward, 2004, 2007; Kamal-Heikman et al., 2007; Mirza et al., 1998), and (c) evaluating historical data of flood events (Islam et al., 2010; Mirza, 2003). Various statistical approaches were used in the above studies instead of using hydrologic model simulations. In recent years, a number of global-scale hydrologic model studies (Haddeland et al., 2011; Haddeland et al., 2012; Pokhrel et al., 2012) have been reported. Although their modeling domains include the GBM basin, these global-scale simulations are not fully reliable due to the lack of model calibration at both the global and basin scales.

A few studies have been conducted to investigate the impact of climate change on the hydrology and water resources of the GBM basin (Biemans et al., 2013; Gain et al., 2011; Ghosh & Dutta, 2012; Immerzeel, 2008; Kamal et al., 2013; Mirza & Ahmad, 2005b). In most of these studies, future streamflow was projected on the basis of linear regression between rainfall and streamflow derived from historical data (Chowdhury & Ward, 2004; Immerzeel, 2008; Mirza et al., 2003). Immerzeel (2008) used the multiple regression technique to predict streamflow at the Bahadurabad station (the outlet of the Brahmaputra basin) under future temperature and precipitation conditions based on a statistically downscaled Global Circulation Model (GCM) output. However, since most hydrologic processes are nonlinear, they cannot be predicted accurately by extrapolating empirically derived regression equations to future projections. The alternative for the assessment of climate change impacts on basin-scale hydrology is well-calibrated hydrologic modeling, but this has rarely been conducted for the GBM basin due to the lack of observed data for model calibration and validation. Ghosh and Dutta (2012) applied a macro-scale distributed hydrologic model to study the change of future flood characteristics in the Brahmaputra basin, but their study domain focused only on the regions inside India. Gain et al. (2011) estimated future trends of the low and high flows in the lower Brahmaputra basin using outputs from a global hydrologic model (grid resolution: 0.5°) forced by multiple GCM outputs. Instead of model calibration, the simulated future streamflow was weighted against observations to assess the climate change impacts.

1.2 Objectives of the Research

Detail hydro-meteorological analyses including climate change impact assessment with an advanced hydrological model aiming to acquire policy-relevant information necessary for climate change adaptation as well as for local water resources management in the GBM basins have rarely been conducted in the previous studies. Therefore, the main objective of the research is to fill this gap, which is achieved by sub-objectives as follows: (1) set up a distributed hydrologic model at a relatively fine grid resolution (10 km) by integrating fine-resolution (~0.5 km) DEM data for accurate delineation of the river network, and calibrate and validate the model with the long-term observed daily streamflow data; (2) investigate the impact of climate changes on the basin-scale hydrology, including runoff, evapotranspiration, soil moisture, and net radiation; (3) investigate the impact of climate changes on manageability of hydrological extremes (both floods and droughts) in terms of necessary storage to smooth out hydrological variations; and (4) investigate the spatiotemporal changes of precipitation and runoff in the most sensitive basin among the three basins.

1.3 Outline of the Thesis

The research work conducted to achieve the stated objectives is presented in six chapters so that the steps involved in the study may be properly delineated. The current chapter introduces the reader to the background of the thesis work and review of previous studies. Descriptions of the methodology and data used in this research are presented in Chapter 2. Chapter 3 describes the impact of climate change on the hydrological processes. The impacts of climate change on manageability of hydrological extremes are reported in Chapter 4. Chapter 5 is dedicated to results and

discussions from the analysis of the impact of climate change on the Meghna basin. Finally, Chapter 6 draws conclusions by summarizing the outcomes of the research and the implications for future water resources management.

2. Methodology

2.1 Introduction

The background of the study as well as previous literature in this area has been described in Chapter 1. This chapter presents the methodology of the research and description of the data to be analyzed.

2.2 Methodology

Figure 2-1 presents the methodology used in this study from hydrologic model setup to investigation of policy-level implications. The methodology can be divided into two major parts: (1) setup of a hydrologic model for future projection to investigate the impact of climate change on hydro-meteorological variables, and (2) duration curve analysis using Flood Duration Curve (FDC) and Drought Duration Curve (DDC) to investigate the impact of climate change on the manageability of floods and droughts of these three basins.

Figure 2-2 presents a detailed flowchart of the first part of the methodology. A global hydrologic model H08 (Hanasaki et al., 2008; Hanasaki et al., 2014) is applied regionally over the GBM basin at a relatively fine grid resolution (10 km) by integrating fine-resolution (~0.5 km) DEM data for accurate delineation of the river networks. The hourly atmospheric forcing data from the Water and Global Change (WATCH) model-inter-comparison project (hereafter referred to as WFD, i.e., WATCH Forcing Dataset; Weedon et al., 2011) are used for the historical simulations. The model has been calibrated and validated based on a rarely obtained long-term (1980–2001) dataset of observed daily streamflow in the GBM basin provided by the Bangladesh Water

Development Board (BWDB). Relative to previous GBM basin studies, it is believed that the availability of this unique long-term streamflow dataset can lead to more precise estimation of model parameters and hence more accurate hydrological simulations and more reliable future projection of the hydrology of the GBM basin. For the future simulations, the model is forced by climate model output under the high-emissions scenario (RCP 8.5) from five different coupled atmosphere–ocean general circulation models (hereafter referred to as GCMs), all of which were included in the Coupled Model Intercomparison Project Phase 5 (CMIP5; Taylor et al., 2012). In order to be consistent with the historical data, for each basin the monthly correction factor (i.e., the ratio between the monthly precipitation of the WFD data and that of the GCM data for each month) is applied to GCM’s future precipitation outputs. Three time-slice experiments are performed for the present-day (1979–2003), the near-future (2015–2039), and the far-future (2075–2099) periods.

In the second part, duration curves analysis has been performed on monthly basin averaged precipitation and daily streamflow data series by using FDCs and DDCs (Takeuchi, 1988) to investigate the impact of climate change on (a) the persistence characteristics of floods and droughts, and (b) the manageability of these hydrological extremes in terms of managing hydrological variations. Finally, to investigate the spatiotemporal changes, this study has been focused on the Meghna basin, which is identified as the most sensitive of the three basins (Masood et al., 2015).

2.2.1 Hydrologic modeling: H08

H08 is a macro-scale hydrological model developed by Hanasaki et al. (2008) that consists of six main modules: land surface hydrology, river routing, crop growth,

reservoir operation, environmental flow requirement estimation, and anthropogenic water withdrawal. For this study, only two modules, land surface hydrology and river routing, were used. The land surface hydrology module calculates the energy and water budgets above and beneath the land surface as forced by the high-temporal-resolution meteorological data.

The runoff scheme in H08 is based on the bucket model concept (Manabe, 1969), but it differs from the original formulation in certain important aspects. Although runoff is generated only when the bucket is overfilled, as in the original bucket model, H08 uses a “leaky bucket” formulation in which subsurface runoff occurs continually as a function of soil moisture. Soil moisture is expressed as a single-layer reservoir with the holding capacity of 15 cm for all the soil and vegetation types. When the reservoir is empty (full), soil moisture is at the wilting point (the field capacity). Evapotranspiration is expressed as a function of potential evapotranspiration and soil moisture (Eq. 2-2). Potential evapotranspiration and snowmelt are calculated from the surface energy balance (Hanasaki et al., 2008).

Potential evaporation E_P is expressed in this model as

$$E_P(T_S) = \rho C_D U (q_{SAT}(T_S) - q_a) \quad (2-1)$$

Where ρ is the density of air, C_D is the bulk transfer coefficient U is the wind speed, $q_{SAT}(T_S)$ is the saturated specific humidity at surface temperature, and q_a is the specific humidity. Evaporation from a surface (E) is expressed as

$$E = \beta E_P(T_S), \quad (2-2)$$

where

$$\beta = \begin{cases} 10.75W_f \leq W \\ W/W_f W < 0.75W_f \end{cases}, \quad (2-3)$$

where W is the soil water content and W_f is the soil water content at field capacity (fixed at 150 kg m^{-2}).

Surface runoff (Q_s) is generated whenever the soil water content exceeds the field capacity:

$$Q_s = \begin{cases} W - W_f & W > W_f \\ 0 & W \leq W_f \end{cases}, \quad (2-4)$$

Subsurface runoff (Q_{sb}) is incorporated in the model as

$$Q_{sb} = \frac{W_f}{\tau} \left(\frac{W}{W_f} \right)^\gamma, \quad (2-5)$$

where τ is a time constant and γ is a parameter characterizing the degree of nonlinearity of Q_{sb} .

The river module accumulates runoff generated by the land surface model and routes it downstream as streamflow. It is identical to the total runoff integrating pathways (TRIP) model (Oki & Sud, 1998). The module has a digital river map covering the whole globe at a spatial resolution of 1° ($\sim 111 \text{ km}$), which is too coarse for the regional simulation in this study, which has a 10-km resolution. Therefore, a new digital river map of the 10-km resolution is prepared for this purpose by integrating finer-resolution ($\sim 0.5 \text{ km}$) DEM data. Effective flow velocity and meandering ratio are

the most sensitive parameters of the river module, and their default values are set at 0.5 m s⁻¹ and 1.5, respectively.

Four parameters from the land surface module of H08 (root-zone depth d , bulk transfer coefficient C_D controlling the potential evaporation, and the parameters sensitive to subsurface flow, that is, τ and γ) and two parameters from the river module (effective flow velocity and meandering ratio) are calibrated. Details of the selection of calibration parameters and calibration processes are given in Subsections 3.1.1 and 3.1.2.

2.2.2 *Duration curve analysis: Flood Duration Curve and Drought Duration Curve*

The flow duration curve, which illustrates the relationship between the frequency and magnitude of streamflow, is the most commonly used method in the field of water resource engineering (Vogel & Fennessey, 1995). It is a graphical representation of the frequency, or the fraction of time during which a specified magnitude of flow is equaled or exceeded. It has a complete signature of streamflow variability with time (Günter Blöschl et al., 2013). However, this flow duration curve can be presented in an alternative way, termed the flood duration curve and drought duration curve. In general, the FDC and DDC present the extreme (lowest or highest) average of a hydrological quantity (precipitation or streamflow) over different duration periods with different probabilities of occurrence. In other words, the curves show extreme values of a hydrological variable, estimated from moving averages of various durations. They contain information that has direct implications on water resources management both for flood control and for effective water use during a drought. Kikkawa and Takeuchi (1975a, 1975b) first defined a DDC with a mathematical expression and proposed it as a tool for regional hydrological characterization and for

reservoir design and operation. Takeuchi (1986) applied DDCs to develop a real-time reservoir operation rule. Then Takeuchi (1988) extended it to both FDCs and DDCs and investigated the hydrological persistence characteristics of floods and droughts in different basins. Yet despite its unique potential of applicability, this way of expressing duration curves has been followed by very few hydrologists (Kyoshi et al., 1993; Matsuda, 1979).

The duration curves present the extreme values of moving averages of precipitation and streamflow over the period m (days or months) estimated from the observed time series (x_t). The variable m has been chosen according to the duration of interest over which smoothing of hydrological variability is necessary for water resource management. In this study it varied from 1 to 1,095 days for streamflow and from 1 to 36 months for precipitation. Equations 2-6 and 2-7 show the annual maxima series, $x_j(m)$ and the annual minima series, $x'_j(m)$ for the period m moving averages of time series x_t . Generalized extreme value (GEV) distribution has been applied on these two series to estimate extreme values for 5-, 10-, 20-, and 50-year return periods (T), which are shown in Figure 2-3.

$$x_j(m) = \max_{t_1 \in j\text{th year}} \frac{1}{m} \sum_{t=t_1}^{t_1+m-1} (x_t) \quad (2-6)$$

$$x'_j(m) = \min_{t_1 \in j\text{th year}} \frac{1}{m} \sum_{t=t_1}^{t_1+m-1} (x_t) \quad , \quad (2-7)$$

where $\frac{1}{m} \sum_{t=t_1}^{t_1+m-1} (x_t)$ is the average of m consecutive values between time t_1 and time $t_1 + m - 1$. $j = 1, \dots, N$ where N is the number of years for which all moving

averages over m starting from any date t_1 are available. N is different for different durations of moving averages concerned.

The FDC and DDC of recurrence interval T -year are defined as $f_T(m)$ and $f'_T(m)$, which are estimated from the sample set of annual maxima series, $x_j(m)$ and annual minima series, $x'_j(m)$, respectively, where

$$f_T(m) = T - \text{yearreturnperiodestimateof } x_j(m), j = 1, \dots, N \quad (2-8)$$

$$f'_T(m) = T - \text{yearreturnperiodestimateof } x'_j(m), j = 1, \dots, N \quad (2-9)$$

Duration curves are drawn for basin-averaged monthly precipitation over three basins and for daily streamflow at Bahadurabad, Hardinge Bridge, and Bhairab Bazar, the outlets of the three basins. However, for the ease of comparing DDCs and FDCs among basins, the curves are normalized on the y -axis by dividing their long-term means. It can be seen from these figures that, in general, FDCs decrease as duration m increases, whereas DDCs increase. This is because both curves approach the long-term mean (toward the average line) as the duration becomes longer. In other words, both floods and droughts may be extreme for a short time, but if a longer time is considered, the averages become less extreme in intensity. Hydrological characteristics such as annual variation, seasonal variation, and severity of extreme events can be explained by three indicators: departure, variation, and angle, respectively of the duration curves that were described by Takeuchi (1988), shown in Figure 2-3. The degree of difficulty of managing extreme events depends on these hydrological characteristics.

Figure 2-4 shows duration curves plotted on both a linear scale and a logarithmic scale. Both ways of presenting these curves have advantages and limitations. The linear plot shows the actual shapes of the duration curves, whereas the logarithmic plot shows distorted shapes. Therefore, regardless of the relative appearance of the curves in a logarithmic paper, differences in absolute values are much larger in FDCs than in DDCs. However, in this study the curves are drawn in logarithmic scale for the following reasons:

- Both FDCs and DDCs can be shown and distinguishably identifiable in a single plot if they are plotted on a logarithmic vertical axis. Therefore, interbasin and interperiod comparisons are possible for both FDCs and DDCs, whereas in a linear plot DDCs cannot be clearly identified separately due to smaller absolute values.
- In logarithmic plots, intra-annual variations (m is between 1 and 365 days) in FDCs and DDCs are easily visible. Therefore, the three important indicators from duration curves can be distinguished and compared easily for different basins and periods.

2.3 Data to be analyzed

Basic information and characteristics (type, source, resolution, and period of data) of input data used in this study are summarized in Table 2-1.

2.3.1 Meteorological Forcing datasets

The WATCH Forcing Dataset (Weedon et al., 2011) is used to drive the H08 model for the historical simulation. The WFD variables, including rainfall, snowfall,

surface pressure, air temperature, specific humidity, wind speed, long-wave downward radiation, and shortwave downward radiation were taken from the ERA-40 reanalysis product of the European Centre for Medium Range Weather Forecasting (ECMWF). The ERA reanalysis data with the one-degree resolution was interpolated into the half-degree resolution on the Climate Research Unit of the University of East Anglia (CRU) land mask, adjusted for elevation changes where needed, and bias-corrected using monthly observations. The WFD is considered one of the best available global climate forcing datasets for providing accurate representation of meteorological events, synoptic activity, seasonal cycles, and climate trends (Weedon et al., 2011). Studies by Lucas-Picher et al. (2011) and Siderius et al. (2013) found that for South Asia and the Ganges, respectively, the WFD rainfall is consistent with the APHRODITE (Yatagai et al., 2012), a gridded (0.25°) rainfall product for the South Asia region developed based on a large amount of rain gauge data. For detailed information on the WFD, see Weedon et al. (2011) and Weedon et al. (2010). The albedo values are based on the monthly albedo data from the Second Global Soil Wetness Project (GSWP2).

2.3.2 *Hydrologic data*

Observed river water level (daily) and discharge (weekly) data from 1980 to 2012 for the hydrological stations located inside Bangladesh (the outlets of the three basins shown in Figure 1-1, i.e., the Ganges basin at Hardinge Bridge, the Brahmaputra basin at Bahadurabad, and the Meghna basin at Bhairab Bazar) were provided by the Hydrology Division, Bangladesh Water Development Board (BWDB). River water levels were regularly measured five times a day (at 6 a.m., 9 a.m., 12 p.m., 3 p.m., and 6 p.m.), and discharges were measured weekly by the velocity-area method. Since the

Brahmaputra River is highly braided, the discharge measurements at Bahadurabad were carried out on multiple channels. In contrast, the Meghna River at Bhairab Bazar is seasonally tidal; after withdrawal of the monsoon, the river near this station becomes tidal, and from December to May the river shows both a horizontal and a vertical tide (Chowdhury & Ward, 2004). Under this condition during the dry season, tidal discharge measurements were made at this station once per month. Daily discharges were calculated from the daily water level data by using the rating equations developed by the Institute of Water Modeling (IWM, 2006) for the Ganges and Brahmaputra Rivers and using the rating equations developed by Masood et al. (2015) for the Meghna River. Discharge (monthly) data of three more stations (Farakka, Pandu, and Teesta) located upstream of these basins (Figure 1-1) were collected from the Global Runoff Data Centre (GRDC) and were also useful for model validation purposes.

2.3.3 Topographic data

DEM data were collected from the Hydrological data and maps based on SHuttle Elevation Derivatives at multiple Scales (HydroSHEDS, 2014). It offers a suite of geo-referenced datasets (vector and raster) including stream networks, watershed boundaries, drainage directions, and ancillary data layers such as flow accumulations, distances and river topology information (Lehner et al., 2006). The HydroSHEDS data were derived from the elevation data of the Shuttle Radar Topography Mission (SRTM) at a ~0.5 km resolution. Preliminary quality assessments indicated that the accuracy of HydroSHEDS significantly exceeds that of existing global watershed and river maps (Lehner et al., 2006).

2.3.4 GCM data

Climate data from five CMIP5 climate models—MIROC5, MIROC-ESM, MRI-CGCM3, HadGEM2-ES (under the RCP 8.5 representative concentration pathway), and MRI-AGCM3.2S (under the SRES A1B)—were used in this study as the forcing data for future hydrological simulations (see Appendix B, Table B1). The climate data were interpolated from their original climate model resolutions (ranging from $0.25 \times 0.25^\circ$ to $2.8 \times 2.8^\circ$) to $5' \times 5'$ (~10-km mesh) using linear interpolation (nearest four-point). In order to be consistent with the historical simulation forced by WFD, the precipitation forcing data in each GBM basin from each GCM were corrected by multiplying them by a monthly correction factor equal to the ratio between the basin-averaged long-term mean precipitation from WFD and that from each GCM for all the months. Among these GCMs, MRI-AGCM3.2S (where the *S* refers to “super-high resolution”) provides higher-resolution (20-km) atmospheric forcing data, which shows improvements in simulating heavy precipitation, global distribution of tropical cyclones, and the seasonal march of the East Asian summer monsoon (Mizuta et al., 2012). The MRI-AGCM3.2S forcing dataset has been used in several recent climate change impact studies focused on South Asia (Endo et al., 2012; Kwak et al., 2012; Rahman et al., 2012).

3. Analysis of the Impact of Climate Change on Hydrological Processes

3.1 Model Performance

3.1.1 Parameter sensitivity

The parameter-sampling simulation is conducted to investigate the sensitivity of the H08 model parameters to the simulation results. The most sensitive parameters in H08 include the root-zone depth d [m], the bulk transfer coefficient C_D [-] controlling the potential evaporation (Eq. 2-1), and the parameters sensitive to subsurface flow, that is, τ [day] and γ [-] (Eq. 2-5; Hanasaki et al., 2014), hence they are treated as calibration parameters in this study. The parameter τ is a time constant determining the daily maximum subsurface runoff. The parameter γ is a shape parameter controlling the relationship between subsurface flow and soil moisture (Hanasaki et al., 2008). Their default parameter values in H08 are 1 m for d , 0.003 for C_D , 100 days for τ , and 2 for γ . For each of these four parameters, five different values were selected from their feasible physical ranges. The parameter-sampling simulations of the H08 model were run by using all of the combinations of four parameters, which consisted of a total of 5^4 (= 625) simulations all conducted by using the same 11 years' (1980–1990) atmospheric forcing data of WFD.

Figure 3-1 plots the 11-year long-term average seasonal cycles of simulated total runoff, surface runoff, and subsurface runoff of the Brahmaputra basin. Each of the five lines in each panel represents the average of 5^3 (=125) runs with one of the 4 calibration parameters fixed at a given value. As shown, the overall sensitivity of the selected model parameters to the flow partitioning is high. When d is low, surface runoff is high (due to higher saturated fractional area; Figure 3-1 b). As d increases, subsurface runoff

increases and surface runoff decreases (Figure 3-1 c and b). Due to these compensating effects, the effect of d on the total runoff becomes more complex: from March to August, higher d causes lower total runoff, but the trend is reversed from August on for the Brahmaputra basin. Similar behaviors can be observed for the other two basins (figure not shown).

The parameter C_D is the bulk transfer coefficient in the calculation of potential evaporation (Eq. 2-1), thus its effect on runoff is relatively small (Figure 3-1 d-f). However, higher C_D causes more evaporation and hence lower runoff (both surface and subsurface; Eq. 2-4 and Eq. 2-5). The sensitivity of parameter γ to runoff is also smaller than that of d and τ . As γ increases, surface runoff increases and subsurface runoff decreases (Figure 3-1 h, i). The overall sensitivity of γ to the total runoff becomes negligible due to the compensating effects (Figure 3-1g).

As shown in Eq. (2-5) and Figure 3-1k-l, the parameter τ has a critical impact on the surface and subsurface flow partitioning. A larger τ corresponds to larger surface runoff and hence smaller subsurface runoff (Figure 3-1k-l), but it has a relatively small impact on total runoff (Figure 3-1j).

These four calibration parameters have combined influences on total runoff partitioning as well as simulations of other hydrologic variables. To summarize, (a) the sensitivity of d to the total runoff is complex, and the trend is reversed between the two halves of a year; (b) parameters d and τ have a significant impact on flow partitioning, whereas C_D and γ have less sensitivity to runoff simulation; and (c) the influence of d and τ is reversed between surface and subsurface runoff, so that surface runoff increases as d decreases and τ increases.

Table 3-1 presents the selected 10 best performance parameter combinations according to the Nash-Sutcliffe coefficient of efficiency (NSE; Nash & Sutcliffe, 1970) for the three basins, and Figure 3-2 e plots the uncertainty bands of the simulated discharges by using these parameter combinations. It is noted from the 10 best performance parameter combinations that in the case of the Brahmaputra basin, the optimal τ is 150, C_D is 0.001, and d and γ range from 3 to 5 and 1.0 to 2.5, respectively. It is also observed that the spread of the uncertainty band is located mainly around the low-flow period (dry season from November to March; Figure 3-2 e). No surface runoff is generated in the dry season, when the soil moisture is lower than the field capacity (Eq. 2-4 and Figure 3-1b). The spread of the uncertainty bands is mainly due to the variations of d and γ . As d increases, the subsurface runoff increases (Figure 3-1c and Figure 3-2 e). On the other hand, in the case of the Ganges and Meghna basins, the spread of uncertainty bands is observed throughout the entire year (in low-flow as well as in peak-flow regimes). Among the 10 best performance parameter combinations for the Ganges (Meghna), it is found that parameter C_D is 0.008 (0.008), τ is 150 (50), d and γ range from 4 to 5 (4 to 5), and 2.5 to 4 (1.5 to 2), respectively. In the dry period, when surface runoff is nearly zero, subsurface runoff increases as d increases. A higher C_D causes higher evaporation, which influences runoff as well (Eq. 2-1). As discussed earlier, the influence of d on the total runoff is complex, which results in the variation of simulated runoff throughout the year. The spread of the uncertainty bands is large in the peak flow period because the sensitivity of both surface and subsurface runoff is also large with respect to the value of d (not shown).

3.1.2 Calibration and validation

The historical simulation from 1980 to 2001 is divided into two periods with the first half (1980-1990) as the calibration period and the second half (1991-2001) as validation. Basic information and characteristics (location, drainage area, and periods of available observed data) of the six validation stations in GBM are summarized in Table 3-2. Model performance is evaluated by comparing observed and simulated daily streamflow by the NSE (Nash & Sutcliffe, 1970), the optimal objective function for assessing the overall fit of a hydrograph (Sevat & Dezetter, 1991). A series of sensitivity analyses of H08 parameters was conducted from which 10 sets of best performance parameters were determined by using the parameter-sampling simulation as discussed earlier, and these parameter sets were used to quantify the uncertainty in both historical and future simulations in the following.

Figure 3-2 plots the daily hydrograph comparisons at the outlets of the three river basins with the corresponding daily observations for both calibration and validation periods. The NSEs obtained for the calibration (validation) period were 0.84 (0.78), 0.80 (0.77), and 0.84 (0.86), while the percent biases (PBIAS) were 0.28% (6.59%), 1.21% (2.23%), and -0.96% (3.15%) for the Brahmaputra, Ganges, and Meghna basins, respectively. For all of the basins, the relative root-mean square error (RRMSE), correlation coefficient (cc), and coefficient of determination (R^2) for the calibration (validation) period ranged from 0.32 to 0.60 (0.32 to 0.59), 0.91 to 0.93 (0.89 to 0.94), and 0.82 to 0.86 (0.79 to 0.88), respectively. These statistical indices (Table 3-3) suggest that the model performance was satisfactory overall. To further evaluate model performance at upstream stations, the monthly discharge data at three

upstream stations (Farakka, Pandu, and Teesta) collected from the Global Runoff Data Centre were used to compare with the model simulations, and the result shows that the mean seasonal cycle of simulated streamflow matches well with the corresponding GRDC observations in these three upstream stations (see Appendix A).

3.1.3 Uncertainty in projection due to model parameters

In recent decades, along with increasing computational power, there has been a trend toward increasing complexity of hydrological models to capture natural phenomena more precisely. However, the increased complexity of hydrological models does not necessarily improve their performance for unobserved conditions due to the uncertainty in the model parameter values (Carpenter & Georgakakos, 2006; Tripp & Niemann, 2008). An increase in complexity may improve the calibration performance due to the increased flexibility in the model behavior, but the ability to identify correct parameter values is typically reduced (Wagener et al., 2003). Model simulations with multiple combinations of parameter sets can perform equally well in reproducing the observations. Another source of uncertainty comes from the assumption of stationary model parameters, which is one of the major limitations in modeling the effects of climate change. Model parameters are commonly estimated under the current climate conditions as a basis for predicting future conditions, but the best performance parameters may not be stationary over time (Mirza & Ahmad, 2005a). Therefore, the uncertainty in future projections due to model parameter specification can be critical (Coron et al., 2012; Merz et al., 2011; Vaze et al., 2010), although it is usually ignored in most climate change impact studies (Lespinas et al., 2014). The results obtained by Vaze et al. (2010) indicated that model parameters can generally be used for climate

impact studies when the model is calibrated using more than 20 years of data and when the future precipitation is not more than 15% lower or 20% higher than that in the calibration period. However, Coron et al. (2012) found a significant level of errors in simulations due to this uncertainty and suggested further research to improve the methods of diagnosing parameter transferability under the changing climate. For the purpose of minimizing this parameter uncertainty, the average results from the 10 simulations using the 10 best performance parameter sets are considered the simulation results for the two future periods in this study. Also, the propagating uncertainty in simulation results due to the uncertainty in model parameters will be quantified and compared among various hydrologic variables in this study.

The upper and lower bounds of the uncertainty of hydro-meteorological variables are plotted in Figure 3-3 for all of the simulation periods. It can be seen from the figure that the uncertainty band of runoff is relatively narrow (the coefficient of variation [CV] ranges between 3 and 7.6% among the three basins), which indicates that future runoff is well predictable through model simulations. In addition, from Figure 3-2 e it is observed that there is no significant uncertainty in simulated peak discharge for the Brahmaputra and Meghna River. Lower uncertainty in simulating runoff is highly desirable for climate change impact studies, such as flood risk assessments in which the runoff estimate (especially the peak flow) is the main focus. However, a relatively wide uncertainty band of runoff can be found in the Ganges in the wet season (Figure 3-3 d2), which might be due to the fact that the upstream water use (diversion) in the Ganges was not well represented in the model. Notice that the lower uncertainty in runoff projection relative to other variables could be expected as the model was calibrated and

validated against observed streamflow at the basin outlet. The uncertainty in the ET projection is also lower (CV: 3.6–11.3%; SD: 0.1–0.4), which could be related to the narrower uncertainty band of net radiation (CV: 1.8–8.6%; SD: 1.8–5.6). On the other hand, the projection of soil moisture is rather uncertain for all three basins (CV: 14.4–31%; SD: 35–104). Large uncertainty in predicting soil moisture can be a serious issue that is significant in land use management and agriculture, and this emphasizes the critical significance of (a) suitable parameterization of soil water physics in the model, (b) a reliable regional soil map for the specification of model parameters, and (c) soil moisture observations for model calibration and validation.

3.2 Hydrological Processes

The calibrated H08 model is applied to the simulations for the following three time-slice periods: the present (1979–2003), the near future (2015–2039), and the far future (2075–2099). The present simulation used both WFD and GCM historical climate forcing data, and the future simulation used only GCM forcing data. The simulation results for the two future periods are then compared with the present period (1979–2003) simulation forced by GCM to assess the effect of climate change on the hydrology and water resources of GBM in terms of precipitation, air temperature, evapotranspiration, soil moisture, and net radiation. The results are presented in the following subsections.

3.2.1 Seasonal cycle

Figure 3-4 plots the 22-year (1980–2001) mean seasonal cycles of the climatic (from WFD forcing) and hydrologic (from model simulations) quantities averaged over the three basins. (The corresponding mean annual amounts of these variables are

presented in Table 3-5.) Figure 3-2 also shows a box-and-whisker plot depicting the range of variability for each month. The interannual variation of precipitation in the Brahmaputra and Meghna is high from May to September (Figure 3-4 a, c), whereas in the Ganges it is high from June to October. However, the magnitude of precipitation differs substantially among the three basins. The Meghna has significantly higher precipitation than the other two basins (Table 3-5), and the maximum (monthly) precipitation during 1980-2001 occurs in May with the magnitude of 32 mm day^{-1} , whereas those in Brahmaputra and Ganges occur in July with the magnitudes of 15 mm day^{-1} and 13 mm day^{-1} , respectively. Moreover, the seasonality of runoff in all three basins corresponds well with that of precipitation. Runoff (Figure 3-4 j-l) in the Ganges is much lower (the monthly maximum of 4.3 mm day^{-1} in August) than in the other two basins (the monthly maximum of 9.3 mm day^{-1} in the Brahmaputra and 15.9 mm day^{-1} in the Maghna, both in July). In addition, ET in the Brahmaputra is significantly lower (251 mm year^{-1}) than that in the other two basins (748 mm year^{-1} in the Ganges and $1000 \text{ mm year}^{-1}$ in the Meghna). The contrasting ET magnitudes among the three basins are attributable to multiple reasons: differences in elevation, amounts of surface water to evaporate, air temperature, and possibly wind and solar irradiance situations. Lower ET in the Brahmaputra basin is likely due to its cooler air temperature, higher elevation, and less vegetated area. The basin-average normalized difference vegetation index (NDVI) in the Brahmaputra is 0.38, whereas those of the Ganges and Meghna are 0.41 and 0.65, respectively (NEO, 2014). However, the patterns of seasonal ET variability in the Brahmaputra and Meghna are quite similar, except there is a drop in July in the Brahmaputra (Figure 3-4 m-o). ET is relatively stable from May to October in the Brahmaputra and Meghna in contrast to that in the Ganges, where ET does not reach its

peak until September. Finally, both the pattern and magnitude of seasonal soil moisture variations are rather different among the three basins (Figure 3-4 p-r). However, the peak of soil moisture occurs consistently in August in all three basins.

Figure 3-4 d-f present the 22-year mean seasonal cycle of basin-average air temperature (T_{air}). The Brahmaputra is much cooler (mean temperature 9.1°C) than the Ganges (21.7°C) and Meghna (23.0°C). Figure 3-4 (g-i) plots the mean seasonal cycle of net radiation averaged over three basins. The seasonal pattern of net radiation is similar, but the magnitudes differ significantly among the three basins: The average net radiation is ~ 31 , 74 , and 84 W m^{-2} in the Brahmaputra, Ganges, and Meghna, respectively, whereas the maximum (monthly average) net radiation is $\sim 47,100$ and 117 W m^{-2} , respectively, in these three basins (Table 3-5).

3.2.2 *Correlation between meteorological and hydrological variables*

Figure 3-5 presents the scatter plots and correlation coefficients between monthly meteorological and hydrological variables in three river basins. The three different colors represent three different seasons: dry/winter (November–March), pre-monsoon (April–June), and monsoon (July–October). From this plot, the following summary can be drawn. Total runoff and surface runoff of the Brahmaputra have a stronger correlation ($cc = 0.95$ and 0.97 ; both are statistically significant at $p < 0.05$) with precipitation than in the other two basins. However, subsurface runoff in the Brahmaputra has a weaker correlation ($cc = 0.62$, $p < 0.05$) with precipitation than that in the Ganges ($cc = 0.75$, $p < 0.05$) and Meghna ($cc = 0.77$, $p < 0.05$). These relationships imply that the deeper soil depths enhance the correlation between subsurface runoff and precipitation. The deeper root-zone soil depth (calibrated $d = 5\text{m}$)

in the Meghna generates more subsurface runoff (69% of total runoff) than in the other two basins. Soil moisture in the Meghna also shows a stronger correlation ($cc = 0.87$, $p < 0.05$) with precipitation than that in the Brahmaputra ($cc = 0.77$, $p < 0.05$), and Ganges ($cc = 0.82$, $p < 0.05$).

The relationships of evapotranspiration with various atmospheric variables (radiation, air temperature) and soil water availability are rather complex (Shaaban et al., 2011). Different methods for estimating potential evapotranspiration (PET) in different hydrological models may also be a source of uncertainty (Thompson et al., 2014). However, the ET scheme in the H08 model uses the bulk formula, in which the bulk transfer coefficient is used to calculate turbulent heat fluxes (Haddeland et al., 2011). In estimating PET (and hence ET), H08 uses humidity, air temperature, wind speed, and net radiation. Figure 3-5 presents the correlation of ET with different meteorological variables in three basins. The ET in the Brahmaputra has a significant correlation with precipitation, air temperature, specific humidity, and net radiation, with the correlation coefficients ranging from 0.70 to 0.89 (all of which are statistically significant at $p < 0.05$). The correlation of ET in the Meghna with the meteorological variables is also relatively strong (cc ranging from 0.61 to 0.80, $p < 0.05$) except for the net radiation ($cc = 0.44$, $p < 0.05$). However, ET in the Ganges has a weak correlation with the meteorological variables (cc from 0.29 to 0.59, $p < 0.05$). A weaker correlation of ET with the meteorological variables is likely attributable to overestimation of the actual ET in the Ganges because the upstream water use (which is larger in the Ganges) may be incorrectly estimated as ET by the H08 model to ensure water balance.

3.2.3 *Interannual variability*

Figure 3-6 presents the interannual variability of meteorological and hydrologic variables from simulations driven by using five different GCMs and that of the multi-model mean (shown by the thick blue line) for three basins. It can be seen from the figure that the magnitude of interannual variations of variables corresponding to individual GCMs is noticeably larger than that of the multi-model mean. However, the long-term trends in the meteorological and hydrologic variables of the multi-model mean are generally similar to those of each GCM. Figure 3-6 (a1-a3) shows that the long-term trend in precipitation is not pronounced in the Brahmaputra and Meghna, but its interannual variability is rather large for each GCM. Among the five GCMs used, the precipitation of MRI-AGCM3 has the largest interannual variability (particularly in the Ganges and Meghna basin). A clear increasing trend in air temperature can be observed for all three basins. As there is a strong correlation between precipitation and runoff (Figure 3-5), their interannual variabilities are similar. There is no clear trend for ET in each basin from the present to the near-future period. However, in the far future, a notable increasing trend is observed for all of the basins (Figure 3-6 e1-e3). Figure 3-6 (f1-f3) plots the interannual variability of soil moisture. Since there are no clear trends (from the present to the near-future period) identified for precipitation and evapotranspiration, the effect of climate change on soil moisture is not pronounced.

3.3 Impact of Climate Change on Climatic and Hydrologic Quantities: Projected Mean Changes

The long-term average seasonal cycles of hydro-meteorological variables in the two projected periods (2015–2039 and 2075–2099) were compared with those of the

base period (1979–2003). All the results presented here are from the multi-model mean of all simulations driven by the climate forcing data from the five GCMs for both base and future periods. The solid lines in Figure 3-3 represent the 25-year monthly means, and the dashed lines represent the upper and lower bounds of the uncertainty bands as determined from the 10 simulations using the 10 best performance parameter sets (identified by ranking the Nash–Sutcliffe efficiency). Figure 3-7 plots the corresponding percentage changes, and Table 3-6 summarizes these relative changes in the hydro-meteorological variables over three basins on an annual and 6-month (dry season and wet season) basis.

3.3.1 Precipitation

Considering the high-emission scenario, by the end of the 21st century, long-term mean precipitation is projected to increase by 16.3%, 19.8%, and 29.6% in the Brahmaputra, Ganges, and Meghna basins, respectively (Table 3-6), in agreement with previous studies that compared GCM simulation results over these regions. For example, Immerzeel (2008) estimated the increase of precipitation in the Brahmaputra basin to be 22% and 14% under the SRES A2 and B2 scenarios, respectively. Endo et al. (2012) considered the SRES A1B scenario and estimated the country-wise increase in precipitation as 19.7% and 13% for Bangladesh and India, respectively. Based on the present study, for the Brahmaputra and Meghna basins the change of precipitation in the dry season (November–April) is expected to be 23% and 33.6%, respectively, both of which are larger than the change in the wet season (May–October) (Brahmaputra: 15.1%, Meghna: 29%; Figure 3-7 b-c). However, the change of precipitation in the dry season in the Ganges (3.6%) is lower than that in the wet season (21.5%).

3.3.2 Air temperature

The GBM basin will be warmer by about 1°C in the near future (Brahmaputra: 1.2°C, Ganges: 1.0°C, Meghna: 0.7°C) and by about 4.3°C in the far future (Brahmaputra: 4.8°C, Ganges: 4.1°C, Meghna: 3.8°C; Table 3-6). According to the projected changes, the cooler Brahmaputra basin will be significantly warmer, with the maximum increase up to 5.9°C in February (Figure 3-7 d). In Immerzeel (2008), the increase of air temperature in the Brahmaputra is projected (under the SRES A2 and B2 scenarios) to be about 2.3°C–3.5°C by the end of the 21st century. However, the rate of increase over the year is not uniform for all of these basins. Temperature will increase more in winter than in summer (Figure 3-7 d-f). Therefore, a shorter winter and an extended spring can be expected in the future of the GBM basin, which may significantly affect the crop growing season as well.

3.3.3 Net radiation

Net radiation is projected to be increased by >4% for all the seasons except summer in the entire GBM basin by the end of the century (Figure 9g-i). Due to the increase in the future air temperature, the downward long-wave radiation would increase accordingly and lead to an increase in net radiation. However, the change of net radiation in the far-future period is larger in the dry season (Brahmaputra: 10.3%, Ganges: 5.3%, Meghna: 6.5%) than in the wet season (Brahmaputra: 3.1%, Ganges: 3.4%, Meghna: 3%). For the near-future period, net radiation is projected to decrease by <1% through almost all seasons due to the smaller increase in air temperature (~1°C) as well as decreased incoming solar radiation (not shown) in this basin.

3.3.4 *Runoff*

Long-term mean runoff is projected to be increased by 16.2%, 33.1%, and 39.7% in the Brahmaputra, Ganges, and Meghna, respectively, by the end of the century (Table 3-6). The percentage increase of runoff in the Brahmaputra will be quite large in May (about 36.5%), which may be due to the increase of precipitation as well as decrease of evapotranspiration caused by lower net radiation (Figure 3-7 g, m). In response to seasonally varying degrees of changes in air temperature, net radiation, and evaporation, the changes of runoff in the wet season (May–October; Brahmaputra: 20.3%, Ganges: 36.3%, Meghna: 41.8%) are larger than that in the dry season (November–April; Brahmaputra: 2.9%, Ganges: -2.3%, Meghna: 24.2%; Figure 3-7 j-k). Runoff in the Meghna shows a larger response to precipitation increase, which could lead to a higher possibility of floods in this basin and prolonged flooding conditions in Bangladesh. These findings are in general consistent with previous findings. Mirza (2002) reported that the probability of occurrence of 20-year floods is expected to be higher in the Brahmaputra and Meghna Rivers than in the Ganges River. However, Mirza et al. (2003) found that the future change in the peak discharge of the Ganges River (as well as the Meghna River) is expected to be larger than that of the Brahmaputra River.

3.3.5 *Evapotranspiration*

It can be seen from Figure 3-7 m-o that the change of ET in the near future is relatively low, but it increases to be quite large by the end of the century (Brahmaputra: 16.4%, Ganges: 13.6%, Meghna: 12.9%). This is due to the increase of net radiation (Brahmaputra: 5.6%, Ganges: 4.1%, Meghna: 4.4%) as well as the higher air

temperature. Following the seasonal patterns of radiation (Figure 3-7 g-i) and air temperature (Figure 3-7 d-f), the change of ET is expected to be considerably larger in the dry season (November–April; Brahmaputra: 25.6%, Ganges: 19.3%, Meghna: 18.2%) than that in the wet season (May–October) (Brahmaputra: 12.9%, Ganges: 10.9%, Meghna: 10.5%).

3.3.6 *Soil moisture*

Soil moisture is expressed in terms of the water depth per unit area within the spatially varying soil depths (3~5 m). The change of soil moisture (ranges from 1.5 ~ 6.9% in the far future) is lower compared to other hydrological quantities, except for the Meghna in April, where the soil moisture is projected to increase by 22%. However, the associated uncertainties through all seasons are relatively high compared to other variables (figure 3-3 f1-f3). Varying initial conditions of soil depth d among 10 simulations might be one of the major reasons of higher uncertainty in estimation of soil moisture, particularly for the Brahmaputra (CV = 31%) and Ganges (CV = 18%) where d 's are 2~4m and 3~5m, respectively (Table 3-1).

4. Analysis of the Impact of Climate Change on Manageability of Hydrological Extremes

4.1 Introduction

This chapter investigates the impact of climate change on the manageability of floods and drought in the three GBM basins. The degree of difficulty of managing hydrological extremes is measured in terms of the difficulty of managing hydrological variations that can be identified from the FDC and DDC. In this section, FDCs and DDCs are plotted for basin averaged precipitation and streamflow at three outlets of those basins for three time periods: the period observed (1980–2009), the near future (2015–2039), and the far future (2075–2099). The future precipitation time series were taken from MRI-AGCM3.2S with the A1B scenario, and the future streamflow time series were taken from the output of hydrological model H08, which was driven using the same GCM. The aims of this chapter are (a) to investigate and compare the hydrological persistence characteristics of floods and droughts in those basins for the present day as well as for the future using those duration curves, (b) to investigate and compare the impact of climate change on the hydrological characteristics that can be identified from the duration curves, and (c) to investigate and compare the degree of difficulty in managing the floods and droughts in terms of the manageability of hydrological variations.

It is necessary to note that if the duration curves are drawn in the normalized scale relative to the long-term mean, the interpretations of the shape of curves should also be made relative to their long-term mean rather than to their real values. The term “manageability” of hydrological variations indicates in this FDC and DDC concepts the

expected amount of storage necessary to smooth out the hydrological variation of floods and droughts, which can be expressed as the area of the largest rectangle that fits in the area surrounded by the duration curve, the horizontal line of the long-term mean streamflow, and the vertical axis from the origin. A detailed explanation of the drought case was given by Kikkawa and Takeuchi (1975a), who identified that the impacts of climate change on the characteristics of the duration curves can be correlated with the changes in the degree of difficulty of managing the extreme hydrological events.

4.2 Persistence Characteristics of Precipitation

The focus of this section is the impacts of climate change on the FDCs and DDCs. Figure 4-1 presents the impacts of climate change in the present, near-future, and future periods (10-year recurrence interval) on the duration curves of the three basins. The following changes in the duration curves due to climate change can be pointed out from these figures:

- As seen in Figure 4-1, the FDCs of the three periods are similar for all three basins, whereas their DDCs of future periods are different from those of the observed period except for the Meghna basin. The FDCs and DDCs of the Meghna are nearly identical for the three periods, which indicates the persistence characteristics of precipitation over the Meghna will not be much affected by climate change, although mean precipitation is projected to increase in the future (Table 4-1).
- The departures of DDCs of the Brahmaputra and the Ganges are lower for the future periods than for the observed period, which indicates the probable lower seasonal variation of low precipitation (relative to its long-term mean) in the

future in those basins. Accordingly, the probability of extreme drought occurrence in those basins is expected to be reduced in the future, which might be due to a projected increase of precipitation in the dry season (Caesar et al., 2015; Masood et al., 2014).

- The gradients of the DDCs of the Brahmaputra are milder for future periods than for the observed period, which makes a narrower open angle between the FDC and the DDC. A milder gradient implies that the extreme events in that basin will be milder in severity in the future (relative to its increased long-term mean), but the recovery to the long-term mean from that extreme event will take a similar period.
- As seen in Figure 4-2, among the three basins, the probabilistic variations (the variation due to recurrence intervals) in the DDCs of the Ganges are the largest and in the FDCs are the smallest for all three periods. That means, the interannual variation of low precipitation is higher and variation of high precipitation is lower in the Ganges basin than in the other two basins.
- The Meghna has larger probabilistic variation in the FDC, which refers to the larger annual variation of high precipitation in the basin. This characteristic is also expected to exist in the future. The Meghna's annual CV of precipitation is also the largest among the three basins (Table 4-1), which is closely connected to the probabilistic variation.
- Probabilistic variation in the DDCs of the Brahmaputra is expected to be reduced in the far future. This implies that the annual variation of low precipitation in that basin will be reduced.

4.3 Persistence Characteristics of Streamflow

Figures 4-3 and 4-4 show the FDCs and DDCs of the daily streamflow series. Compared to the duration curves of precipitation, those of streamflow are quite different, especially the DDCs. For all m , the departure of DDC curves from the average line is smaller for streamflow than for precipitation. This is due to having natural storage of water in rivers, ponds, and underground, which reduces the seasonal variation of streamflow. Some of the significant changes in the duration curves of streamflow due to climate change are identified as follows:

- As seen in Figure 4-3, for the Brahmaputra the departure of future FDCs is lesser than that of the observed period, which indicates the intensities of seasonal variation of future high streamflow are expected to be reduced. For the Ganges and the Meghna, the larger departure of future FDCs indicates probable higher seasonal variation of future high streamflow in those rivers. On the other hand, for all three basins, the departures of DDCs are the lowest in the near-future period, which indicates the probable lower seasonal variation of low streamflow. It is important to note that the characteristics of low flow in the Meghna River are expected to change much in the future. As seen in Figure 4-3, short-term extreme low flow that could cause drought is expected to be eliminated from the Meghna basin.
- The open angle between the FDC and DDC is the smallest in the near future for the Brahmaputra. The narrow open angle implies that the speed of recovery of the extreme event to the long-term average in that basin will slow. For the Ganges and the Meghna, however, the open angles are larger in the future than in

the observed period, which indicates that the recovery rate from extreme events will be high in the future in those basins. Note that the high or low recovery rate does not signify and is independent of a quicker or slower recovery, as the recovery time itself depends on the severity of the extreme situation at the start of recovery.

- Figure 4-4 shows that for the observed period, probabilistic variations (variation due to recurrence interval) of the FDCs are small and almost similar; however, those of the DDCs are quite different among the three basins. The Ganges has the largest variation, whereas the Brahmaputra has the smallest variation. However, in the far future, probabilistic variations of both the FDCs and the DDCs of the Meghna are the highest among the three basins. This implies that the annual variations in streamflow of the Meghna are expected to be the largest in the far future.

4.4 Manageability of Hydrological Extremes and Interbasin Comparisons

Figure 4-2 and Figure 4-4 present the duration curves of basin-averaged precipitation over the three basins and streamflow at their outlets, respectively, for the three periods. All subplots in the same figure are shown on the same scale, and therefore every pair can be directly compared with the others. The following distinct characteristics of the duration curves can be identified from these figures:

- As seen in Figure 4-2, for precipitation the FDCs are quite similar, whereas the DDCs are very different from each other. This implies that the characteristics of low precipitation in these three basins are different. However, this distinction is expected to be more prominent in the future.

- From the duration curves of streamflow (Figure 4-4), it is observed that following a similar pattern of duration curves of precipitation, the Ganges has the highest departure of FDC and the Meghna has the highest departure of DDC from the average line. This would indicate that among the three basins, seasonal variation of high flow and low flow is the highest in the Ganges and the Meghna, respectively, for all three periods. Again, this statement is relative to their long-term means and not their absolute values. In the future, the FDCs and DDCs of the Brahmaputra have the lowest departure from the average line, which means seasonal streamflow variation is expected to be the lowest in that basin among these three basins. This is because the relative difference between the projected runoff increment in the wet season and that in the dry season is the lowest in the Brahmaputra among the three basins (Masood et al., 2015). The Brahmaputra's CVs of monthly values of streamflow (ranging from 0.67 to 0.74) are also the smallest among the three basins (Table 4-1), which is closely connected to the seasonal variation.
- A large departure means a large amount of reservoir storage is necessary to adjust the seasonal variation (Takeuchi, 1988). As seen in Figure 4-4, the departures of the DDCs of the Ganges and the Meghna are much larger than that of the Brahmaputra, which means to manage drought in the Ganges and the Meghna, larger reservoir storage is necessary relative to its basin size.
- For all three periods, the Ganges has the steepest gradient of curves, which makes the highest open angle between the FDC and the DDC (Figure 4-2 and 4-4). The steep gradient of the Ganges implies that the extreme events in the basin have a high recovery rate once it starts to recover from that extreme event. On the other

hand, the Brahmaputra has the smallest departure and the smallest open angle, which means the magnitude of extreme events of the basin is smaller and the rate of recovery is lower than those of the other basins.

Some basic statistics regarding the data used in this analysis are listed in Table 4-1. Among the basic properties, the coefficient of variation of monthly values seems most closely connected to the angle between FDC and DDC (Takeuchi, 1988). The Ganges's CVs are the largest, and the Brahmaputra's CVs are the lowest. This order is exactly the same as the order of angles in Figures 4-2 and 4-4. As for probabilistic variation, the coefficient of variation of annual values has the closest relation (Takeuchi, 1988). The smallest variation is seen in the Brahmaputra's, which has the lowest CVs.

The degree of difficulty of managing hydrological extremes depends on hydrological characteristics such as annual variation, seasonal variation, and severity (intensity and duration) of extreme events. Therefore, the impact of climate change on the manageability of floods and droughts in these three basins can be investigated and compared by observing changes in the hydrological variations that can be easily identified from the duration curves. According to the findings from the duration curves of streamflow, three study basins are ranked, as presented in Table 4-2. It is observed that the manageability of the Meghna basin is expected to be more difficult than that of other two basins due to increases of seasonal and annual variations of streamflow in the future. However, the severity of extreme events will be larger in the Ganges.

5. Analysis of the Impact of Climate Change on the Meghna Basin

5.1 Introduction

According to the earlier discussion, the impact of climate change is expected to be stronger on the hydro-meteorology of the Meghna (Figure 5-1) than those of the Brahmaputra and the Ganges, which has also been reported in previous literature (Masood et al., 2015; Mirza et al., 2003). A study by Kamal et al. (2013) found that the peak flow of the Lower Meghna River (at the confluence of the three major rivers, the Ganges, Brahmaputra, and Upper Meghna) may increase up to 39.1% during the monsoon, and the low flows may decrease up to 26.9% in the dry season at the end of this century. Mirza et al. (2003) identified that the Meghna river will play a major role in the future flooding in Bangladesh. The Meghna Basin is also very important to Bangladesh in many aspects. First, while the Ganges and the Brahmaputra occupy 59% of Bangladesh territory, only 4.8% of the catchments belong to Bangladesh. In the case of the Meghna, it occupies 24% of the territory, but 43% of catchment belongs to Bangladesh (FAO-AQUASTAT, 2014). This implies that the Meghna Basin can be intensively managed by Bangladesh itself. Second, the area under Bangladesh supports the country's economy as a rice production base during the dry season and as a fishing ground filled with ample fish during the rainy season. In the last two decades, the area has developed remarkably in terms of crop production growth (Quddus, 2009). The contribution of this area is above 16% of the country's total rice production. Third, abundant precipitation in the Meghna Basin has remarkable consequences for flash floods in the northeastern region of Bangladesh (Mirza, 2003). Agriculture in that area has frequently suffered from flash floods. Fourth, the duration of flooding in the basin is

exceptionally prolonged (Mirza, 2003). Because the flood discharge from the Meghna river is usually obstructed either by the combined flow of the Ganges and the Brahmaputra (Mirza et al., 2003) or by back-water effects caused by its tidal effect (Chowdhury & Ward, 2004). During the severe flood in 1998, river water stayed above the danger level for 68 days at Bhairab Bazar station, which was significantly higher than for the other two rivers, the Ganges and the Brahmaputra (Mirza, 2003). All those major aspects imply that if the climate change impacts are to be analyzed, the fine spatiotemporal analyses of the basin are necessary to assess local impacts such as on agriculture and floods. Therefore, this chapter analyzes the impacts of climate change on the spatiotemporal characteristics of the Meghna Basin hydro-meteorology by the high-resolution MRI-AGCM projection with the A1B scenario (Mizuta et al., 2012).

5.2 About the Meghna Basin

Major statistics of the Meghna Basin are summarized in Table 5-1. The Meghna River originates in Manipur in India as the Barak and divides into two branches after entering Bangladesh. The northern branch, called the Surma, flows southwards through the eastern side of Bangladesh next to Sylhet town, and the southern branch, called the Kushiara flows through India and then enters Bangladesh. First the Surma joins the Meghna River near Kuliar Char, and then the Kushiara joins the Meghna River near Ajmiriganj. The Surma, Kushiara, Bhogaikangsha, and numerous other rivers contribute to the Upper Meghna at Bhariab Bazar (Figure 5-1). The Upper Meghna and the Padma (joint flow of the Ganges and the Brahmaputra) join as the Lower Meghna, which ultimately flows into the Bay of Bengal. The Lower Meghna River is one of the

largest rivers in the world, being the mouth of three great rivers, the Ganges, Brahmaputra, and Meghna. The total drainage area of the Meghna Basin is about 65,000 km² (Nishat & Faisal, 2000) considering the outlet at Bhairab Bazar, which is shared by India (67% of the total catchment area) and Bangladesh (33%). The world's top two wettest places, Mawsynram and Cherrapunji in Meghalaya state, India, with annual precipitation of 11,871 and 11,777 mm, respectively, are located in this basin (Parry, 2013). The warm, moist winds coming from the Bay of Bengal during the monsoon are forced to suddenly rise to 1,400 m and converge into the narrower zone over the Khasi Hills, thus concentrating their moisture and causing heavy precipitation over the region. The basin's average annual precipitation is about 3,212 mm year⁻¹ concentrated in the monsoon months May to September (>80% of the annual precipitation). Elevations of the basin range from -1 to 2,579 m a.s.l. (Lehner et al., 2006). However, the average elevation of the basin is 307 m a.s.l., and 75% of the area has an elevation of less than 500 m a.s.l. The mountainous region mostly falls in India, whereas the flat and low-lying areas belong to Bangladesh (Figure 5-2a). Forest covers about 54% of the area of the basin, mostly located in the Indian part, and about 27% of the area is used for agriculture, mostly in Bangladesh (Figure 5-2b; Tateishi et al., 2014). The major crop of this area is Boro rice, a dry season variety of rice planted in lower fields (Haruhisa et al., 2005). Annual production of Boro rice from this area is above 3 million metric tons, which is about 17% of the country's total production. The contribution in production of local Boro rice (a local variety of Boro rice) is about three quarters of total production (estimated from BBS, 2011). However, this crop frequently suffers during the start of the rainy season from flash floods caused by river water flowing into the Meghna River from the mountainous regions in India.

5.3 Variability of Precipitation

5.3.1 Spatial variation of precipitation

The spatial distribution of mean annual precipitation over 25-year time periods and changes across the catchment are presented in Figure 5-3. Approximately one quarter of the basin in the north experiences above the mean annual precipitation (3,211 mm year⁻¹) during the base period (1979–2003). The spatial distribution of projected mean annual precipitation for the near future indicates further expansion of higher-precipitation areas, resulting in a contraction of low-precipitation areas (Figure 5-3b). Also, the amount of annual precipitation in much higher-precipitation areas (7,000 mm and above) is increased. The distribution of projected precipitation for the far future is similar to that of the near future, but the magnitudes are quite high in the far-future periods. The area with precipitation ranging from 3,001 to 4,000 mm year⁻¹ is expected to expand from 27% (in the base period) to 29% and 33% in the near future and the far future, respectively (Table 5-2). The area with higher precipitation (7,000 mm and above) increases from 1.9% (in the base period) to 5.6% and 6.7% in the near future and the far future, respectively.

Figure 5-3d and e show the percentage change of mean annual precipitation in the future compared to the base period. The projected maximum increment of mean annual precipitation is up to 23% and 31% in the near future and the far future, respectively (Figure 5-3d and e). However, the mean annual precipitation is projected to decrease by up to 3% during the near future in about one quarter of the area (22.5%) of the basin located in the southeast region. In general, a high precipitation increment will happen in higher-precipitation areas, while a low precipitation increment will happen in

low-precipitation areas. The increment of precipitation shows a gradual increase from the southeast corner to the northwest end of the basin (Figure 5-3d and e). Above 20% of the precipitation increment will be experienced in an area equal to 7.6% of the basin in the far future.

5.3.2 Temporal variation of precipitation

The probabilities of exceedance of monthly precipitation for the base period and projected periods at the two gauging stations of the basin are presented in Figure 5-4. The figure also presents variations of precipitation of different magnitude from the corresponding contributing basin at the gauging stations over time. Here, high precipitation refers to precipitation that has a percentage of monthly precipitation exceedance (PME) of 0–25, while medium precipitation has a PME of 26–75 and low precipitation has a PME of 76–100 (Figure 5-4). Across the basin, high, medium, and low precipitation varied differently in magnitude, following a pattern of change. In general, a greater increment of precipitation is observed for higher precipitation with an increasing magnitude of increment from PME of about 25 upwards.

During the near future, compared to the base period, all monthly precipitation, including low monthly precipitation, is projected to increase across the basin with various magnitudes. The gap between monthly precipitation of the base period and projected monthly precipitation widens medium to high precipitation. Medium-range monthly precipitation (which usually occurs during pre- or post-monsoon months) in the far future is quite higher than that of the near future, especially at Bhairab Bazar. Very low monthly precipitation (PME of 85% and above) is projected to be same in the near future and the far future.

5.4 Variability of Runoff

5.4.1 Spatial variation of runoff

The spatial distribution of mean annual runoff over a 25-year timescale for the observed and projected periods is presented in Figure 5-5. The figure also shows the percentage change of mean annual runoff for the projected periods with respect to the base period. In general, like precipitation, runoff varied across the basin from southeast to northwest as low (700 mm) to high (8,200 mm). The projected runoff increment pattern is also similar to that of the precipitation increment pattern. During the near future, the runoff increment is projected up to 34% across the basin compared to the base period (Figure 5-5d). For the far future, the runoff increment is projected up to 39% (Figure 5-5e). The area with runoff ranging from 3,001 to 4,000 mm year⁻¹ is expected to expand from 27% (in the base period) to 29% and 33% in the near future and the far future, respectively (Table 5-2). The area with higher runoff (above 6,000 mm) increases from 0.8% (in the base-period) to 2.4% and 2.6% in the near future and the far future, respectively. However, the mean annual runoff is projected to be decreased in low-precipitation areas near the southeast part of the basin in the near future and the far future by up to 6% and 1%, respectively (Figure 5-5d, e). Above 20% of the runoff increment will be experienced in 21.4% and 35% of the area of the basin in the near future and the far future, respectively (Table 5-3).

5.4.2 Temporal variation of runoff

The probability of exceedance of annual runoff for observed and projected periods at the two gauging stations is presented in Figure 5-6 for different time slices which also shows the temporal variability of runoff over the time periods. The basins'

average monthly runoffs (medium and low) at Bhairab Bazar for three different time slices are not prominently different. However, the high monthly runoffs of both the near future and the far future are significantly higher than that of the base period (Figure 5-6a). At Amalshid, all monthly runoffs (high, medium, and low) except extreme runoffs of the near future (PME of 1) are projected to remain similar to that of the base period. However, later this century (2075–2099), all monthly runoffs (high, medium, and low) are projected to rise significantly at Amalshid (Figure 5-6c). It is also observed that low runoffs are expected to increase in the future at both gauging stations (Figure 5-6b, d).

5.5 Effect of Climate Change on Discharge

The accumulated runoff from upstream grids comes downstream through the river channel in the form of river discharge; hence, the expected spatiotemporal changes of runoff obviously have an impact on the pattern of river discharge. Figure 5-7 summarizes the changes in monthly discharges at Bhairab Bazar station for three time slices. It is observed that changes in discharge of dry months (December–April) are not significant, while increments of discharges in wet months, especially in May–July, are quite high. The projected increase in the median value of monthly discharge during the near future (far future) is 44% (104%) in May, 38% (25%) in June, and 38% (26%) in July. However, in the peak flow period (June and July), discharges of the far future are projected to be lower than those of the near future.

Mean seasonal cycles of discharge at the basin outlet for the three time periods are shown in Figure 5-7 b. In general, monsoonal peak discharges have larger increments in both the near future and the far future, and the peaks are expected to come earlier than in the base period. For example, the peak of the near future (far future) is

expected to shift in mid-June (July), which is about 1.5 (1) month prior to that of the base period. In fact, the expected shifting of peaks ultimately leads to a higher possibility of earlier flash flooding in the future. Hence, the changes in monsoonal peak discharges in terms of magnitude and temporal shift are of greater concern for agriculture and flood management in the basin.

The Gumbel distribution (Gumbel, 1941), with parameters estimated by using the L-moment method, was selected to estimate trends in high flow frequencies because the Gumbel distribution has been recommended, for flood frequency analyses for the major rivers in Bangladesh (Mirza, 2002), and it is also suitable for a relatively smaller data sample (Hirabayashi et al., 2013). Figure 5-8 presents the non-exceedance probability plot of annual maxima series of discharges at Bhairab Bazar for different time slices. The figure shows a very strong increase in annual peak discharge in the future, which may have a severe impact for flooding in the basin. The 50-year discharge (probability of non-exceedance is 0.98) is projected to increase from about $28,000 \text{ m}^3 \text{ s}^{-1}$ at the base period to about $45,000 \text{ m}^3 \text{ s}^{-1}$ ($50,000 \text{ m}^3 \text{ s}^{-1}$) in the near future (far future), and a peak flow that currently occurs every 50 years will occur at least once every five years in the future. Such a high increase would require serious attention, although it is based on only one projection, MRI-AGCM3.2S.

5.6 Decadal Changes of Precipitation and Runoff

Decadal changes of precipitation and runoff are estimated to show evidence of the impact of climate change in the shorter term, and my aim is to develop a tool that would be useful for planning future water resources. Figure 5-9 presents the decadal mean of annual precipitation increment and corresponding runoff increment at the

Meghna basin's outlet for the projected periods, considering 1979–2003 as the base period. Each point represents a decadal change of runoff with respect to the decadal change of precipitation. A relatively strong relationship is observed between precipitation increments and corresponding runoff increments, though the relationship is not uniform over time. The trend lines cut the x-axis at about 3–4, which means that there would be no runoff increases for up to 3–4% of the precipitation increase. This excess water will be balanced by increasing evapotranspiration, as it is controlled by the availability of water. However, the ratio of the projected decadal increment of runoff to precipitation during the far future is 1.63, less than the ratio during the near future (2.32).

6. Conclusions and Policy Implications

6.1 Conclusions

In this study, most contemporary advanced technology has been successfully applied and climate change implications to water resources of Bangladesh are demonstrated. For detail hydro-meteorological analyses including climate change impact assessment, the use of fine resolution hydro-meteorological forcing data and well-calibrated distributed hydrological models are indispensable, which are successfully achieved in this study. The model has been calibrated at a relatively fine grid resolution (10 km) via analysing model parameter sensitivity and validated based on long-term (32 years) observed daily streamflow data. The impacts of climate change on hydrology of the GBM basins have been assessed by using 5 CMIP5 GCMs. In addition, the impacts of climate change on manageability of hydrological extremes (both floods and droughts) in terms of necessary storage to smooth out hydrological variations are assessed by using Flood Duration Curves (FDCs) and Drought Duration Curves (DDCs). Summarized research findings and conclusions are presented in the following three sub-sections.

6.1.1. *Hydrological modelling*

For this research a macro-scale distributed hydrological model H08 was chosen because of its (a) capability of long-term simulation using globally-available meteorological data, (b) accessibility, (c) performance, (d) widely acceptance in global climate change impact analyses and (e) parsimonious nature with having minimal parameters to be calibrated. To simulate at fine grid resolution (10 km) a new river map

has been created from fine-resolution (~0.5 km) DEM data. The model could efficiently simulate the historical time period with Nash-Sutcliff efficiency (NSE) ranging from 0.80 to 0.84. Other statistical indices also suggest that the model performance is overall satisfactory (Table 3-3). A series of sensitivity analysis of H08 parameters was conducted from which 10 sets of best performance parameters are determined by using the parameter-sampling simulation and these parameter sets are used to quantify the uncertainty in both historical and future simulations. It is observed that the uncertainty due to model parameters in runoff projection is lower than that of other hydrologic variables. The uncertainty in ET projection is also lower, which can be related to the narrower uncertainty band of net radiation. On the other hand, the projection of soil moisture is rather uncertain, partly due to uncertainty in parameter specification of soil depth in the model.

6.1.2. Climate change impact assessment

The future projection has been conducted by the model with the 10 best calibrated performance parameters forced by five CMIP5 GCMs through three time-slice experiments; the present-day (1979–2003), the near-future (2015-2039) and the far-future (2075–2099) periods. The average results of the 10 simulations have been used to investigate the climate change impacts on basin-scale hydrology. The following findings and conclusions were drawn from the model analysis:

- ✧ (a) All of the GBM basins are projected to be warmer by the range of 1–4.3°C in the near future and far future. Also, the cooler Brahmaputra basin will be warmer than the Ganges and Meghna. (b) Considering a high-emissions scenario, by the end of the 21st century, the long-term mean precipitation is projected to increase by

+16.3, +19.8, and +29.6%, and the long-term mean runoff is projected to increase by +16.2, +33.1, and +39.7% in the Brahmaputra, Ganges, and Meghna basins, respectively. (c) The change of ET in the near future is relatively low, but it increases and becomes quite large by the end of the century due to the increase in net radiation as well as the higher air temperature. (d) The change in soil moisture is lower compared to that of other hydrological quantities.

- ✧ Overall, it is observed that climate change impact on the hydrological processes of the Meghna basin is larger than that of the other two basins. For example, in the near future, runoff of the Meghna is projected to increase by 19.1%, whereas it is expected to increase by 6.7% and 11.3% for the Brahmaputra and Ganges, respectively. In the far future, a larger increase in precipitation (29.6%) and a lower increase in ET (12.9%) and consequently larger increase in runoff (39.7%) will lead to a higher possibility of floods in this basin.

As the Meghna basin has been identified as the most sensitive to climate change, further focus has been given to the basin to investigate the spatio-temporal changes in precipitation and runoff analyses under MRI-AGCM3.2S with the A1B scenario. The following findings and conclusions are drawn from this analysis:

- ✧ The spatial distribution of projected changes in precipitation and runoff shows that the expected changes are not uniform across the basin. The increment pattern shows a gradual increase from the southeast corner toward the northwest end of the basin. The maximum increment of mean annual precipitation (runoff) is up to 23% (34%) and 31% (39%) in the near future and the far future, respectively, with decreases in a few areas of the Southeast.

- ✧ The projected increment of the median value of monthly discharges at the basin outlet is significantly high in the wet period (May–July), ranging from 38–44% and 25–104% in the near-future and the far future, respectively. The probability plot of the annual maxima series of discharges also shows higher probability of the strong annual peak in the future, which may have the severe impact of flooding in the basin. Moreover, the monsoonal peaks are expected to come about 1~1.5 months earlier, which will ultimately lead to a higher possibility of earlier flash floods in the future.
- ✧ Although the highest impact in terms of a larger change of precipitation or runoff is on the northwestern part of the basin, the probable major affected area will be the northeastern part of Bangladesh (downstream of the basin) in terms of flood occurrence due to its lower ground elevation. The projected maximum percentage precipitation (runoff) increment in this region is 15% (30%) and 20% (30%) in the near future and the far future, respectively. Therefore, frequency and magnitudes of flash floods are most likely to increase in this area.

6.1.3. Duration curve analysis

The study plots FDCs and DDCs for basin-averaged monthly precipitation and daily streamflow at the outlets of the three basins for three time periods. This is done to investigate and compare climate change impact on the manageability of floods and droughts in terms of the persistence characteristics of hydrological variations from the long-term mean in these basins. Significant impacts on the characteristics of the duration curves have been identified, which can be correlated with the degree of

difficulty of managing these extreme hydrological events. The findings are summarized below:

- ✧ On the basin-averaged precipitation among the three basins, the probabilistic variation in the DDCs of the Ganges is the largest and in the FDCs is the smallest, indicating higher annual variation of low precipitation and lower annual variation of high precipitation in the Ganges basin. For the Meghna, FDCs with larger probabilistic variation refer to its larger annual variation of high precipitation, which is expected to exist in future periods as well. Similar to precipitation pattern, annual variations of both high and low streamflow of the Meghna are larger than those of the other two basins relative to their long-term means.
- ✧ Regarding streamflow, the Ganges and the Meghna have higher FDC-DDC departures and angles than does the Brahmaputra, which implies that relative to its long-term mean, the extreme events in these basins will be more severe, although the recovery rate from that extreme event will be high when the extreme situation begins to recover to normal. Meanwhile, the Brahmaputra has the smallest departure and a similar angle, which indicates a weak severity of extreme events and a similar recovery rate in the three basins. These significant characteristics are also expected to exist in future periods.
- ✧ On the ranking according to the degree of difficulty, it is observed that the manageability of the Meghna basin is expected to be lower than that of the other two basins due to increases in seasonal and annual variations of streamflow relative to its long-term mean in the future.

6.2 Policy Implications

This study presents detail hydro-meteorological analyses including climate change impact assessment aiming to acquire policy-relevant information necessary for climate change adaptation as well as for local water resources management in the GBM basins. The findings of this research have a number of policy level implications for the government, non-government and donor agencies, which can also be utilized in policy making for preparedness, prevention, mitigation of disaster risk.

Larger uncertainty in the estimation of soil moisture by the model can be significant in land use management and agriculture in particular. For the efficient use of the hydrological model result, priority should be put on soil moisture observation. This also emphasizes the significance of suitable parameterization of soil water physics in the model.

For efficient water resource development, a planner and policymaker can obtain useful information from a basin ranking on difficulty of manageability in terms of reservoir storage indicators. Basin rankings can be utilized for prioritization, and storage indicators can be used for concrete development and target adjustment. As the development of storage capacity is impossible or marginal in Bangladesh due to its limited resources and geographical location, more human adjustment would be necessary against increasing hydro-meteorological variability.

Although policymakers and water resource planners are interested in knowing about climate change impact on precipitation and runoff in the longer term, they are more interested in knowing about its impact in the shorter term. To meet these groups'

needs, decadal changes in precipitation and runoff are estimated and presented in Figure 5-9. This might be used as a tool for water resource planning because, from the plot, for a particular change in future precipitation, the likely change in future runoff can be calculated in the decadal time period. For example, in the near future, a 10% increment of mean annual precipitation (compared to the base period, 1979–2003) will result in an estimated 15% increment of runoff. As the amount of mean annual precipitation and runoff in the past is a known quantity, the corresponding quantity for any desired assumption can be calculated.

Compared with the Brahmaputra, the Ganges and the Meghna are more serious in the persistence of hydro-meteorological variability. The anticipated future shifting of the seasonal cycle of Meghna's flow will be significant for flood disaster managers and farmers. Flood disaster managers are most concerned about the timing of the peak and maximum probable flood levels, which need to be considered during the planning and designing of flood control measures. Therefore, the expected future changes in discharge imply that design flood level should be shifted to a higher level than the present one in order to design flood control structures in that region.

Climate change is expected to reduce the crop yield by crop failure due to increasing the frequency and severity of droughts and floods or by altering pest and disease outbreaks (Harvey et al., 2014). Particularly, in the low-lying area downstream of the Meghna, where farmers can cultivate one crop per year, if a flash flood comes earlier and damages the crops, the livelihoods of the farmers become unstable. *Boro* rice, the major crop of this area, is planted in January to February and harvested in April to May (Mirza et al., 1998). During this season, precipitation is scarce, and there might

occasionally be droughts, but *Boro* is grown under abundant sunshine and moderate temperature conditions (Haruhisa et al., 2005). However, this crop frequently suffers as a result of either a flash flood before harvesting or longer inundation during the cultivation period due to the late recession of the flood peak. Usually, the crops are saved from flash floods up to the harvesting period by submergible embankment, a type of earthen embankment that can protect from a flood up to certain level and then allows water to enter to submerge lower lands. The deadline of building or repairing the existing embankment is the end of April. Therefore, in the future, this target of completing the repair/building of the embankment needs to shift earlier in order to protect the crop from expected earlier flash floods. Alternately, the crop yield can be achieved by supplying high-yielding variety (HYV) crops to farmers. A recent study found that two varieties of winter rice with higher yields attained maturity by the end of the first week of April, when they have a high potential to avoid flash-flood risks (Anik & Khan, 2012). However, other alternative adaptive measures, such as agroforestry (Thorlakson & Neufeldt, 2012) and agricultural diversity (Reidsma & Ewert, 2008), suggested by many literatures can also be used to reduce their vulnerability to climate change. Within the field of interest of concern, each agency should formulate and implement policies for building capacity at a local level as well as for reducing the vulnerability and damage.

6.3 Recommendations for Future Studies

This study still has some limitations which can be addressed in future research.

(a) Results presented in the assessment of climate change impact on hydrology of the GBM basins are basin-averaged. The basin-averaged large scale changes and trends are

difficult to translate to regional and local scale impacts. Moreover, the changes in averages do not reflect the changes in variability and extremes. (b) Anthropogenic and industrial water use in upstream are important factors in altering hydrologic cycle, however, they were not considered in present study due to data constraints. (c) Urbanizing watersheds are characterized by rapid land use changes and associated landscape disturbances can shift the rainfall–runoff relationships away from natural processes. Hydrological changes in future can also be amplified by changing land uses. However, in this study future changes of demography and land uses were not considered.

References

- Abrams, P. (2003). River Ganges. Retrieved 13 July 2014, from <http://www.africanwater.org/ganges.htm>
- Anik, S. I., & Khan, M. A. S. A. (2012). Climate change adaptation through local knowledge in the north eastern region of Bangladesh. *Mitigation and Adaptation Strategies for Global Change*, 17(8), 879-896. doi: 10.1007/s11027-011-9350-6
- BBS. (2011). Estimates of Boro Rice, 2009-2010 (M. o. P. Agricultural Wing, Government of the People's Republic of Bangladesh, Trans.). Dhaka, Bangladesh: Bangladesh Bureau of Statistics, Agricultural Wing.
- BBS. (2014). Statistical Pocketbook of Bangladesh-2013 (M. o. P. Statistics and Informatics Division (SID), Government of the People's Republic of Bangladesh, Trans.). Dhaka, Bangladesh: Bangladesh Bureau of Statistics.
- Biemans, H., Speelman, L. H., Ludwig, F., Moors, E. J., Wiltshire, A. J., Kumar, P., . . . Kabat, P. (2013). Future water resources for food production in five South Asian river basins and potential for adaptation — A modeling study. *Science of The Total Environment*, 468–469, Supplement(0), S117-S131. doi: <http://dx.doi.org/10.1016/j.scitotenv.2013.05.092>
- BWDB. (2012). *Rivers of Bangladesh*. Dhaka: Bangladesh Water Development Board.
- Caesar, J., Janes, T., Lindsay, A., & Bhaskaran, B. (2015). Temperature and precipitation projections over Bangladesh and the upstream Ganges, Brahmaputra and Meghna systems. *Environmental Science: Processes & Impacts*. doi: 10.1039/C4EM00650J

- Carpenter, T. M., & Georgakakos, K. P. (2006). Intercomparison of lumped versus distributed hydrologic model ensemble simulations on operational forecast scales. *Journal of Hydrology*, 329(1–2), 174-185. doi: <http://dx.doi.org/10.1016/j.jhydrol.2006.02.013>
- Chowdhury, M. R. (2000). An Assessment of Flood Forecasting in Bangladesh: The Experience of the 1998 Flood. *Natural Hazards*(22), 139–163.
- Chowdhury, M. R., & Ward, M. N. (2004). Hydro-meteorological variability in the greater Ganges-Brahmaputra-Meghna basins. *International Journal of Climatology*, 24(12), 1495-1508. doi: 10.1002/joc.1076
- Chowdhury, M. R., & Ward, M. N. (2007). Seasonal flooding in Bangladesh – variability and predictability. *Hydrological Processes*, 21(3), 335-347. doi: 10.1002/hyp.6236
- Endo, H., Kitoh, A., Ose, T., Mizuta, R., & Kusunoki, S. (2012). Future changes and uncertainties in Asian precipitation simulated by multiphysics and multi–sea surface temperature ensemble experiments with high-resolution Meteorological Research Institute atmospheric general circulation models (MRI-AGCMs). *Journal of Geophysical Research*, 117(D16). doi: 10.1029/2012jd017874
- FAO-AQUASTAT. (2014). Ganges-Brahmaputra-Meghna river basin *Irrigation in Southern and Eastern Asia in figures –AQUASTAT Survey – 2011* (pp. 1).
- Gain, A. K., Immerzeel, W. W., Sperna Weiland, F. C., & Bierkens, M. F. P. (2011). Impact of climate change on the stream flow of the lower Brahmaputra: trends in high and low flows based on discharge-weighted ensemble modelling. *Hydrology and Earth System Sciences*, 15(5), 1537-1545. doi: 10.5194/hess-15-1537-2011

- Ghosh, S., & Dutta, S. (2012). Impact of climate change on flood characteristics in Brahmaputra basin using a macro-scale distributed hydrological model. *Journal of Earth System Science*, 121(3), 637-657. doi: 10.1007/s12040-012-0181-y
- Gumbel, E. J. (1941). The return period of flood flows. *The Annals of Mathematical Statistics*, 12, 163–190.
- Günter Blöschl, Murugesu Sivapalan, Thorsten Wagener, A., & Savenije, V. a. H. (2013). *Runoff Prediction in Ungauged Basins: Synthesis across Processes, Places and Scales* (Vol. Edited): CAMBRIDGE UNIVERSITY PRESS.
- Haddeland, I., Clark, D. B., Franssen, W., Ludwig, F., Voß, F., Arnell, N. W., . . . Yeh, P. (2011). Multimodel Estimate of the Global Terrestrial Water Balance: Setup and First Results. *Journal of Hydrometeorology*, 12(5), 869-884. doi: 10.1175/2011jhm1324.1
- Haddeland, I., Heinke, J., Voß, F., Eisner, S., Chen, C., Hagemann, S., & Ludwig, F. (2012). Effects of climate model radiation, humidity and wind estimates on hydrological simulations. *Hydrology and Earth System Sciences*, 16(2), 305-318. doi: 10.5194/hess-16-305-2012
- Hanasaki, N., Kanae, S., Oki, T., Masuda, K., Motoya, K., Shirakawa, N., . . . Tanaka, K. (2008). An integrated model for the assessment of global water resources – Part 1: Model description and input meteorological forcing. *Hydrol. Earth Syst. Sci.*(12), 1007–1025.
- Hanasaki, N., Saito, Y., Chaiyasaen, C., Champathong, A., Ekkawatpanit, C., Saphaokham, S., . . . Thongduang, J. (2014). A quasi-real-time hydrological simulation of the Chao Phraya River using meteorological data from the Thai

- Meteorological Department Automatic Weather Stations. *Hydrological Research Letters*, 8(1), 9-14. doi: 10.3178/hrl.8.9
- Haruhisa, A., Jun, M., & Rahman, R. (2005). Impact of Recent Severe Floods on Rice Production in Bangladesh. *Geographical Review of Japan*, 78(12), 783-793.
- Harvey, C. A., Rakotobe, Z. L., Rao, N. S., Dave, R., Razafimahatratra, H., Rabarijohn, R. H., . . . Mackinnon, J. L. (2014). Extreme vulnerability of smallholder farmers to agricultural risks and climate change in Madagascar. *Philos Trans R Soc Lond B Biol Sci*, 369(1639), 20130089. doi: 10.1098/rstb.2013.0089
- Hirabayashi, Y., Mahendran, R., Koirala, S., Konoshima, L., Yamazaki, D., Watanabe, S., . . . Kanae, S. (2013). Global flood risk under climate change. *Nature Climate Change*, 3(9), 816-821. doi: 10.1038/nclimate1911
- HydroSHEDS. (2014). Hydrological data and maps based on SHuttle Elevation Derivatives at multiple Scales. 2014, from <http://hydrosheds.cr.usgs.gov/hydro.php>
- Immerzeel, W. (2008). Historical trends and future predictions of climate variability in the Brahmaputra basin. *International Journal of Climatology*, 28(2), 243-254. doi: 10.1002/joc.1528
- Islam, A. S., Haque, A., & Bala, S. K. (2010). Hydrologic characteristics of floods in Ganges-Brahmaputra-Meghna (GBM) delta. *Natural Hazards*, 54, 797-811.
- IWM. (2006). Updating and Validation of North West Region Model (NWRM). Bangladesh: Institute of Water Modelling.
- Kamal-Heikman, S., Derry, L. A., Stedinger, J. R., & Duncan, C. C. (2007). A Simple Predictive Tool for Lower Brahmaputra River Basin Monsoon Flooding. *Earth Interactions*, 11(21), 1-11. doi: 10.1175/ei226.1

- Kamal, R., Matin, M. A., & Nasreen, S. (2013). Response of River Flow Regime to Various Climate Change Scenarios in Ganges-Brahmaputra- Meghna Basin. *Journal of Water Resources and Ocean Science*, 2(2), 15-24. doi: 10.11648/j.wros.20130202.12
- Kikkawa, H., & Takeuchi, K. (1975a). Characteristics of drought duration curve and its application. *Proc JSCE*, 234, 62-71.
- Kikkawa, H., & Takeuchi, K. (1975b). Use of statistical knowledge of drought for alleviating drought problems. *Proc. Second World Congr. IWRA, New Delhi*, 4, 197-203.
- Kwak, Y., Takeuchi, K., Fukami, K., & Magome, J. (2012). A new approach to flood risk assessment in Asia-Pacific region based on MRI-AGCM outputs. *Hydrological Research Letters*, 6, 70-75. doi: 10.3178/HRL.6.70
- Kyoshi, T., Shimoda, A., & Watanabe, K. (1993). A Study of Dam Control with DDC Rule Curve. *JHHE*, 37, 87-92.
- Lehner, B., Verdin, K., & Jarvis, A. (2006). HydroSHEDS technical documentation.
- Lespinas, F., Ludwig, W., & Heussner, S. (2014). Hydrological and climatic uncertainties associated with modeling the impact of climate change on water resources of small Mediterranean coastal rivers. *Journal of Hydrology*, 511, 403-422. doi: 10.1016/j.jhydrol.2014.01.033
- Lucas-Picher, P., Christensen, J. H., Saeed, F., Kumar, P., Asharaf, S., Ahrens, B., . . . Hagemann, S. (2011). Can Regional Climate Models Represent the Indian Monsoon? *Journal of Hydrometeorology*, 12(5), 849-868. doi: 10.1175/2011jhm1327.1

- Masood, M., Yeh, P. J. F., Hanasaki, N., & Takeuchi, K. (2014). Model study of the impacts of future climate change on the hydrology of Ganges–Brahmaputra–Meghna (GBM) basin. *Hydrol. Earth Syst. Sci. Discuss.*, *11*(6), 5747-5791. doi: 10.5194/hessd-11-5747-2014
- Masood, M., Yeh, P. J. F., Hanasaki, N., & Takeuchi, K. (2015). Model study of the impacts of future climate change on the hydrology of Ganges–Brahmaputra–Meghna basin. *Hydrology and Earth System Sciences*, *19*(2), 747-770. doi: 10.5194/hess-19-747-2015
- Matsuda, S. (1979). Study on Rainfall During Periods of Deficient Precipitation in Kochi Prefecture. *Transactions of The Japanese Society of Irrigation, Drainage and Reclamation Engineering*, *1979*(84), 29-35,a21. doi: 10.11408/jsidre1965.1979.84_29
- Mirza, M. M. Q. (2002). Global warming and changes in the probability of occurrence of floods in Bangladesh and implications. *Global Environmental Change*, *12*(12), 127–138.
- Mirza, M. M. Q. (2003). Three Recent Extreme Floods in Bangladesh: A Hydro-Meteorological Analysis. *Natural Hazards*, *28*(1), 35-64. doi: 10.1023/A:1021169731325
- Mirza, M. M. Q., & Ahmad, Q. K. (2005a). *Climate Change And Water Resources In South Asia*. Leiden, Netherlands: A. A. Balkema Publishers.
- Mirza, M. M. Q., & Ahmad, Q. K. (Eds.). (2005b). *Climate Change And Water Resources In South Asia*. Leiden, Netherlands: A. A. Balkema Publishers.

- Mirza, M. M. Q., Warrick, R. A., & Ericksen, N. J. (2003). The implications of climate change on floods of the Ganges, Brahmaputra and Meghna rivers in Bangladesh. *Climate Change*(57), 287-318.
- Mirza, M. M. Q., Warrick, R. A., Ericksen, N. J., & Kenny, G. J. (1998). Trends and persistence in precipitation in the Ganges, Brahmaputra and Meghna river basins. *Hydrological Sciences-Journal*, 43(6), 345-858.
- Mizuta, R., Yoshimura, H., Murakami, H., Matsueda, M., Endo, H., Ose, T., . . . Kitoh, A. (2012). Climate Simulations Using MRI-AGCM3.2 with 20-km Grid. *Journal of the Meteorological Society of Japan*, 90A(0), 233-258. doi: 10.2151/jmsj.2012-A12
- Moffitt, C. B., Hossain, F., Adler, R. F., Yilmaz, K. K., & Pierce, H. F. (2011). Validation of a TRMM-based global Flood Detection System in Bangladesh. *International Journal of Applied Earth Observation and Geoinformation*, 13(2), 165-177. doi: <http://dx.doi.org/10.1016/j.jag.2010.11.003>
- Nash, J. E., & Sutcliffe, J. V. (1970). River flow forecasting through conceptual models part I – a discussion of principles. *J. Hydrol.*, 10, 282–290.
- Nishat, A., & Faisal, I. M. (2000). An assessment of the Institutional Mechanism for Water Negotiations in the Ganges–Brahmaputra–Meghna system. *International Negotiations*(5), 289–310.
- Oki, T., & Sud, Y. C. (1998). Design of Total Runoff Integrating Pathways (TRIP)-A Global River Channel Network. *Earth Interactions*, 2.
- Parry, L. (2013). Think the weather bad's here? Spare a thought for these Indian villagers who live in the wettest place in the world with 40 FEET of rain a year. Retrieved 23 Jan 2015, from <http://www.dailymail.co.uk/news/article->

2471421/Indias-Mawsynram-villagers-live-wettest-place-world-40-FEET-rain-year.html

- Pokhrel, Y., Hanasaki, N., Koirala, S., Cho, J., Yeh, P. J. F., Kim, H., . . . Oki, T. (2012). Incorporating Anthropogenic Water Regulation Modules into a Land Surface Model. *Journal of Hydrometeorology*, 13(1), 255-269. doi: 10.1175/jhm-d-11-013.1
- Quddus, M. A. (2009). Crop production growth in different agro-ecological zones of Bangladesh. *J. Bangladesh Agril. Univ.*, 7(2), 351–360.
- Rahman, M. M., Ferdousi, N., Sato, Y., Kusunoki, S., & Kitoh, A. (2012). Rainfall and temperature scenario for Bangladesh using 20?km mesh AGCM. *International Journal of Climate Change Strategies and Management*, 4(1), 66-80. doi: 10.1108/17568691211200227
- Reidsma, P., & Ewert, F. (2008). Regional Farm Diversity Can Reduce Vulnerability of Food Production to Climate Change. *Ecology and Society*, 13(1)(38).
- Sevat, E., & Dezetter, A. (1991). Selection of calibration objective functions in the context of rainfall-runoff modeling in a Sudanese savannah area. *Hydrological Sci. J.*, 36(4), 307-330.
- Siderius, C., Biemans, H., Wiltshire, A., Rao, S., Franssen, W. H., Kumar, P., . . . Collins, D. N. (2013). Snowmelt contributions to discharge of the Ganges. *Sci Total Environ*, 468-469 Suppl, S93-S101. doi: 10.1016/j.scitotenv.2013.05.084
- Takeuchi, K. (1986). Chance-Constrained Model for Real-Time Reservoir Operation Using Drought Duration Curve. *Water Resources Research*, 22(4), 551-558.
- Takeuchi, K. (1988). Hydrological Persistence Characteristics of floods and droughts- International comparisons. *Journal of Hydrology*, 102, 49-67.

- Tateishi, R., Hoan, N. T., Kobayashi, T., Alsaadeh, B., Tana, G., & Phong, D. X. (2014). Production of Global Land Cover Data – GLCNMO2008. *Journal of Geography and Geology*, 6(3), 99-122. doi: 10.5539/jgg.v6n3p99
- Thorlakson, T., & Neufeldt, H. (2012). Reducing subsistence farmers' vulnerability to climate change: evaluating the potential contributions of agroforestry in western Kenya. *Agriculture & Food Security*, 1(1), 15.
- Tripp, D. R., & Niemann, J. D. (2008). Evaluating the parameter identifiability and structural validity of a probability-distributed model for soil moisture. *Journal of Hydrology*(353), 93-108. doi: 10.1016/j.jhydrol.2008.01.028
- Vogel, R. M., & Fennessey, N. M. (1995). Flow Duration Curves II: A Review of Applications In Water Resources Planning. *Water Resources Bulletin*, 31(6), 1029-1039.
- Wagner, T., McIntyre, N., Lees, M. J., Wheeler, H. S., & Gupta, H. V. (2003). Towards reduced uncertainty in conceptual rainfall-runoff modelling: dynamic identifiability analysis. *Hydrological Processes*, 17(2), 455-476. doi: 10.1002/hyp.1135
- Weedon, G. P., Gomes, S., Viterbo, P., Österle, H., Adam, J. C., Bellouin, N., . . . Best, M. (2010). The watch forcing data 1958-2001: A meteorological forcing dataset for land surface- and hydrological-models. (pp. 1-41).
- Weedon, G. P., Gomes, S., Viterbo, P., Shuttleworth, J., Blyth, E., Osterle, H., . . . Best, M. (2011). Creation of the WATCH Forcing Data and its use to assess global and regional reference crop evaporation over land during the twentieth century. *J. Hydrometeorol*, 12, 823–848. doi: 10.1175/2011JHM1369.1

Yatagai, A., Kamiguchi, K., Arakawa, O., Hamada, A., Yasutomi, N., & Kitoh, A. (2012). APHRODITE: Constructing a Long-Term Daily Gridded Precipitation Dataset for Asia Based on a Dense Network of Rain Gauges. *Bulletin of the American Meteorological Society*, 93(9), 1401-1415. doi: 10.1175/BAMS-D-11-00122.1

Table 1-1

Major Characteristics of the Ganges, Brahmaputra, and Meghna River Basin

Item		Brahmaputra	Ganges	Meghna
Basin area (km ²)		583,000 ^b	907,000 ^b	65,000 ^b
		530,000 ^{f,g}	1087,300 ^h	82,000 ^h
		543,400 ^h	1000,000 ^c	
River length (km)		1,800 ^b	2,000 ^b	946 ^b
		2,900 ^f	2,510 ^c	
		2 896 ^a	2 500 ^a	
Elevation (m a.s.l.) ^e	Range	8 ~ 7,057	3 ~ 8,454	-1 ~ 2,579
	Average	3,141	864	307
	Area below 500 m:	20%	72%	75%
	Area above 3000 m:	60%	11%	0%
Discharge (m ³ s ⁻¹)	Station	Bahadurabad	Hardinge bridge	Bhairab bazar
	Lowest	3,430 ^d	530 ^d	2 ^d
	Highest	102,535 ^d	70,868 ^d	19,900 ^d
	Average	20,000 ^g	11,300 ^d	4,600 ^d
Land use (% area) ⁱ	Agriculture	19%	68%	27%
	Forest	31%	11%	54%
Basin-averaged Normalized Difference Vegetation Index (NDVI) ^j		0.38	0.41	0.65
Total number of dams (both for hydropower and irrigation purpose) ^k		6	75	-

^a Moffitt et al. (2011)^b Nishat and Faisal (2000)^c Abrams (2003)^d BWDB (2012)

^e Estimated from SRTM DEM data by Lehner et al. (2006)

^f Gain et al. (2011)

^g Immerzeel (2008)

^h FAO-AQUASTAT (2014)

ⁱ Estimated from Tateishi et al. (2014)

^j Estimated from NEO (2014)

^k Lehner et al. (2008)

Table 2-1

Basic Input Data Used in This Study

Type	Description	Source/Reference(s)	Original spatial resolution	Period	Remarks
Physical Data	Digital Elevation Map (DEM)	HydroSHE DS ^a (HydroSHE DS, 2014)	15" (~0.5 km)	-	Global data
	Basin mask	HydroSHE DS ^a (HydroSHE DS, 2014)	30" (~1 km)	-	
Meteorological data	Rainfall, snowfall, surface pressure, air temperature, specific humidity, wind speed, long-wave downward radiation, shortwave downward radiation	WFD ^b (Weedon et al., 2010; Weedon et al., 2011)	0.5°	1980–2001	5' (~10 km-mesh) data has been prepared by linear interpolating for this study
	albedo	GSWP2 ^c	1°	1980–1990	Mean monthly 5' (~10 km-mesh) data has been prepared for this study
Hydrologic data	Water level, discharge	Bangladesh Water Development Board (BWDB)	Gauged	1980–2012	Water level (daily), discharge (weekly) data at outlets of three basins, i.e. the Ganges basin at Hardinge Bridge, the Brahmaputra

					basin at Bahadurabad, and the Meghna basin at Bhairab Bazar obtained from BWDB.
	Discharge	Global Runoff Data Centre (GRDC)	Gauged	1949–1973 (Farakka), 1975–1979 (Pandu), 1969–1992 (Teesta) with missing data	Discharge (monthly) data at Three upstream stations, i.e. at Farakka (Ganges), Pandu (Brahmaputra) and Teesta (Brahmaputra).
GCM data	Rainfall, snowfall, surface pressure, air temperature, specific humidity, wind speed, long-wave downward radiation, shortwave downward radiation	MRI-AGCM3.2S ^d	0.25° (~20 km-mesh)	1979–2003, 2015–2039, 2075–2099	Bias of precipitation dataset has been corrected by multiplying using monthly correction coefficient (ratio between basin averaged long term monthly mean precipitation from WFD and that from each GCM) for each GBM basins
		MIROC5	1.41×1.39°		
		MIROC-ESM	2.81×2.77°		
		MRI-CGCM3	1.125×1.11°		
		HadGEM2-ES	1.875×1.25°		

^aHydroSHEDS is hydrological data and maps based on shuttle elevation derivatives at multiple scales,

^bWFD is WATCH forcing data

^cGSWP2 is Second Global Soil Wetness Project

^dMRI-AGCM is Meteorological Research Institute-Atmospheric General Circulation Model

Table 3-1

Sensitive Parameters in the H08 Model and 10 Best Performance Parameter Combinations out of 625 Simulations

Basin	Parameter combinations	Soil Depth, d	Bulk transfer co-efficient, C_D	Runoff parameter, γ	Runoff parameter (time constant), τ
Brahmaputra	1	3	0.001	1	150
	2	3	0.001	1.5	150
	3	3	0.001	2	150
	4	2	0.001	1	150
	5	4	0.001	2	150
	6	4	0.001	2.5	150
	7	2	0.001	1	100
	8	3	0.002	1	150
	9	2	0.002	1	100
	10	4	0.001	1.5	150
Ganges	1	4	0.008	4	150
	2	5	0.008	4	150
	3	3	0.008	4	150
	4	4	0.008	2.5	150
	5	4	0.008	4	100
	6	5	0.004	4	150
	7	3	0.008	2.5	150
	8	4	0.008	2	150
	9	3	0.008	2	150
	10	3	0.008	4	100
Meghna	1	5	0.008	1	50
	2	5	0.008	1.5	50
	3	5	0.004	1	50
	4	5	0.003	1	50
	5	5	0.008	2	50
	6	5	0.004	1.5	50
	7	5	0.008	1	70
	8	5	0.002	1	50
	9	5	0.003	1.5	50
	10	5	0.008	2.5	50

Table 3-2

Basic Information of the Streamflow Validation Stations in the GBM Basin

Basin name	Brahmaputra			Ganges		Meghna
Station name	Bahadurabad	Pandu	Teesta	Hardinge bridge	Farakka	Bhairab bazar
Latitude	25.18° N	26.13° N	25.75° N	24.08° N	25° N	25.75° N
Longitude	89.67° E	91.7° E	89.5° E	89.03° E	87.92° E	89.5° E
Drainage area (km ²)	583,000	405,000	12,358	907,000	835,000	65,000
Available observed data period (with missing)	1980–2001	1975–1979	1969–1992	1980–2001	1949–1973	1980–2001

Table 3-3

Statistical Indices That Measure the Model Performance at Three GBM Basins during Both Calibration and Validation Period Considering Best Model Parameter Set

Statistical indices	Brahmaputra		Ganges		Meghna	
	Calibration	Validation	Calibration	Validation	Calibration	Validation
Nash–Sutcliffe efficiency (NSE)	0.84	0.78	0.80	0.77	0.84	0.86
Percent bias (PBIAS)	0.28%	6.59%	1.21%	2.23%	0.96%	3.15%
Root-Mean Square Error (RRMSE)	0.32	0.38	0.60	0.59	0.38	0.32
Correlation coefficient (cc)	0.93	0.89	0.91	0.89	0.93	0.94
Coefficient of determination (R^2)	0.86	0.79	0.82	0.79	0.86	0.88

Table 3-4

Statistical Indices (the Coefficient of Variation [CV] and Standard Deviation [SD]) of the Uncertainty in Model Simulations Due to the Uncertainty in Model Parameters

Variable	Period	Brahmaputra		Ganges		Meghna	
		Coefficient of variation (CV) of mean (Figure 3-3) (%)	Standard deviation (SD) of mean (Figure 3-3)	Coefficient of variation (CV) of mean (Figure 3-3) (%)	Standard deviation (SD) of mean (Figure 3-3)	Coefficient of variation (CV) of mean (Figure 3-3) (%)	Standard deviation (SD) of mean (Figure 3-3)
Net radiation	Present-day	8.6	5.4	2.0	2.0	2.1	2.4
	Near-future	8.6	5.4	1.9	1.9	2.1	2.3
	Far-future	8.4	5.6	1.8	1.8	2.0	2.4
Total runoff	Present-day	3.2	0.1	7.6	0.1	6.7	0.4
	Near-future	3.0	0.1	7.2	0.1	5.4	0.4
	Far-future	3.1	0.1	6.6	0.1	4.6	0.4
ET	Present-day	7.9	0.1	3.6	0.1	11.3	0.4
	Near-future	7.9	0.1	3.7	0.1	10.6	0.4
	Far-future	7.8	0.1	3.7	0.1	9.7	0.4
Soil moisture	Present-day	31.0	103.7	18.5	34.5	15.9	53.5
	Near-future	30.8	104.1	18.5	35.5	15.4	54.5
	Far-future	30.5	103.7	18.3	36.1	14.4	51.6

Table 3-5

The 22-Year (1980–2001) Averages of the Meteorological (from the WFD Forcing Data) and Hydrologic Variables in the GBM River Basins

	Unit	Brahmaputra	Ganges	Meghna
(a) Meteorological variables				
Precipitation (Prcp)	mm year ⁻¹	1,609	1,157	3,212
Temperature (Tair)	°C	9.1	21.7	23.0
Net radiation (Net rad)	W m ⁻²	31	74	84
Specific humidity	g/kg	9.3	11.8	14.4
(b) Hydrological variables				
Runoff	mm year ⁻¹	1,360	406	2,193
Evapotranspiration (ET)	mm year ⁻¹	251	748	1,000
Potential evapotranspiration (PET)	mm year ⁻¹	415	2,359	1,689

Table 3-6

The 10-Simulation Average of Annual Mean and Percentage Changes of Hydrological and Meteorological Variables

Variable	Period	Brahmaputra				Ganges				Meghna			
		annual mean	% change (Tair: °C)			annual mean	% change (Tair: °C)			annual mean	% change (Tair: °C)		
			dry season (November-April)	wet season (May-October)	annual		dry season (November-April)	wet season (May-October)	annual		dry season (November-April)	wet season (May-October)	annual
(a) Meteorological variables													
Precipitation (mm year ⁻¹)	Present day	1632	-	-	-	1154	-	-	-	3192	-	-	-
	Near future	1720	4.2	5.6	5.4	1218	-0.1	6.2	5.6	3598	11.4	12.9	12.7
	Far future	1897	23.0	15.1	16.3	1383	3.6	21.5	19.8	4139	33.6	29.0	29.6
Tair (°C)	Present day	5.5	-	-	-	21.7	-	-	-	23.0	-	-	-
	Near future	6.7	1.4	1.0	1.2	22.8	1.1	0.9	1.0	23.7	0.8	0.6	0.7
	Far future	10.3	5.5	4.1	4.8	25.9	4.6	3.7	4.1	26.8	4.3	3.4	3.8
Net radiation (W m ⁻²)	Present day	63	-	-	-	97	-	-	-	114	-	-	-
	Near future	62	2.0	-1.6	-0.4	97	-0.2	-0.9	-0.7	112	-0.4	-2.2	-1.5
	Far future	66	10.3	3.1	5.6	101	5.3	3.4	4.1	119	6.5	3.0	4.4
(b) Hydrological variables													
Total runoff (mm year ⁻¹)	Present day	1166	-	-	-	372	-	-	-	1999	-	-	-
	Near future	1244	0.5	8.6	6.7	414	2.5	12.1	11.3	2380	10.5	20.2	19.1
	Far future	1355	2.9	20.3	16.2	495	-2.3	36.3	33.1	2793	24.2	41.8	39.7
ET (mm year ⁻¹)	Present day	467	-	-	-	785	-	-	-	1193	-	-	-
	Near future	477	5.5	0.9	2.1	808	4.9	2.1	3.0	1216	5.2	0.4	1.9
	Far future	543	25.6	12.9	16.4	892	19.3	10.9	13.6	1347	18.2	10.5	12.9
Soil moisture (mm)	Present day	335	-	-	-	186	-	-	-	336	-	-	-
	Near future	338	0.4	1.2	0.9	192	2.7	3.4	3.1	354	6.6	5.1	5.5
	Far future	340	0.2	2.3	1.5	197	0.4	8.3	5.8	359	6.7	6.9	6.9

Table 4-1

Basic Statistics of Precipitation and Streamflow Data for Three Periods

Item		Brahmaputra	Ganges	Meghna
Outlet station		Bahadurabad	Hardinge Bridge	Bhairab Bazar
Precipitation ^b				
Mean (mm year ⁻¹)	Observed	1611	1149	3195
	Near future	1798	1201	3428
	Far future	1906	1290	3658
Monthly standard deviation (SD) (mm)	Observed	120	113	246
	Near future	120	115	271
	Farfuture	131	121	280
Annual SD (mm)	Observed	151	105	499
	Near future	104	120	485
	Far future	149	146	458
Monthly CV	Observed	0.006	0.008	0.006
	Near future	0.006	0.008	0.007
	Far future	0.006	0.008	0.006
Annual CV	Observed	0.094	0.092	0.156
	Near future	0.058	0.100	0.141
	Far future	0.078	0.113	0.125
Streamflow ^c				
Mean (m ³ s ⁻¹)	Observed	23148	13880	5142
	Near future	21816	8697	4498
	Far future	22867	9504	4755
Monthly SD (m ³ s ⁻¹)	Observed	17172	15957	4648
	Near future	14571	11989	4410
	Far future	16506	13011	4533
Annual SD (m ³ s ⁻¹)	Observed	5229	5074	1304
	Near future	1751	2197	967
	Far future	2419	2311	950
Monthly CV	Observed	0.74	1.15	0.90
	Near future	0.67	1.38	0.98
	far-future	0.72	1.37	0.95
Annual CV	Observed	0.23	0.37	0.25
	Near-future	0.08	0.25	0.21
	Far-future	0.11	0.24	0.20

^b Estimated from WFD precipitation dataset (1980–2001)

^c Estimated from observed data from [BWDB \(2012\)](#)

Table 4-2

Basin Ranking According to Degree of Difficulty with Managing Extreme Events Using the Indicators of Duration Curves

Hydrological characteristics	Seasonal variation		Annual variation		Severity of extreme events (intensity and duration)
Indicator from duration curves (Fig. 2-3)	Departure		Variation		Departure and Angle between FDC and DDC*
From which duration curves (for streamflow)	FDC	DDC	FDC	DDC	Both FDC and DDC
Basin ranking (high to low), also indicates the ranking according to the degree of difficulty to manage extreme events	Ganges	Meghna	Meghna	Meghna	Ganges
	Meghna	Ganges	Brahmaputra	Ganges	Meghna
	Brahmaputra	Brahmaputra	Ganges	Brahmaputra	Brahmaputra

* Departure and Angle closely relate to the amount of storage necessary to smooth out hydrological variations.

Table 5-1

Major Statistics of the Meghna River Basin

Item		value
Basin area (km ²) considering outlet at Bhairab Bazar	Total	65,000 ^a 64,956 ^b
	India portion (% to the total basin area)	43,521 (67%) ^b
	Bangladesh portion (% to the total basin area)	21,436 (33%) ^b
River length (km) ^a		946
Elevation (m a.s.l.) ^c	Range	-1 ~ 2,579
	Average	307
	Area below 500 m	75%
Land use (% of total basin area) ^d	Forest	54%
	Agriculture	27%
	Herbaceous/sparse tree/open tree	18%
Meteorological variables (basin averaged) ^e	Precipitation (mm year ⁻¹)	3,212
	Temperature (°C)	23
	Net radiation (W m ⁻²)	84
	Specific humidity (g/kg)	14.4
Hydrological variables (basin averaged) ^f	Runoff (mm year ⁻¹)	2,193
	Evapotranspiration (mm year ⁻¹)	1,000
	Potential Evapotranspiration (mm year ⁻¹)	1,689
Discharge at Bhairab Bazar station (m ³ s ⁻¹) ^g	Lowest	2
	Highest	19,900
	Average	4,600
Net cultivated area (km ²) in Bangladesh portion (% to the Bangladesh's total) ^h		11,624 (15.1%)
Rice crop production (metric tons) in Bangladesh portion (% to the Bangladesh's total) ⁱ	Local Boro	154,619 (72.1%)
	Hybrid Boro	510,456 (15.8%)
	HYV Boro	2427 343 (16.6%)
	Total Boro (Local+Hybrid+HYV)	3092,418 (17.1%)
	Aus	266,210 (15.6%)
	Aman	1785,855 (14.6%)
Population in Bangladesh		19.4 million

portion (% to the Bangladesh's total) ^j	(13.5%)
--	---------

^a Nishat and Faisal (2000)

^b From this study

^c Estimated from SRTM DEM data by Lehner et al. (2006)

^d Estimated from Tateishi et al. (2014)

^e Estimated from WFD (data period: 1980-2001) by Weedon et al. (2011)

^f From model simulation with WFD

^g BWDB (2012)

^h Estimated from Agriculture Census, 2008 (BBS, 2014)

ⁱ Estimated from crop production, 2009-2010 (BBS, 2011)

^j Estimated from Population Census, 2011 (BBS, 2014)

Table 5-2

Percent Area of the Basin for Different Classes of Average Annual (a) Precipitation and (b) Runoff in Three Different Time Slices

Classes (unit: mm year ⁻¹)	Base period (1979–2003)	Near future (2015–2039)	Far future (2075–2099)
(a) Precipitation			
below 2000	5.9	6.1	3.0
2001-3000	48.6	40.7	36.9
3001-4000	27.4	29.0	32.9
4001-5000	6.9	9.8	10.8
5001-6000	4.9	4.4	5.7
6001-7000	4.4	4.3	4.1
7001-8000	1.9	3.0	2.7
8001-9000	-	1.9	2.3
above 9000	-	0.7	1.7
(b) Runoff			
below 1000	3.3	3.3	1.3
1001-1500	27.5	22.7	19.2
1501-2000	32.0	29.0	30.1
2001-3000	20.4	23.8	26.9
3001-4000	6.8	7.9	8.5
4001-5000	5.1	4.9	4.4
5001-6000	3.9	4.1	4.5
above 6000	0.8	2.4	2.6

Table 5-3

Percent Area of the Basin for Different Classes of Percentage Change of (a) Precipitation and (b) Runoff in the Near Future (2015–2039) and the Far Future (2075–2099) Compared to the Base Period

Classes (unit: %)	Near Future (2015-2039)	Far Future (2075-2099)
(a) Precipitation		
below 0	22.5	-
1 - 5	30.8	8.7
6 - 10	13.6	21.6
11 - 15	16.4	25.8
16 - 20	12.5	36.3
21 - 25	2.7	4.7
above 25	-	2.9
(b) Runoff		
below 0	23.7	3.5
1 - 10	34.8	26.4
11 - 20	19.6	35.1
21 - 30	20.2	31.1
above 30	1.2	3.9

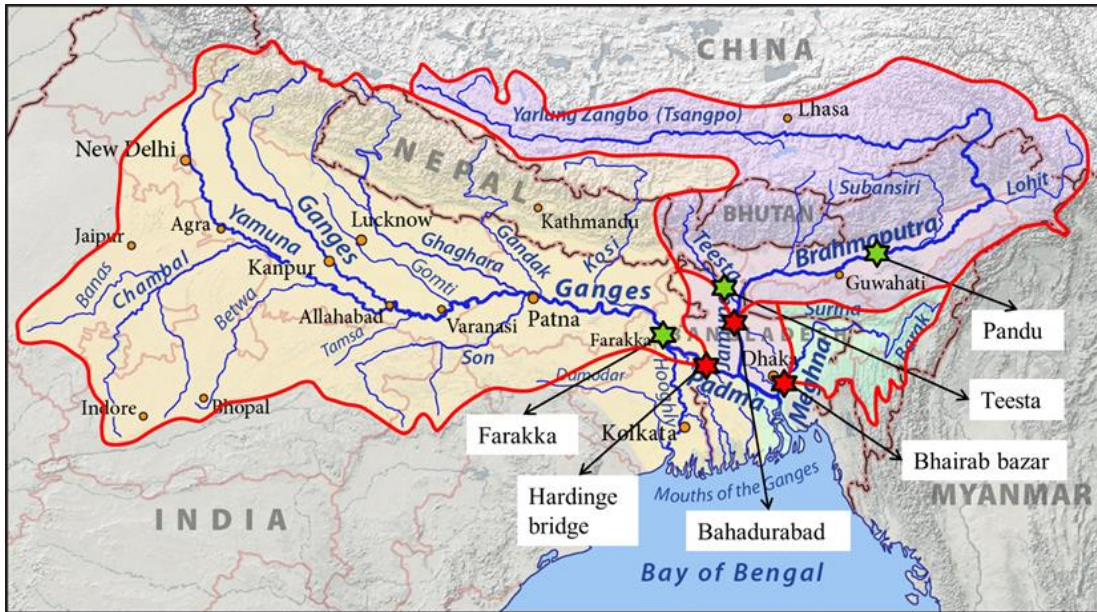


Figure 1-1. The boundary of the Ganges-Brahmaputra-Meghna (GBM) river basin (thick red line), the three outlets (red star): Hardinge bridge, Bahadurabad, and Bhairab bazar for the Ganges, Brahmaputra, and Meghna river basins, respectively. Green stars indicate the locations of three additional upstream stations: Farakka, Pandu, and Teesta (modified from Pfly, 2011).

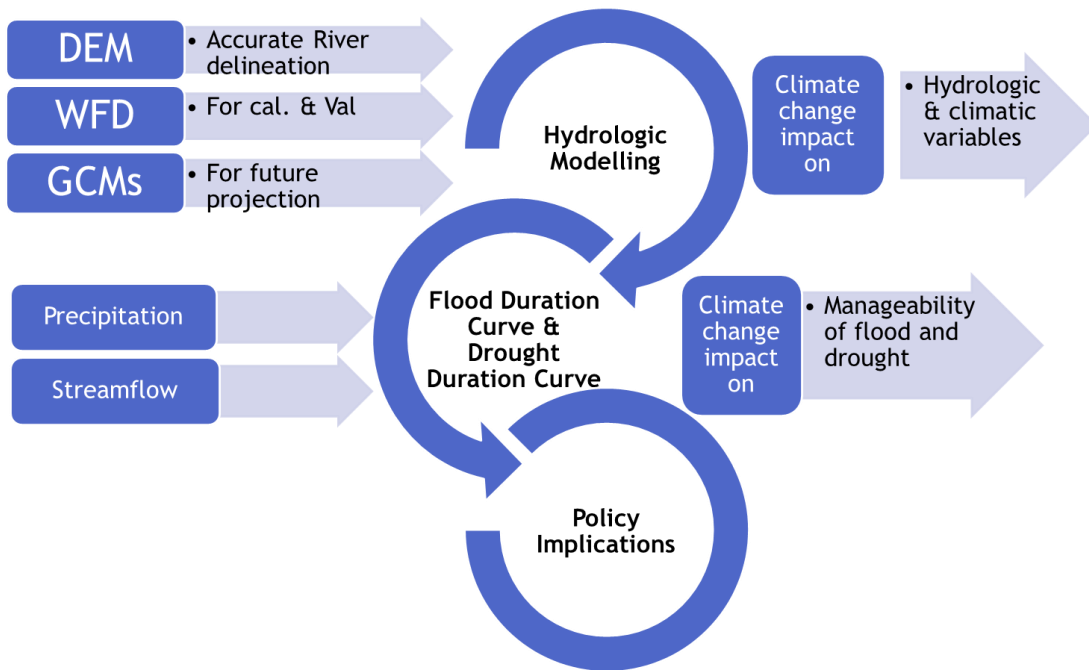


Figure 2-1. Flow chart of the methodology with input (left) and output (right).

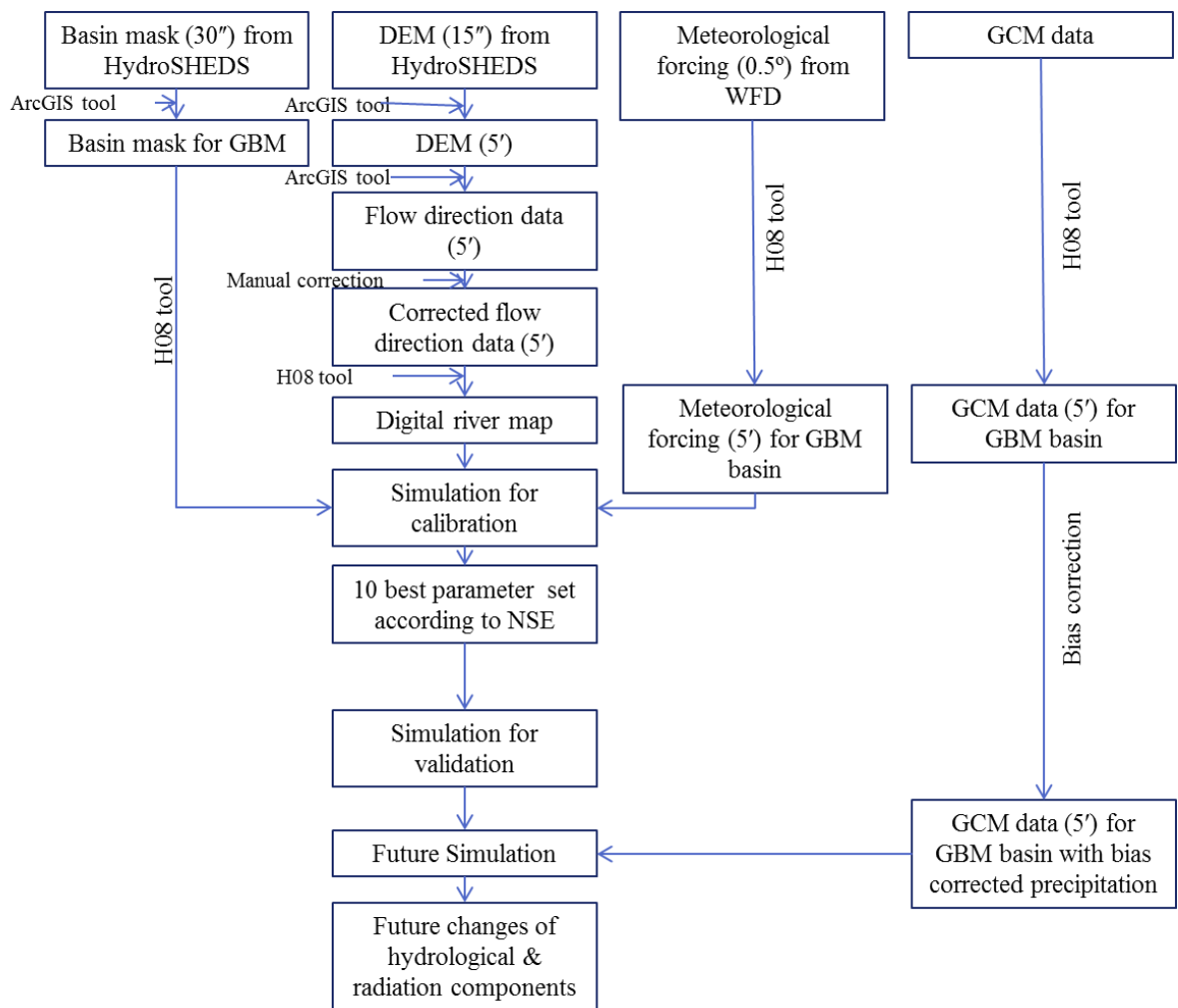
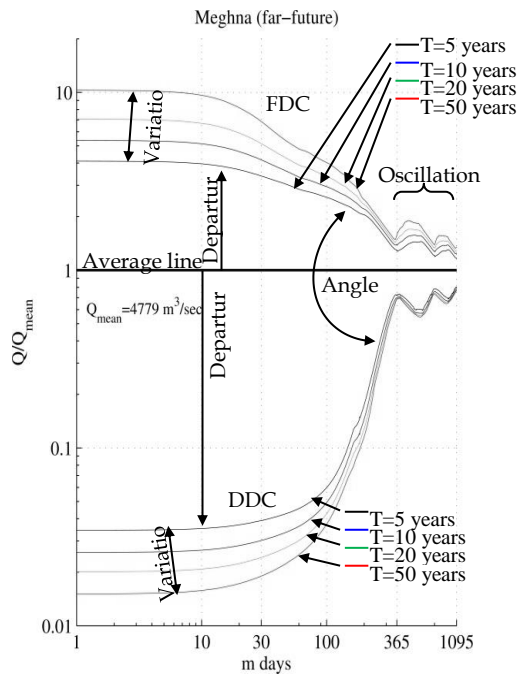


Figure 2-2. Flow chart of the methodology followed for future projection.



Angle: refers the recovery rate from an extreme event. A steeper gradient (wider angle) of the curve represents a situation when the extreme event lasts for a shorter duration and the average situation recovers quickly.

Departure: refers the intensity of seasonal variation around long-term mean. A large departure means a large reservoir storage is necessary to adjust the seasonal variation. It also refers the severity of an extreme event.

Oscillation: corresponds the degree of seasonality.

Figure 2-3. A typical Flood duration curve (FDC) and Drought duration curve (DDC) of daily discharge series and its basic terminologies

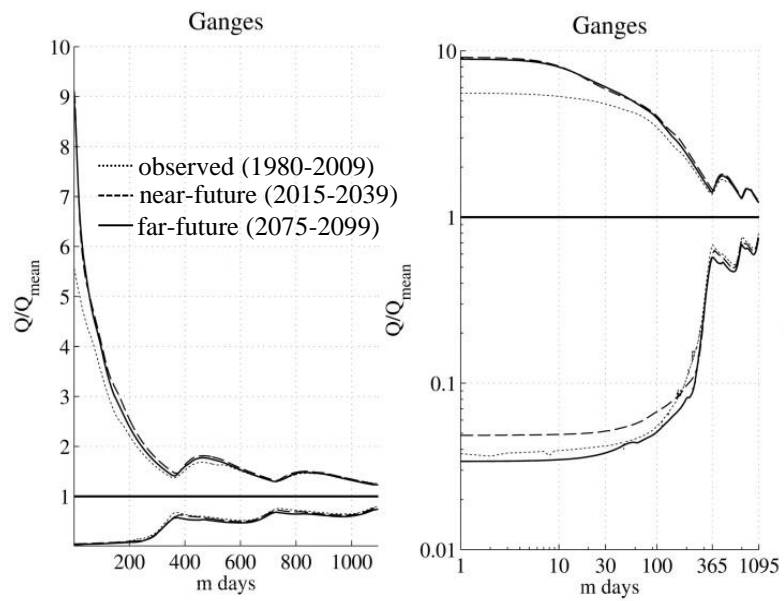


Figure 2-4. Duration curves of daily streamflow series of three periods with 10-year return period for the Ganges, plotted in linear scale (left) and logarithmic scale (right).

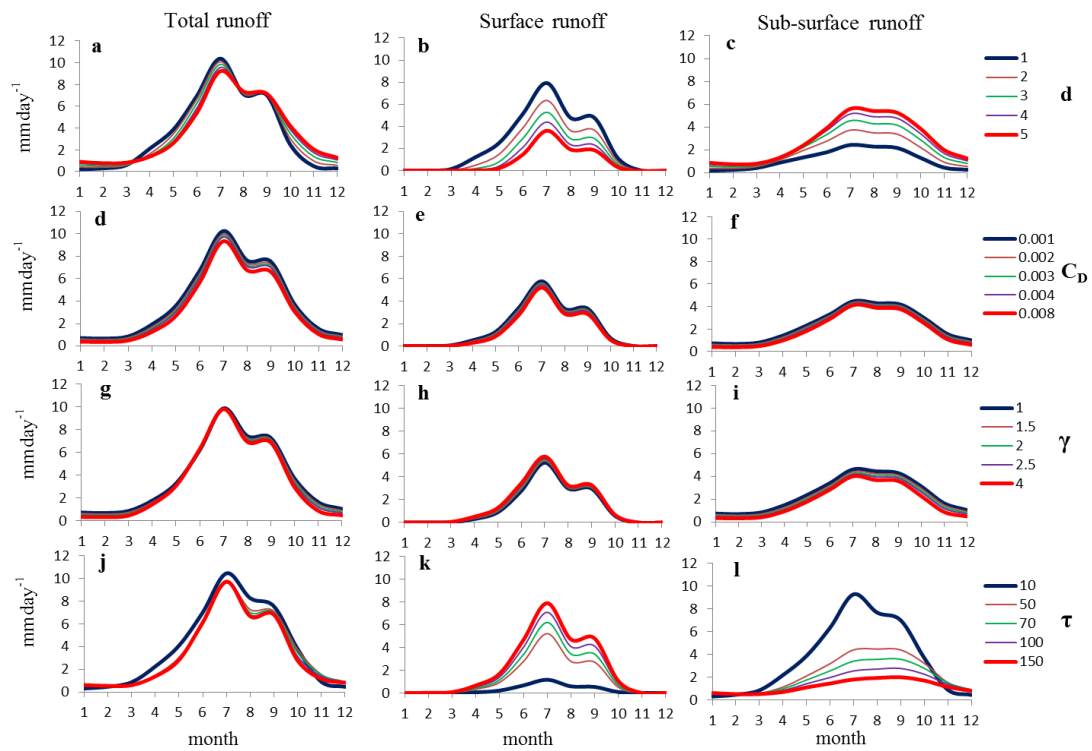


Figure 3-1. The 11-year (1980–1990) mean seasonal cycles of the simulated total runoff, surface runoff, and sub-surface runoff (unit: mm day^{-1}) in the Brahmaputra basin. Each of the five lines in each panel represents the average of 5^3 ($=125$) runs with one of the four calibration parameters fixed at a given reasonable value.

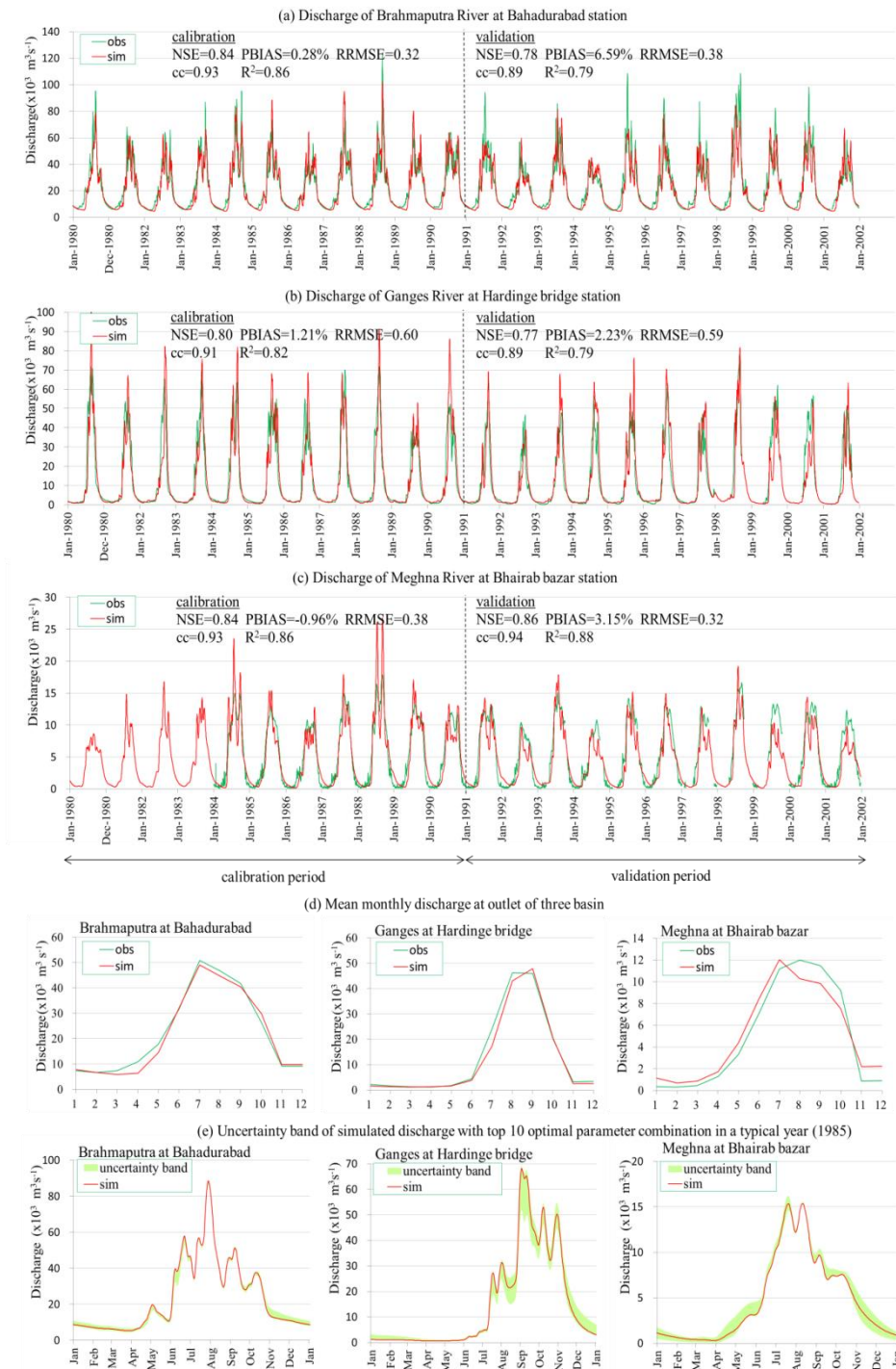


Figure 3-2. The simulated discharges (red line) using the WFD forcing data (both calibration and validation period) compared with observations (green line) at outlets of the (a) Brahmaputra, (b) Ganges, (c) Meghna River, and (d) mean monthly (1980–2001) simulated discharges compared with that of observations at outlets, (e) simulated discharges by using the 10 optimal parameter sets (red line) and the associated uncertainty bands (green shading) in a typical year (1985). Nash–Sutcliffe efficiency (NSE), percent bias (PBIAS), relative Root-Mean Square Error (RRMSE), correlation coefficient (cc), and coefficient of determination (R²) for both calibration and validation period are noted at sub-plot (a), (b), and (c).

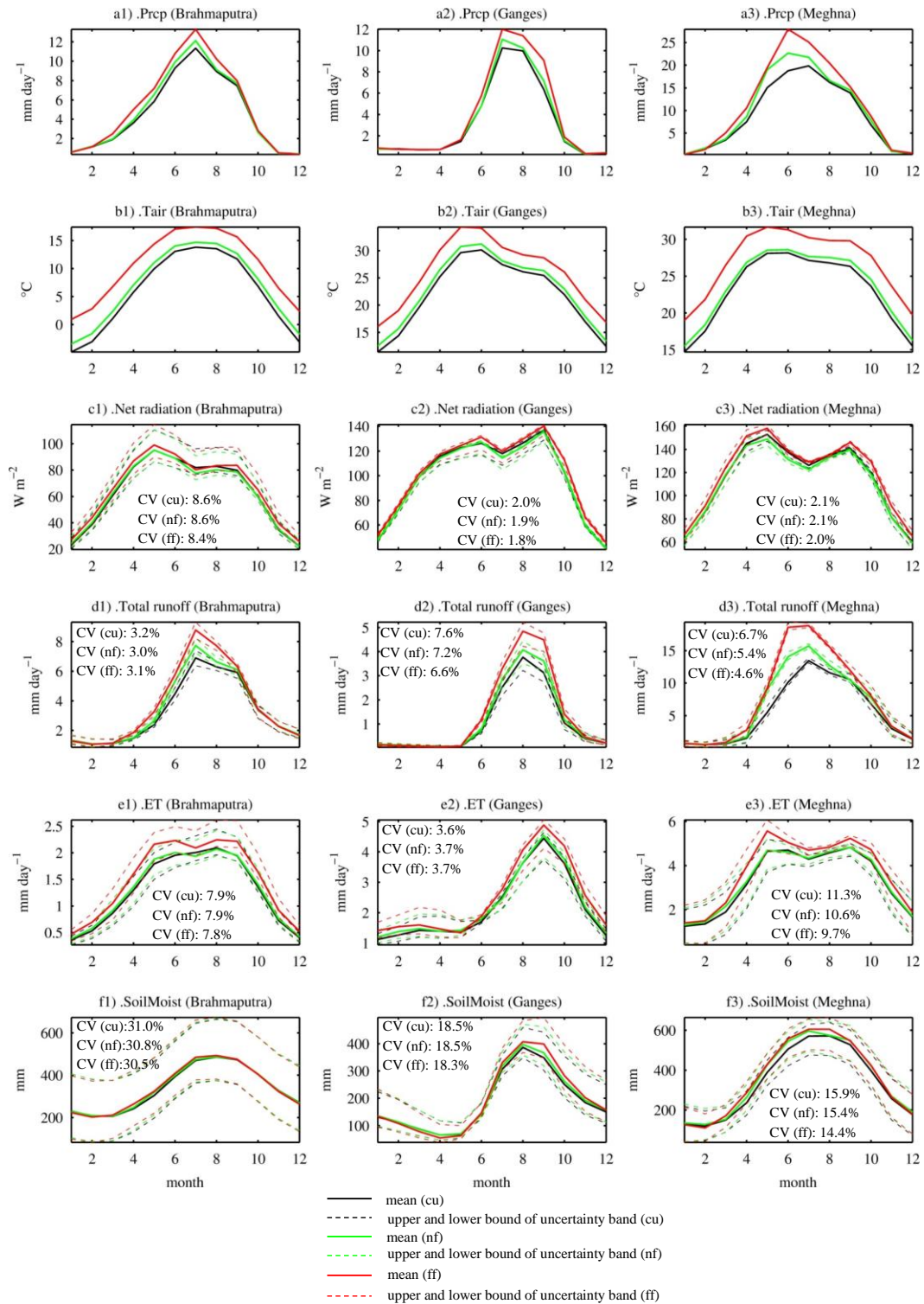


Figure 3-3 (a1)-(f3). The mean (solid line) and upper and lower bounds (dashed line) of the uncertainty band of the hydrological quantities and net radiation components for the present-day (black), near-future (green), and far-future (red) simulations as determined found from 10 simulation results, considering 10 optimal parameter set according to Nash–Sutcliffe efficiency (NSE) (cu: present-day, nf: near-future, ff: far-future). Coefficient of variations (CV) for all periods (Table 3-4) are noted on each sub-plot.

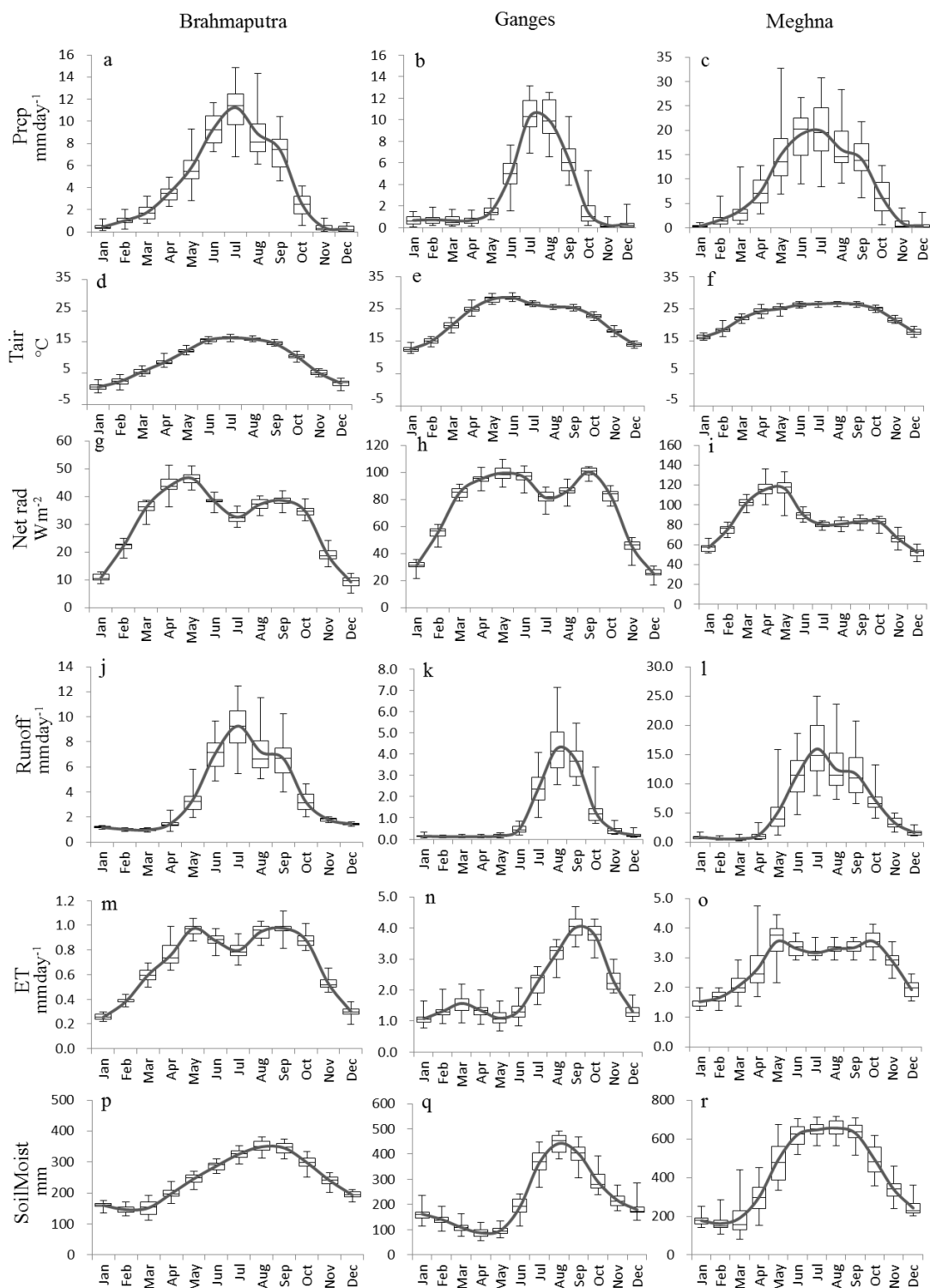


Figure 3-4 (a)-(r). Seasonal cycle of climatic and hydrologic quantities during 1980–2001. Box-and-whisker plots indicate minimum and maximum (whiskers), 25th and 75th percentiles (box ends), and median (black solid middle bar). Solid curve line represents interannual average value. All abbreviated terms here refer to Table 3-5.

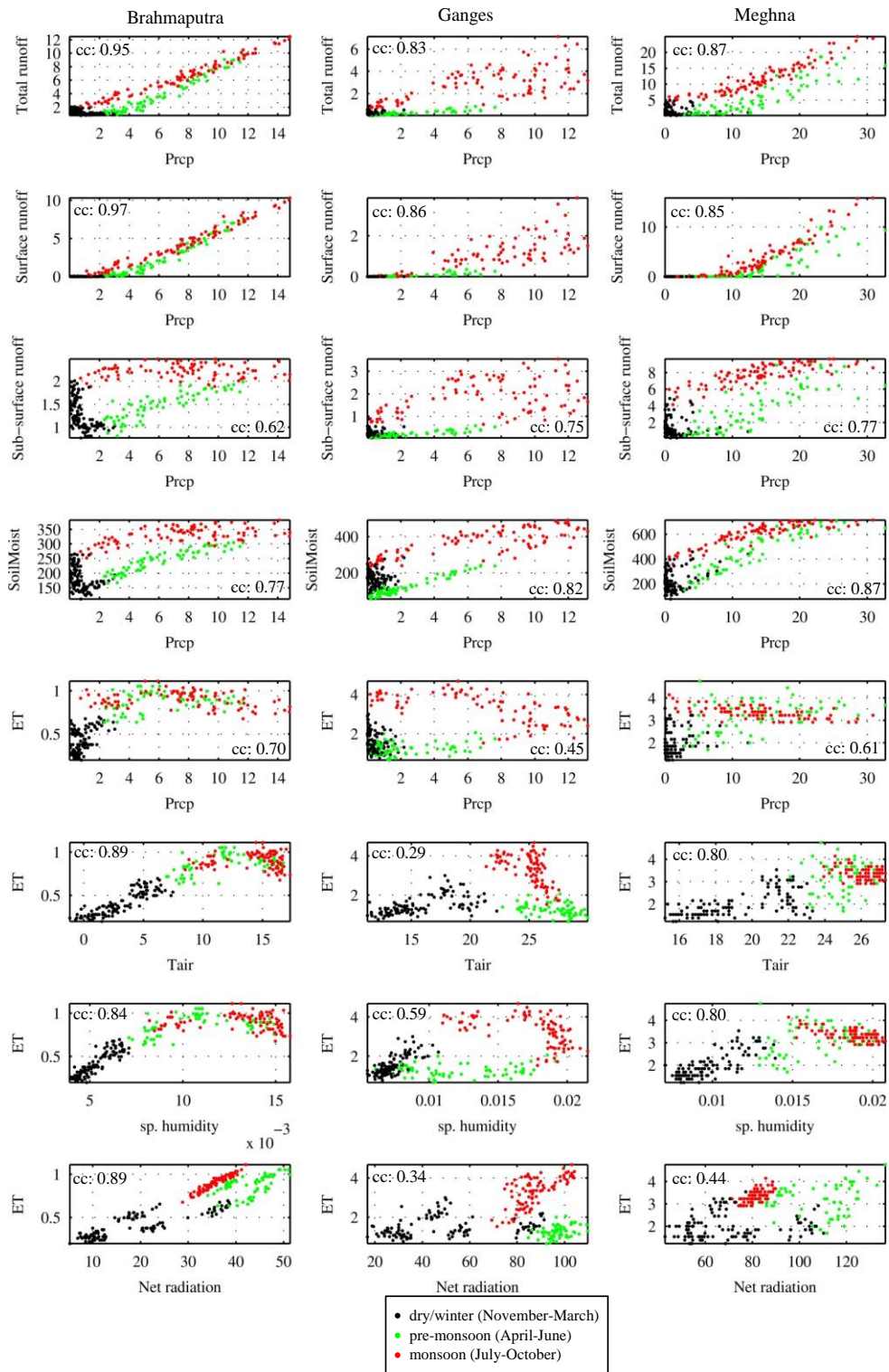


Figure 3-5. The correlation between the monthly means of meteorological variables (WFD) and that of hydrological variables for the Brahmaputra, Ganges, and Meghna basins. Three different colors represent the data in three different seasons: Black: dry/winter (November-March); Green: pre-monsoon (April-June); and Red: monsoon (July-October). The correlation coefficient (cc) for each pair (all 3 seasons together) is noted at each sub-plot. The units are mm day⁻¹ for Prec, ET, runoff, mm for SoilMoist, °C for T_{air}, and W m⁻² for net radiation. All abbreviated terms here refer to Table 3-5.

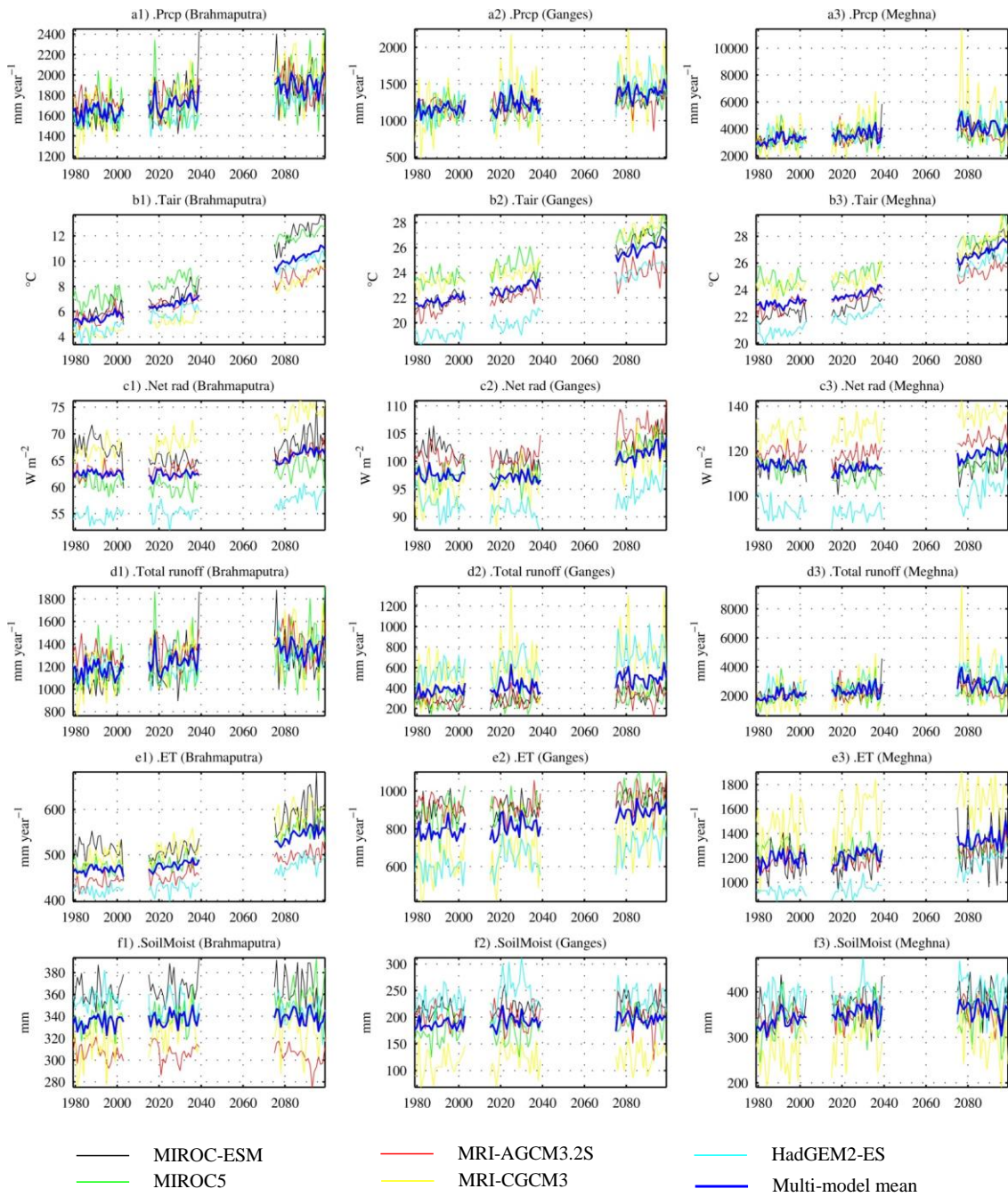


Figure 3-6 (a1-f3). Interannual variation of mean of meteorological and hydrological variables of 5 GCMs for the present day (1979–2003), near future (2015–2039), and far future (2075–2099). Thick blue lines represent the means of 5 GCMs.

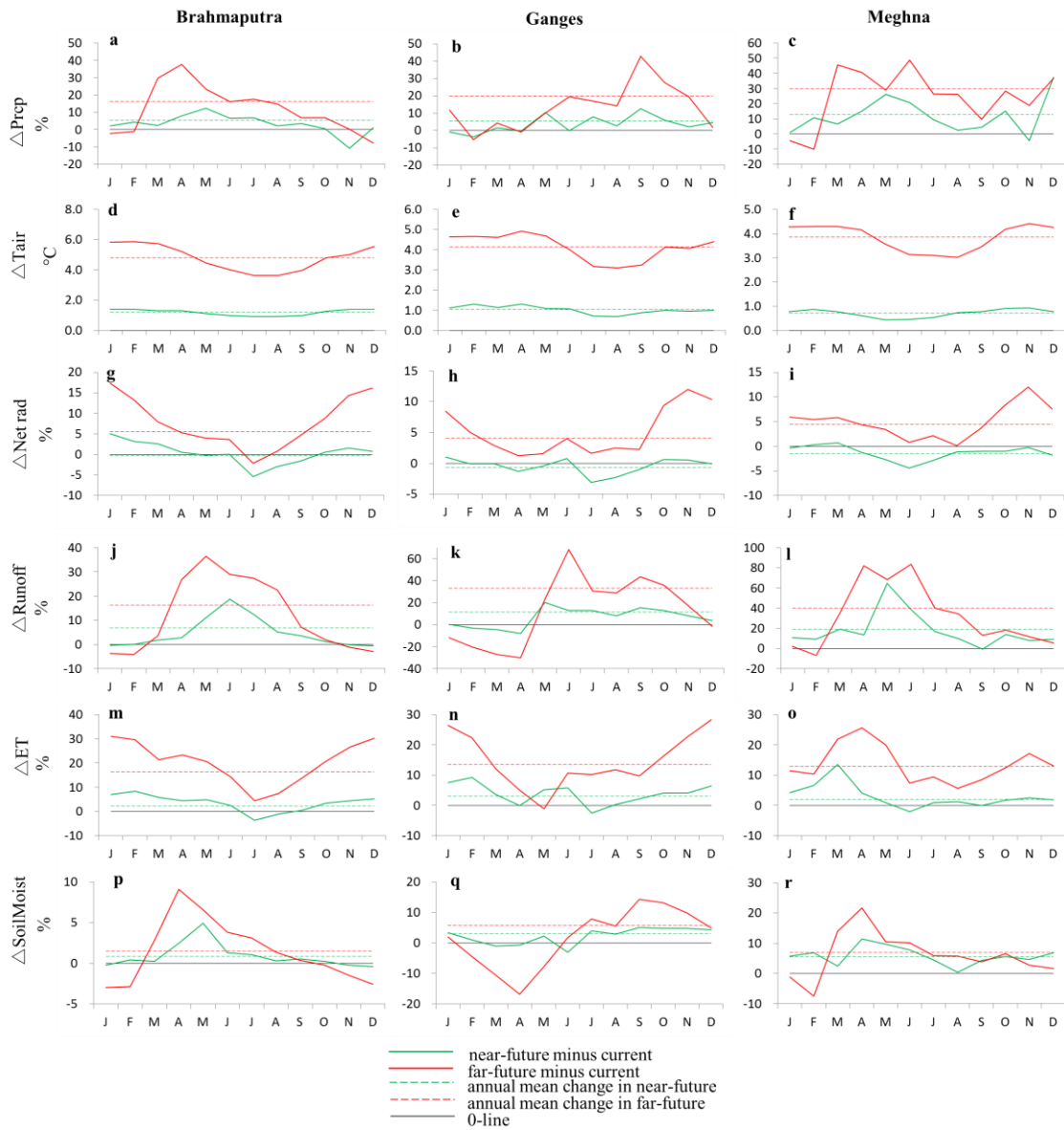


Figure 3-7 (a)-(r). Percentage changes in the monthly means of the climatic and hydrologic quantities from the present-day period to the near-future and far-future periods. The dashed lines represent the annual mean changes.

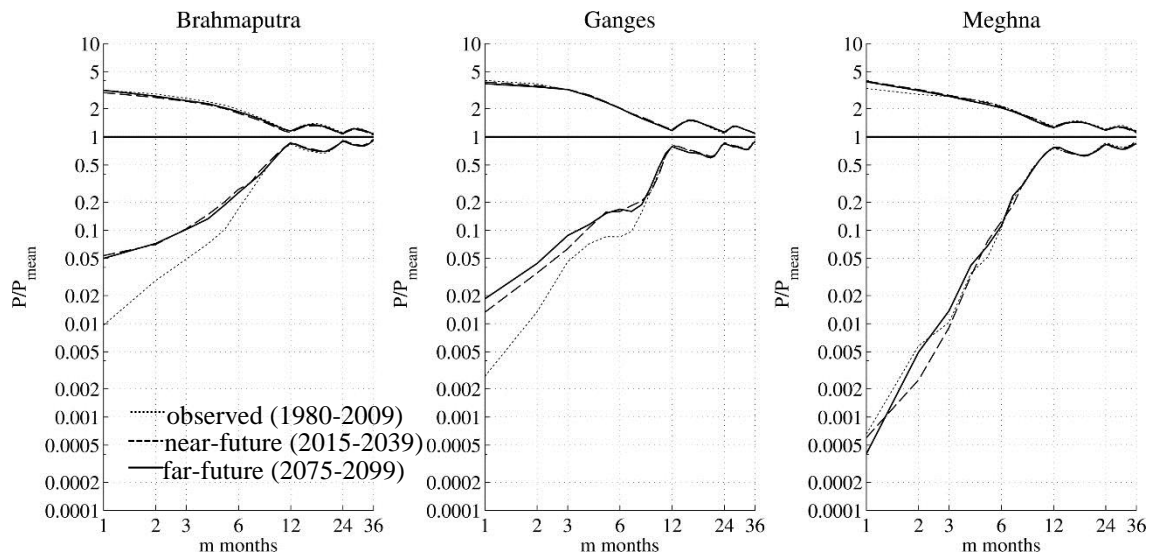


Figure 4-1. Comparison of duration curves of basin-averaged monthly precipitation (P) series of three periods with 10-year return period for three basins.

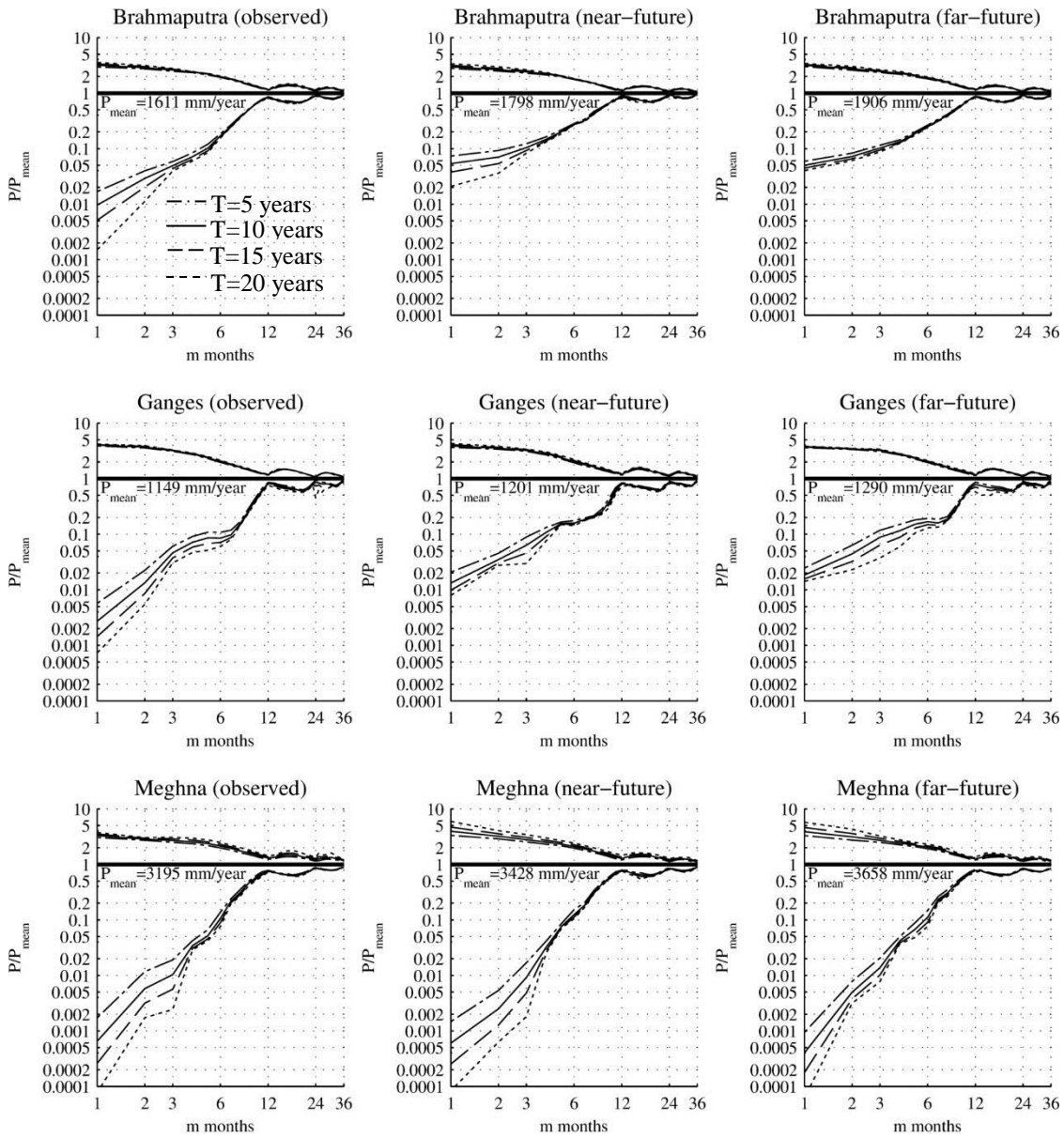


Figure 4-2. Flood and drought duration curves of basin-averaged monthly precipitation (P) series of three periods; observed (1980–2009), near future (2015–2039), and far future (2075–2099) with 5-, 10-, 20-, and 50-year return period (T) for the three basins.

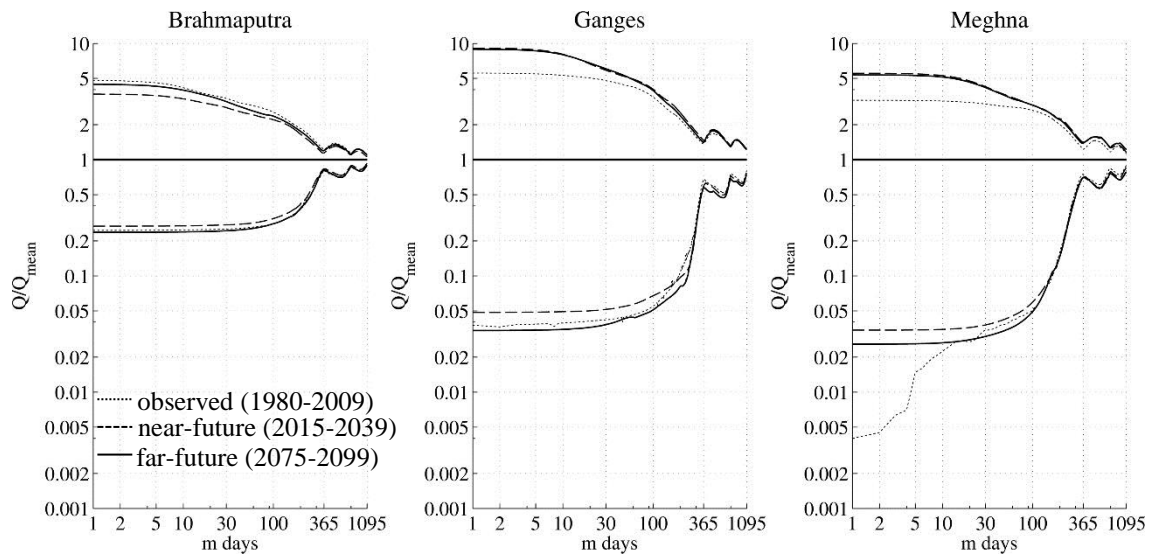


Figure 4-3. Comparison of duration curves of daily streamflow series of three periods; observed (1980–2009), near future (2015–2039), and far future (2075–2099) with 10-year return period for the three basins.

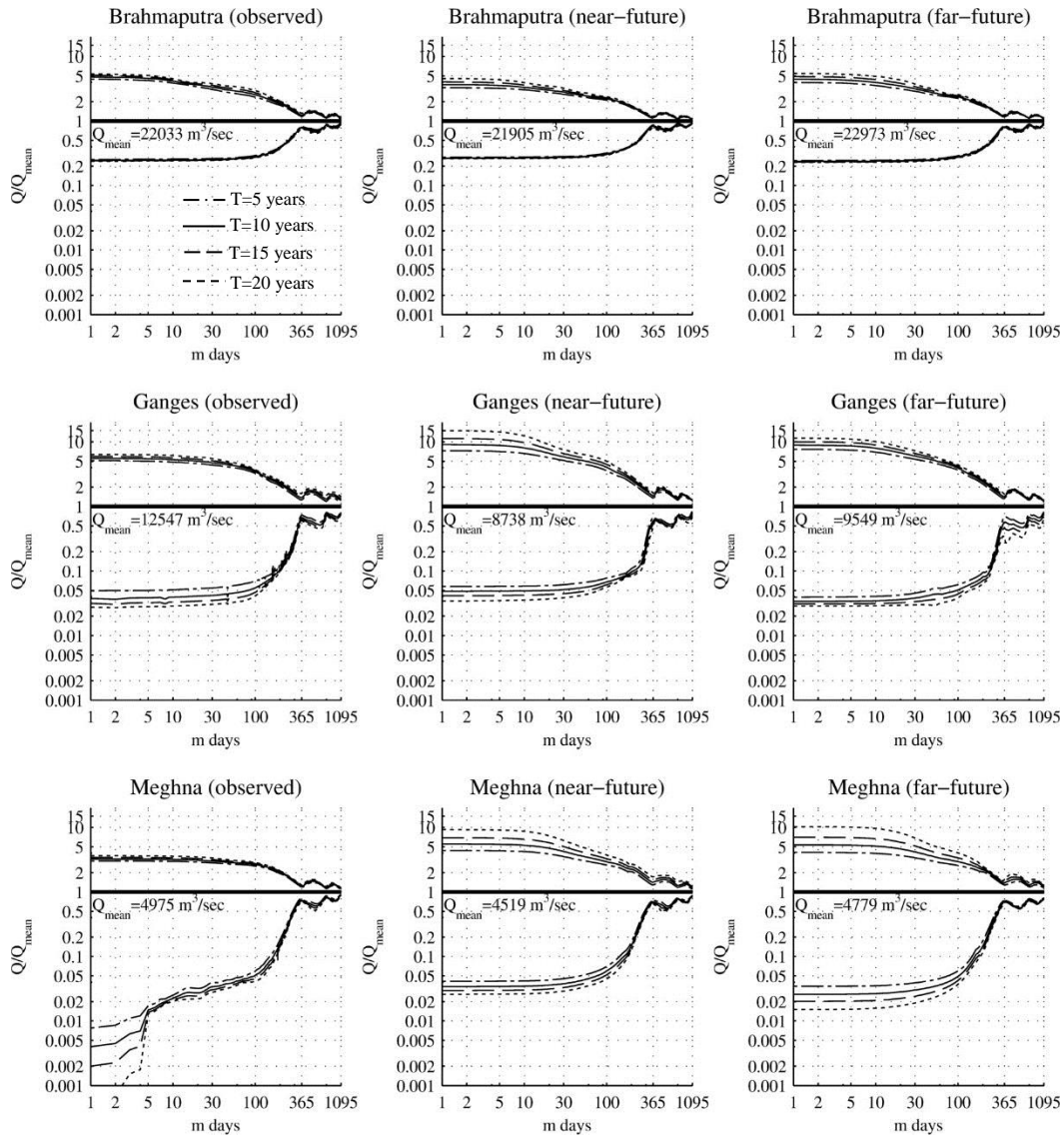


Figure 4-4. Flood and drought duration curves of daily streamflow (Q) series of three periods: observed (1980–2009), near future (2015–2039), and far future (2075–2099) with 5-, 10-, 20-, and 50-year return period (T) at basin outlets for the three basins.

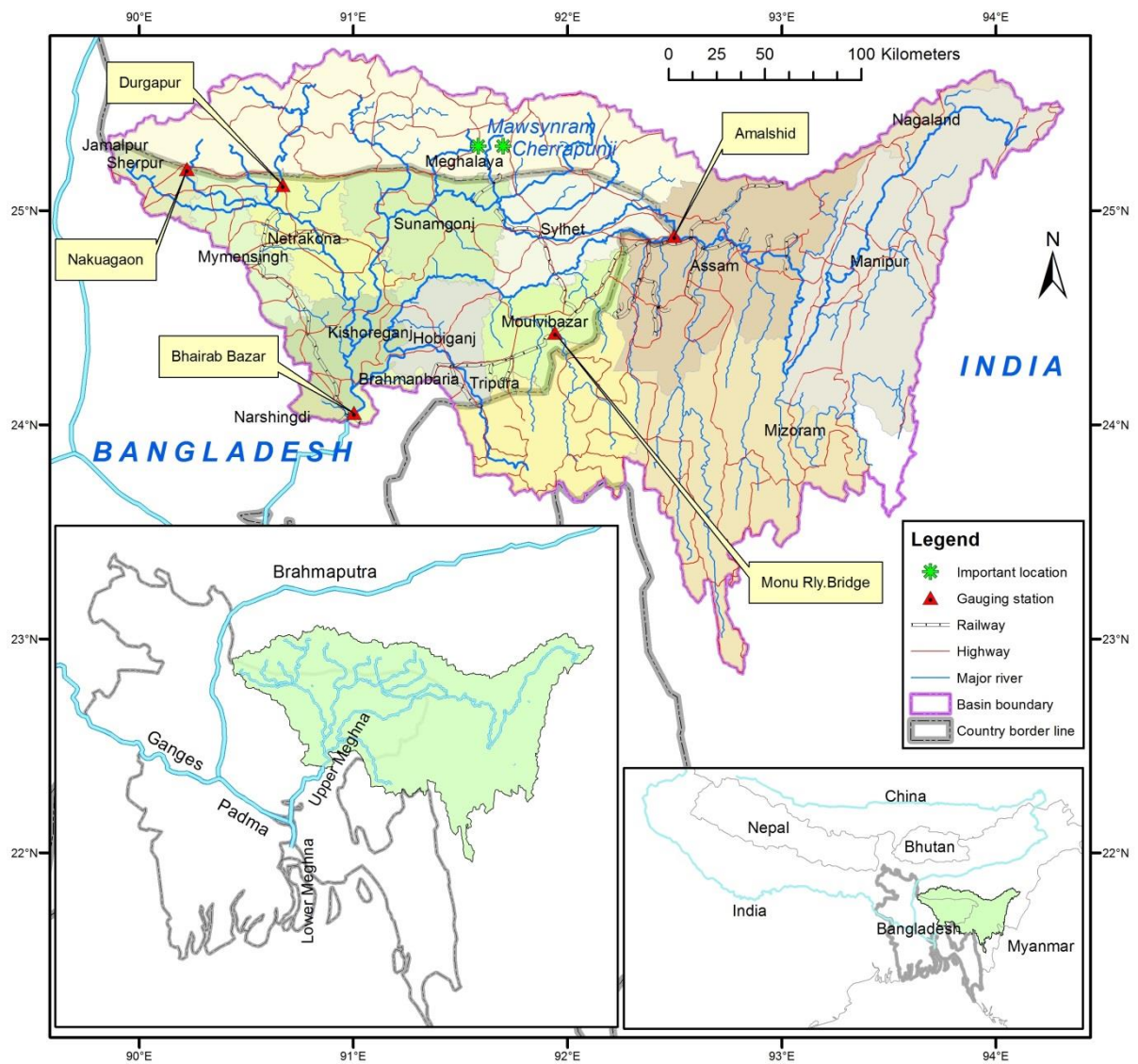


Figure 5-1. The Meghna river basin map with major rivers, transportation network, and gauging stations in the study area.

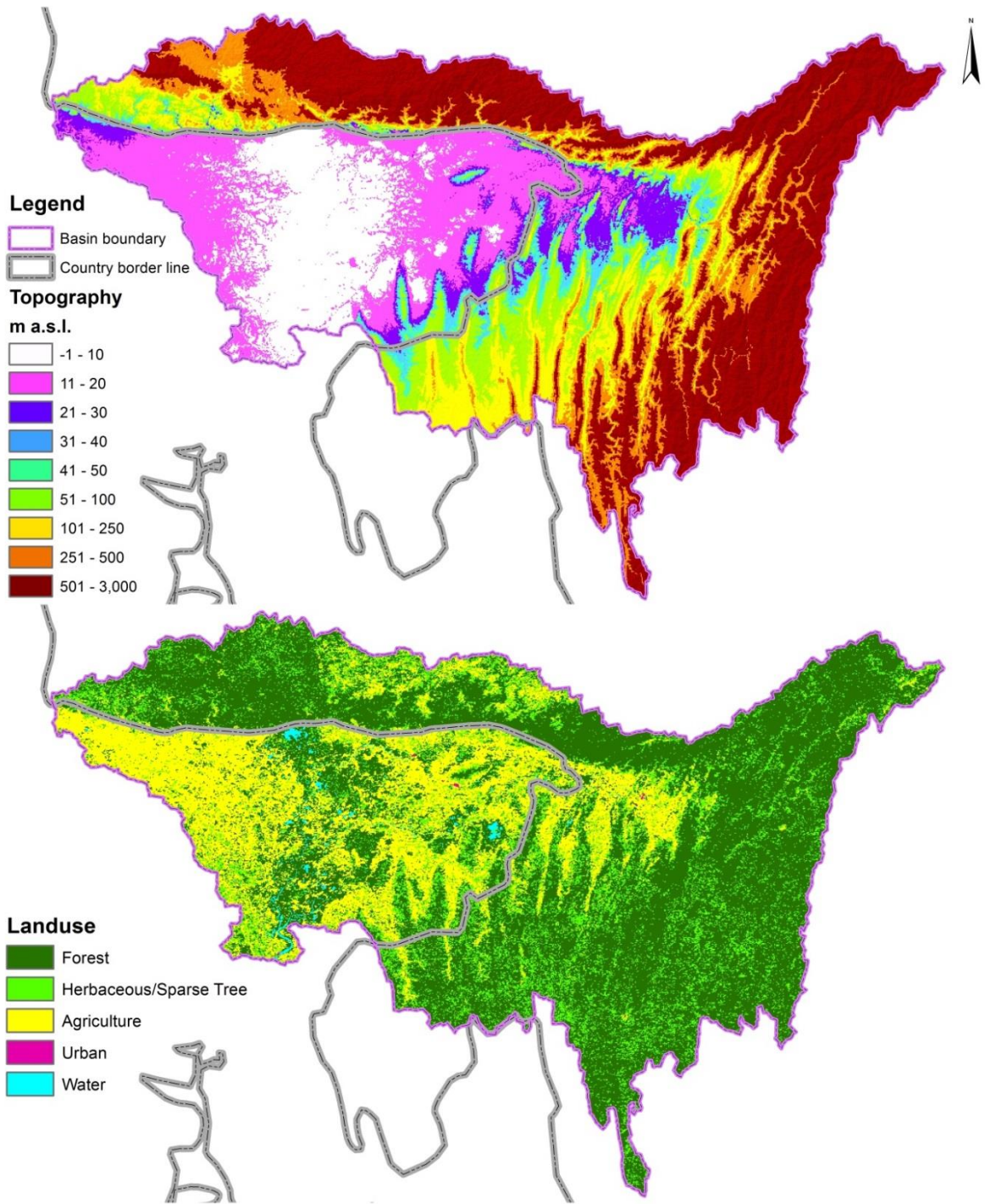


Figure 5-2. Topography and land use of the Meghna river basin.

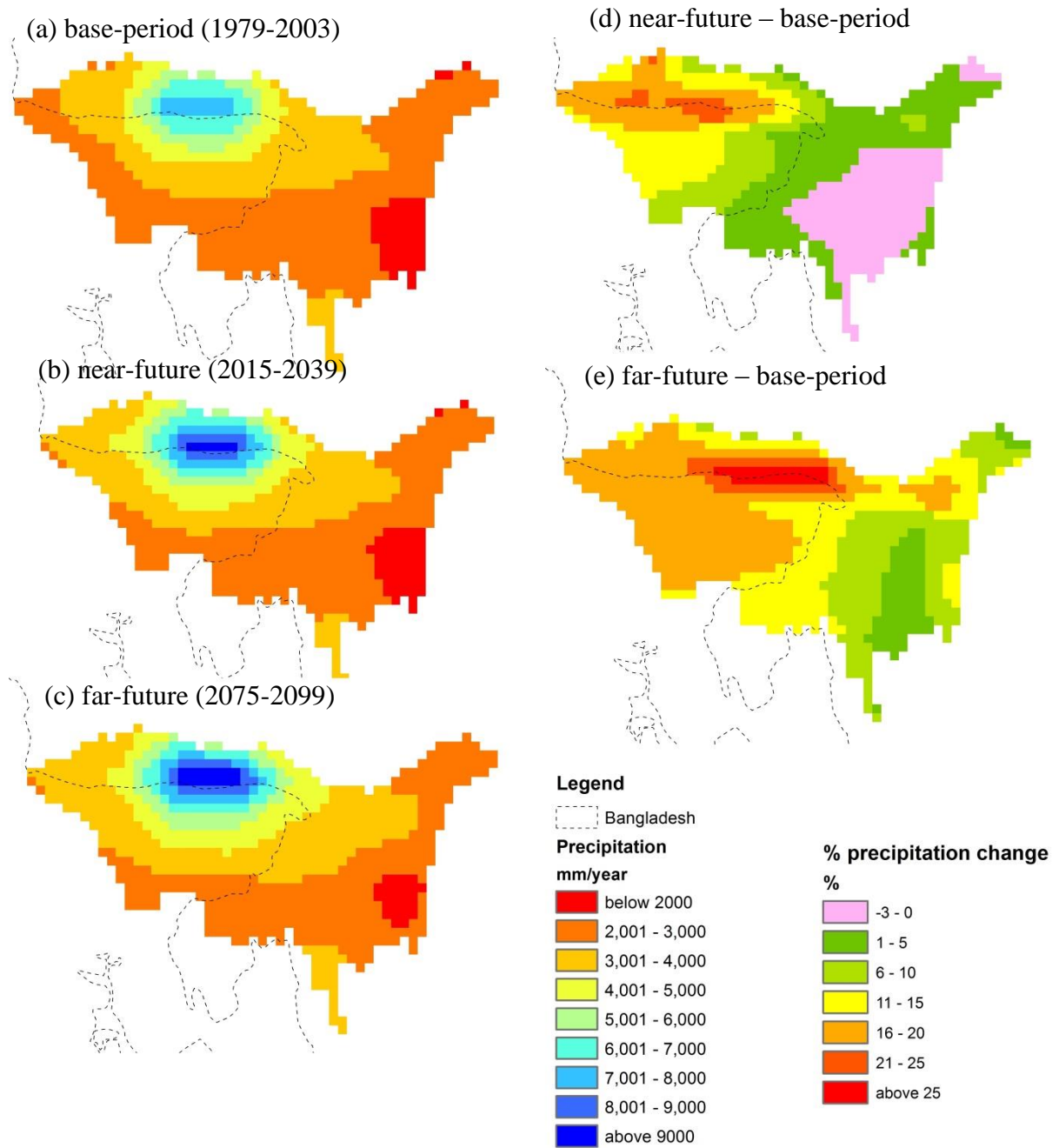


Figure 5-3. Spatial distribution of projected precipitation and percentage changes in average annual precipitation of the Meghna basin. All mean annual precipitation presented in the figure is a 25-year mean, and changes are calculated considering the 1979–2003 as the base period. (a), (b), and (c) are for the base-period, the near future, and the far future, respectively. Percentage changes in projected precipitation are presented as (d) and (e) for the near future and the far future, respectively. Light violet colored cells in (d) indicate the area where projected precipitation is zero or negative.

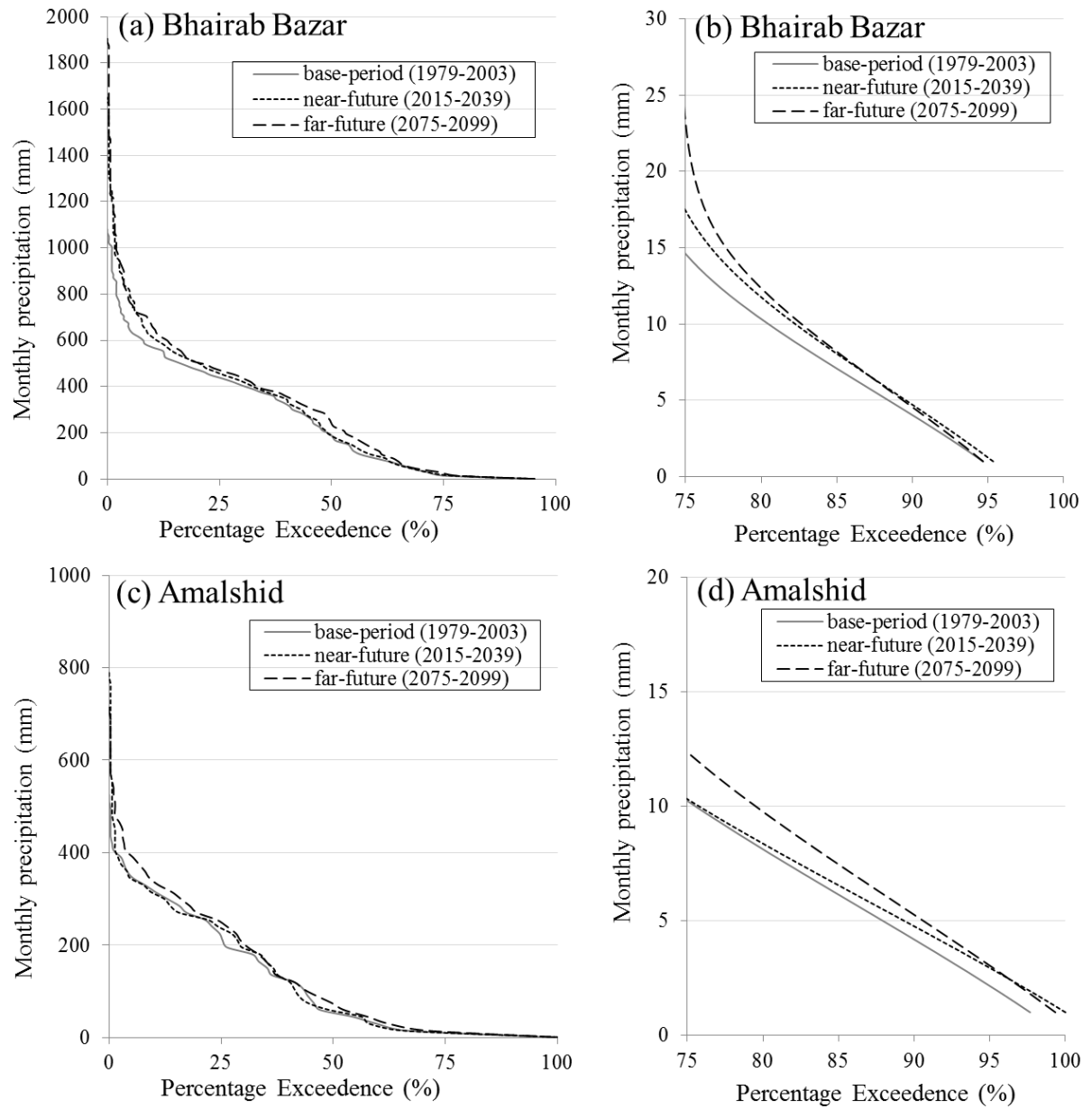


Figure 5-4. Probability of exceedance of basin averaged monthly precipitation of the Meghna basin at two gauging stations: (a) and (b) at Bhairab Bazar, (c) and (d) at Amalshid for three time slices: the base period, the near future, and the far future. (b) and (d) are the magnified view of (a) and (c) at 75–100 percentage exceedance (which represent the probability of exceedance of monthly low-precipitation) at Bhairab Bazar and Amalshid, respectively.

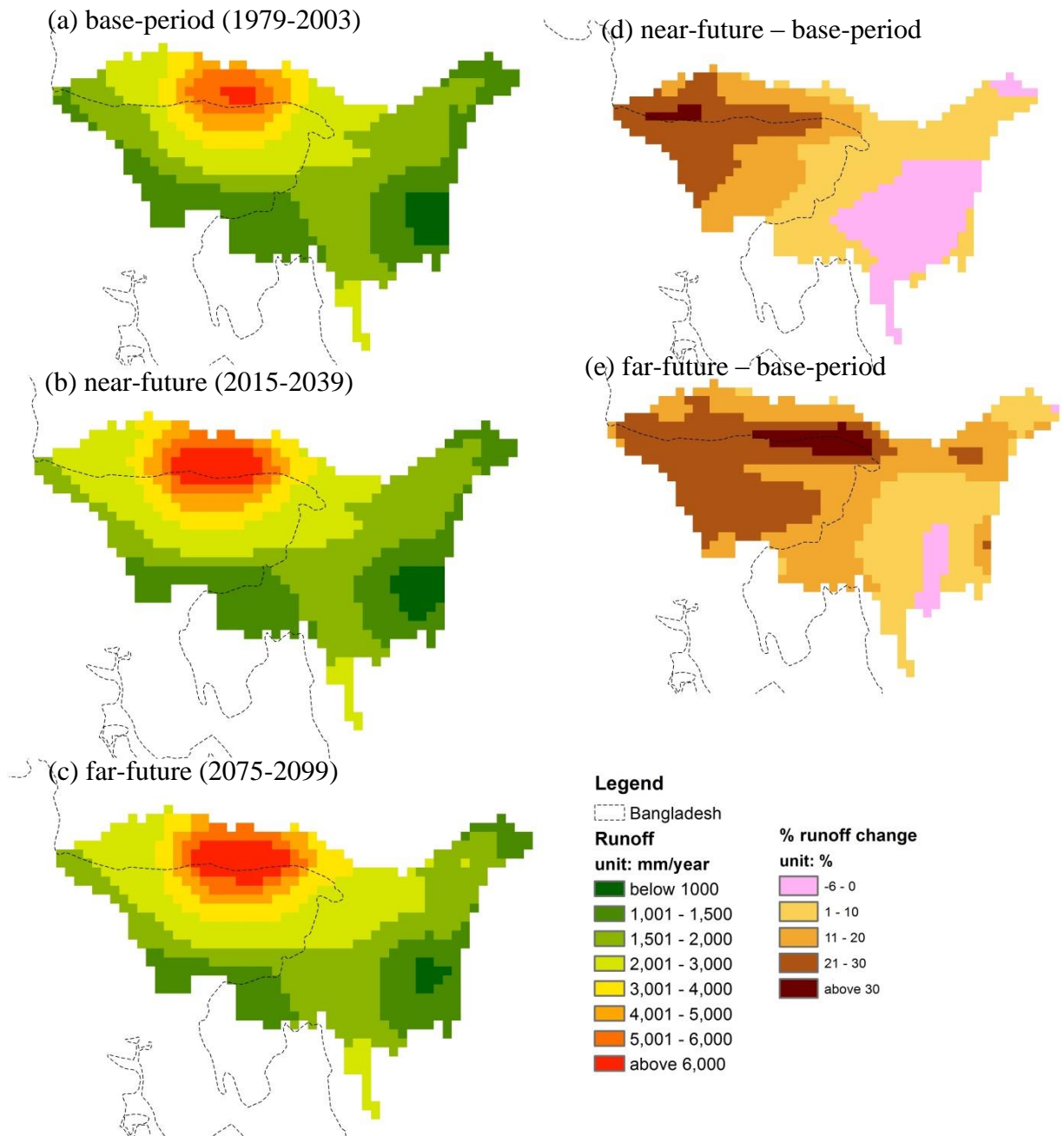


Figure 5-5. Spatial distribution of projected runoff and percentage changes in average annual runoff of the Meghna basin. All mean annual runoff presented in the figure is a 25-year mean and changes are calculated considering 1979–2003 as the base period. (a), (b), and (c) are for the base period, the near future, and the far future, respectively. Percentage changes in projected runoff are presented as (d) and (e) for the near future and the far future, respectively. Light violet colored cells in (d) and (e) indicate the area where projected runoff is zero or negative.

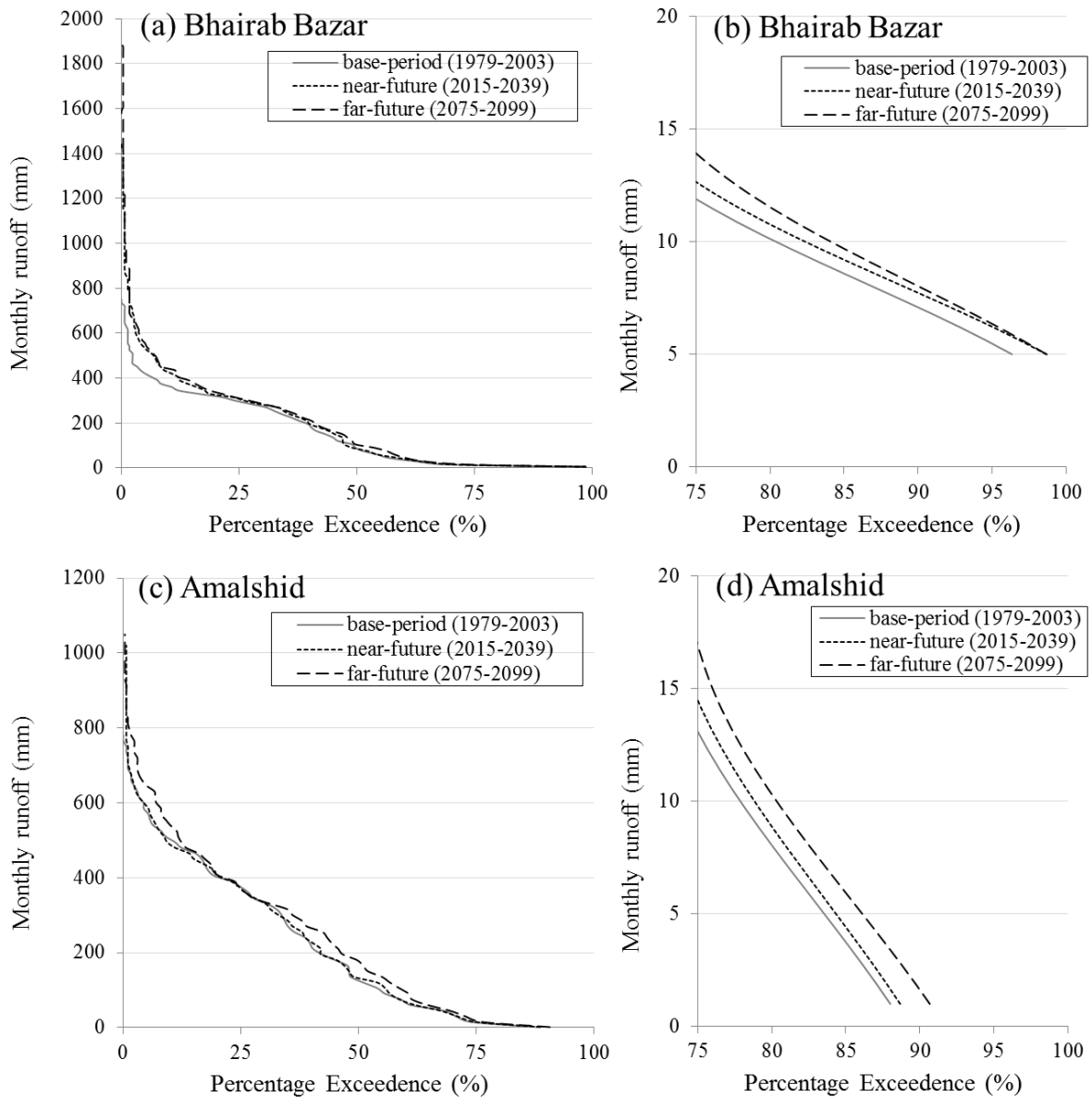


Figure 5-6. Probability of exceedance of basin averaged monthly runoff of the Meghna basin at two gauging stations: (a) and (b) at Bhairab Bazar, (c) and (d) at Amalshid for three time slices: the base period, the near future, and the far future. (b) and (d) are the magnified view of (a) and (c) at 75–100 percentage exceedance (which represent the probability of exceedance of monthly low-flow) at Bhairab Bazar and Amalshid, respectively.

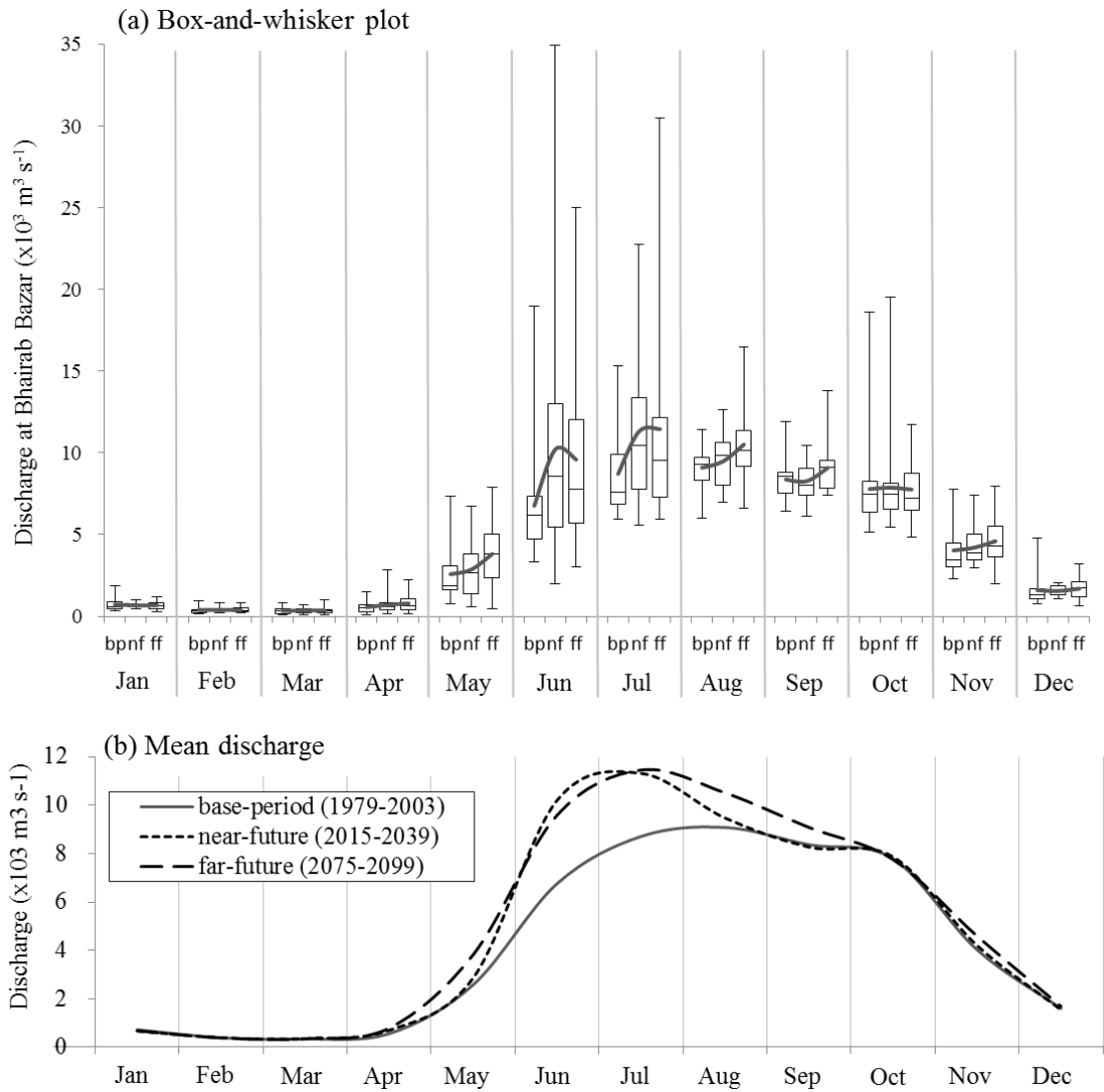


Figure 5-7. (a) Discharge of the Meghna river at Bhairab Bazar station for three time slices: the base-period (bp), the near future (nf), and the far future (ff). Box-and-whisker plots indicate minimum and maximum (whiskers), 25th and 75th percentiles (box ends), and median (black solid middle bar). Solid curve line represents mean monthly value.

(b) Mean discharges at Bhairab Bazar station for three time slices.

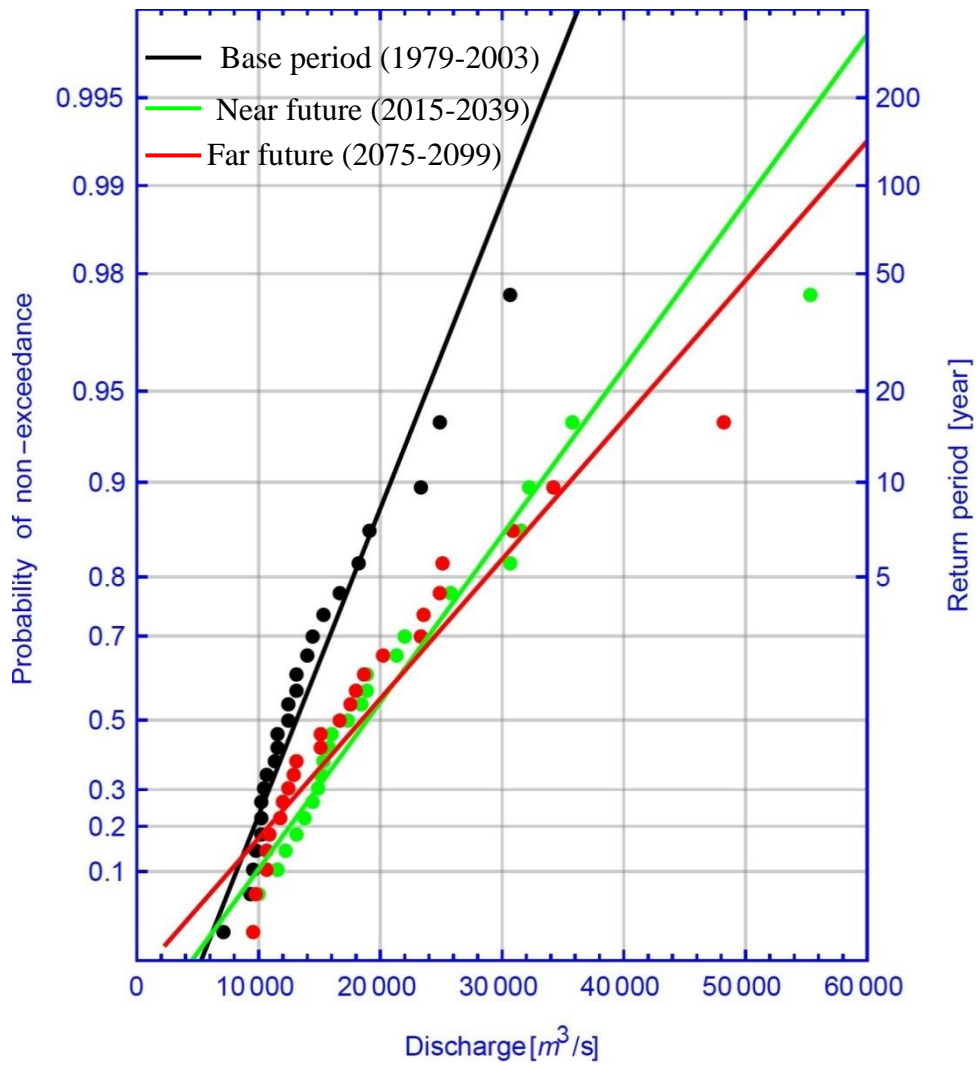


Figure 5-8. Probability of non-exceedance and return period for Gumbel distribution of annual maxima discharges ($m^3 s^{-1}$) at Bhairab Bazar for three time slices, the base period (1979–2003), the near future (2015–2039), and the far future (2075–2099), plotted in a Gumbel probability paper.

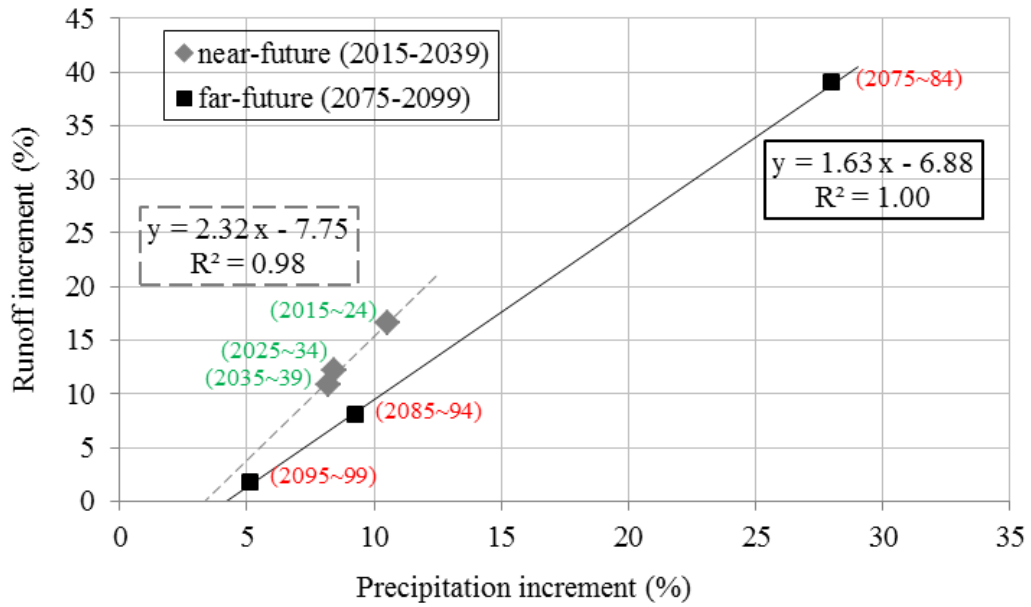


Figure 5-9. Projected precipitation and runoff change for the near future and the far future. Each point in the plot represents the 10-year mean of runoff increment associated with the corresponding precipitation increment at Bhairab Bazar gauging station. For 2035–2039 and 2095–2099, the mean is taken over 5 years. All increments are computed considering 1979–2003 as the base period.

Appendix A: Model validation at three upstream stations

The model performance was further evaluated by comparing the simulated monthly streamflow with the observed data from the Global Runoff Data Centre (GRDC) at three upstream gauging stations (Farakka, Pandu, and Teesta) in the GBM basin. The locations and drainage areas of these three stations are summarized in Table 3-2. Although the available data period do not cover the study period of 1980–2001 (except for the Teesta, which has the data from 1985–1991), the mean seasonal cycle and the mean, maximum, minimum, and standard deviation of the streamflow are compared in Figure A1 and Table A1. It can be seen that the mean seasonal cycle of simulated streamflow matches well with the corresponding GRDC data (Fig. A1d-f). Also, the agreement of the simulated and observed 1985–1991 monthly streamflow at the Teesta station of the Brahmaputra basin is excellent (Fig. A1c).

Table A1

Comparison between Observed (Data Source: GRDC) and Simulated Discharge ($m^3 s^{-1}$) at the Farakka Gauging Station in the Ganges Basin as well as the Pandu and Teesta Stations in the Brahmaputra Basin

Basin	Ganges		Brahmaputra		Brahmaputra	
Station	Farakka		Pandu		Teesta	
Data type	observed	simulate d	observed	simulate d	observed	simulate d
Data period (with missing)	1949- 1973	1980- 2001	1975- 1979	1980- 2001	1969- 1992	1980- 2001
Mean	12,037	11,399	18,818	15,868	915	920
Maximum	65,072	69,715	49,210	46,381	3,622	4,219
Minimum	1,181	414	4,367	3,693	10	122
Standard deviation	14,762	15,518	12,073	11,709	902	948

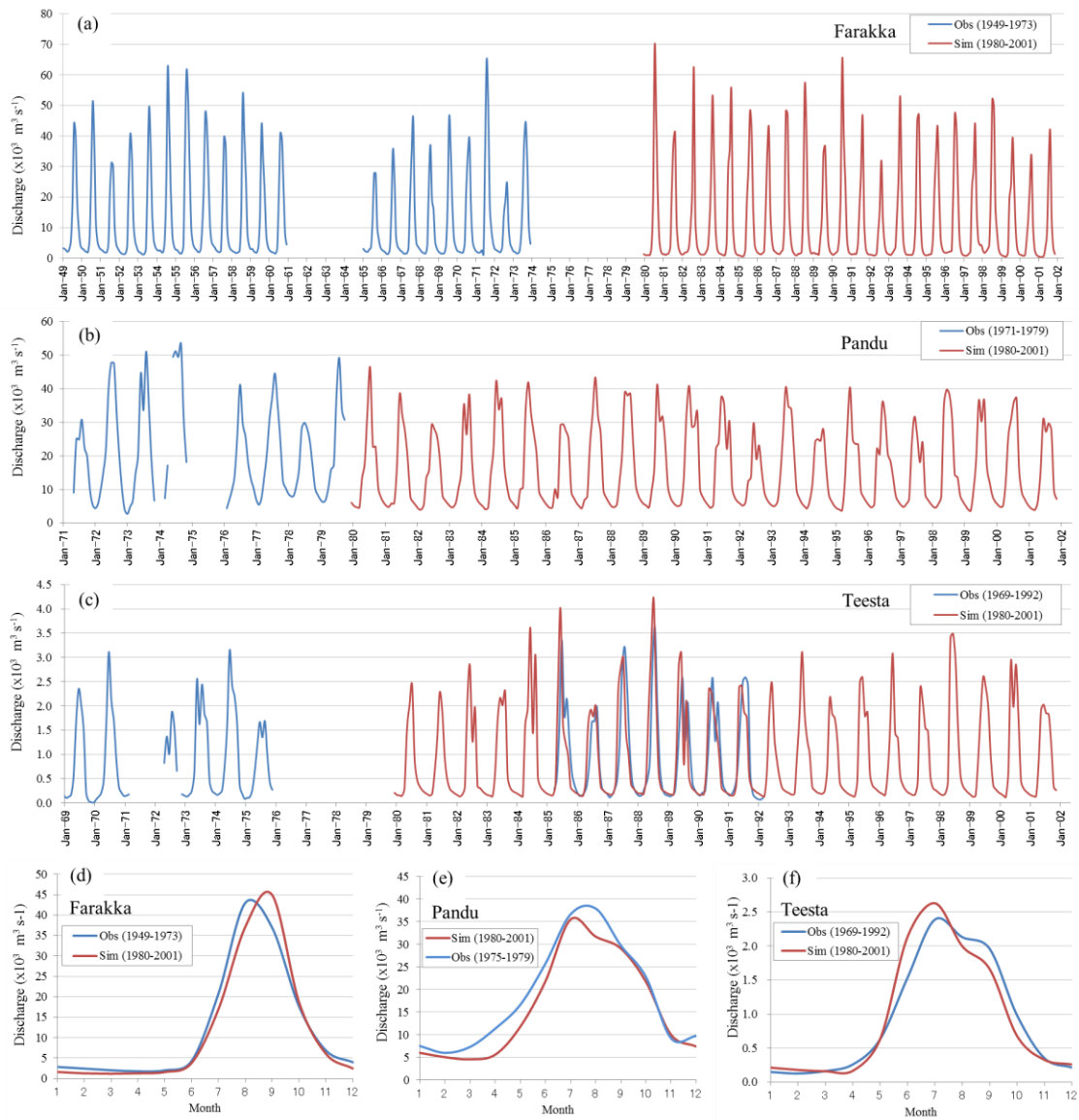


Figure A1. Comparisons between simulated (magenta line) and observed GRDC (blue line) data for (a–c) the monthly time series of discharges and (d–f) long-term mean seasonal cycles at the Farakka gauging station in the Ganges basin and at the Pandu and Teesta stations in the Brahmaputra basin.

Appendix B: Salient features of GCMs used

Table B1:

Salient features of CMIP5 climate models used in the analysis

Model name	MIROC-ESM	MIROC5	MRI-AGCM3.2S	MRI-CGCM3	HadGEM2-ES
Modelling centre	Japan Agency for Marine-Earth and Technology, and Atmosphere and Ocean Research Institute (The University of Tokyo), and National Institute for Environmental Studies	Atmosphere and Ocean Research Institute (The University of Tokyo), National Institute for Environmental Studies, and Japan Agency for Marine-Earth Science and Technology	Meteorological Research Institute (MRI), Japan and Meteorological Agency (JMA), Japan	Meteorological Research Institute (MRI), Japan	Met Office Hadley Centre, UK
Scenario	RCP 8.5	RCP 8.5	SRES A1B	RCP 8.5	RCP 8.5
Nominal horizontal resolution	2.81 × 2.77°	1.41×1.39°	0.25×0.25°	1.125×1.11°	1.875×1.25°
Model type	ESM ^a	ESM ^a	AMIP ^b	ESM ^a	ESM ^a
Aerosol component name or type	SPRINTARS	SPRINTARS	Prescribed		Interactive
Atmospheric Chemistry	Not implemented	Not implemented	Not implemented	Not implemented	Included
Land surface component	MATSIRO	MATSIRO	SiB0109	HAL	Included
Ocean Biogeochemistry	NPZD-type	Not implemented	Not implemented	Not implemented	Included
Sea ice	Included	Included	Not implemented	Included	Included

^aESM is Earth System Model. Atmosphere–Ocean General Circulation Models (AOGCMs) with representation of biogeochemical cycles.

^bAMIP refers to models with atmosphere and land surface only, using observed sea surface temperature and sea ice extent.